Proceedings of the International Workshop on e^+e^- collisions from ϕ to ψ (PHIPSI15)

Hefei, September 23 ~ 26, 2015

FORWARD

ZHAO Zhengguo
(for the PHIPSI15 Local Organizing Committee)
University of Science and Technology of China, Hefei 230026, China

The "International Workshop on e^+e^- collisions from ϕ to ψ" (PHIPSI15), was held at University of Science and Technology of China (USTC), Hefei, China, from Wednesday, September 23 to Saturday, September 26, 2015. This is the 10th workshop in a series, which started in Karlsruhe in 1996 and continued in Novosibirsk (1999), SLAC (2001), Pisa (2003), Novosibirsk (2006), Frascati (2008), Beijing (2009), Novosibirsk (2011) and Rome (2013), carrying now the name "from ϕ to ψ" first used at the Novosibirsk workshop in 1999. The aim of the workshop is to discuss in detail the state of art of various problems in hadronic physics at low energy e^+e^- colliders and the potential of existing and future facilities.

The subjects of the Workshop include: (1) R-measurements; (2) Radiative corrections; (3) Form factors and OZI rule violation; (4) Spectroscopy (light and heavy); (5) Muon $g-2$, experimental measurements and theoretical calculations; (6) Flavor physics; (7) Proton radius puzzle; (8) Gamma-gamma physics; (9) Tau lepton physics; (10) Machines and detectors.

We thank all the participants and the international advisory committee for making a very successful Workshop.

The Workshop was sponsored by the Chinese Center for Advanced Science and Technology (CCAST), the National Natural Science Foundation of China (NSFC), the Ministry of Science and Technology of China, the Chinese Academy of Sciences (CAS), and the University of Science and Technology of China (USTC).

中国科学技术大学学报

第 46 卷　第 6 期(总第 278 期)　2016 年 6 月

目　　次

[**期刊基本参数**]　CN34-1054/N * 1965 * m * A4 * 102 * zh/en * P * ￥30.00 * 1200 * 12 * 2016-06

责任编辑　李玉红　　**英文编辑**　崔海建　Federick Firstbrook

JOURNAL OF UNIVERSITY OF SCIENCE AND TECHNOLOGY OF CHINA

Vol. 46 No. 6 (Serial No. 278) May 2016

CONTENTS

Article ID:0253-2778(2016)06-0449-07

$\gamma\gamma$ physics analyses at BESⅢ

REDMER C. F. (the BESⅢ collaboration)

(*Institut Für Kernphysik, Johannes Gutenberg-Universität Mainz* 55128, *Germany*)

Abstract: The BESⅢ Collaboration has recently embarked on a two-photon physics program. Its main motivation is given by the large uncertainty of the contribution of hadronic light-by-light scattering to the anomalous magnetic moment of the muon α_μ, and the need of electromagnetic transition form factors (TFF) as experimental input to improve the calculations. Data acquired with the BESⅢ detector at center-of-mass energies from 3.77 to 4.6 GeV allow for the determination of TFFs of light pseudoscalar mesons. The measurements are performed with a single-tag technique and result in unprecedented accuracy at momentum transfers below 2 GeV^2, the region of highest importance for the calculations of α_μ. Employing the same approach, the first double-tagged measurement of the pion transition form factor has been started. It is the first step towards a model independent parameterization of the TFF of the π^0. Additionally, measurements of multi-meson final states have been engaged.

Key words: anomalous magnetic moment of the muon; hadronic light-by-light scatteringg; pseudoscalar mesons; transition form factor; single-tag measurement **CLC number**: O572.3 **Document code**: A
doi:10.3969/j.issn.0253-2778.2016.06.001

Citation: REDMER C F(the BESⅢ collaboration). $\gamma\gamma$ physics analyses at BESⅢ[J]. Journal of University of Science and Technology of China, 2016,46(6): 449-455.
REDMER C F(代表BESⅢ合作组). BESⅢ上双光子物理分析[J]. 中国科学技术大学学报,2016,46(6): 449-455..

BESⅢ上双光子物理分析

REDMER C. F.

(约翰内斯堡大学, 德国美因茨, 55128)

摘要:BESⅢ合作组最近开始双光子物理研究,主要源于强子 light-by-light 散射对缪子反常磁矩的贡献有很大不确定性,电磁跃迁形状因子作为实验输入是改善计算精度的需要。在BESⅢ探测器上获得的质心能量3.77 GeV到4.6GeV的数据使得我们能够测量轻赝标量介子的跃迁形状因子。在动量转移低于2 $(GeV/c)^2$时单标记技术测量的结果达到前所未有的精确,该区域对于 α_μ 的计算十分重要,并且也首次开始了 π 介子跃迁形状因子的双标记测量。这是 π^0 跃迁形状因子模型无关参数化研究的第一步。另外,多介子末态测量也在进行中.

关键词:缪子反常磁矩; 强 light-by-light 散射; 赝标介子; 跃迁形状因子;单标记测量

Received:2015-11-30;**Revised**:2016-04-20

Foundation item:Supported by the German Research Foundation DFG under Contract(CRC-1044).

Biography:REDMER C. F.(corresponding author), Professor/PhD. Research field: high energy physics. E-mail: redmer@uni-mainz.de

0 Introduction

The anomalous magnetic moment of the muon is one of the most precisely known observables in particle physics. Over the recent decades enormous efforts have been made to reach a precision in the order of 10^{-10} in the direct experimental measurement, as well as in the Standard Model prediction of α_μ. However, there remains a discrepancy of 3 to 4 standard deviations between the measured and the calculated values of α_μ. The potential origin of this difference has triggered a lot of activity, since, even if not being significant enough to claim a discovery, it might be a hint for New Physics.

Newly proposed experiments aim at a fourfold improvement of the current precision of the direct measurements of α_μ[1-2]. These experimental endeavors have given rise to numerous theory efforts in order to improve the Standard Model prediction on the same level. While the dominating QED contribution has been calculated including corrections up to tenth order[3], and the weak contribution also being well understood by means of perturbation theory[4], the error of the prediction of α_μ is completely dominated by the hadronic contributions. The main challenge is that QCD cannot be handled by perturbative methods at the relevant energy regime.

The largest hadronic contribution α_μ^{hVP} is due to the hadronic vacuum polarization. It is handled within a dispersive framework, which requires $\sigma(e^+e^- \rightarrow \text{hadrons})$ as experimental input[5]. Various laboratories world wide have measured hadronic cross section in scan experiments and exploiting the technique of Initial State Radiation(ISR), as has been reported in this workshop. These results can be used to significantly reduce the uncertainty of α_μ related to hadronic vacuum polarization in the near future.

Another hadronic contribution to the muon anomaly α_μ is due to the hadronic light-by-light scattering (HLbL), α_μ^{HLbL}. In contrast to α_μ^{hVP}, it cannot be directly related to experimentally measurable quantities. The HLbL involves the coupling of real and virtual photons to virtual hadronic states, described by transition form factors(TFF), while only transitions of real mesons to real and virtual photons can be measured. Calculations of the HLbL process are possible in the low energy regime by means of chiral perturbation theory, or at high energies, using perturbative QCD(pQCD). The energy scale relevant for the magnetic moment of the muon is, however, the intermediate regime, which cannot be addressed by perturbative means. Thus, hadronic models have been developed and used for the calculations of α_μ^{HLbL}. The contributions of individual hadronic processes to the models is dominated by the transitions of the pseudoscalar mesons π^0, η and η', followed by multi-meson states and higher resonances[6]. The validity of the models can be tested with measurements of the momentum transfer dependence of the respective TFF. The uncertainties of the resulting values of α_μ^{HLbL} depend strongly on the models. Two of the frequently quoted examples are the so called " Glasgow Consensus" by Prades, de Rafael and Vainshtain[7] and the recent calculations by Jegerlehner and Nyffeler[8]. The relative uncertainties of the respective results of α_μ^{HLbL} differs by approximately 30%.

In order to reduce the model dependency for the calculation of α_μ^{HLbL}, recently, the development of data driven approaches has been started. The goal is to provide a more reliable estimate of the uncertainty of α_μ^{HLbL}, based on dispersive analysis[9-10]. Important inputs to these calculations are the TFF of π^0, of two pions and the pion polarizabilities.

The need for additional data on TFF, in order to improve the calculations of HLbL and, thus, to improve the prediction of α_μ, has motivated the $\gamma\gamma$ physics program, recently started at BES Ⅲ. Experiments at e^+e^- colliders can provide data on space-like TFF through the measurement of meson production in two-photon collision. The differential cross section of this production mechanism is directly proportional to the square of the TFF, but it is peaked towards small polar angles of the scattered leptons. Common detector setups cannot cover smallest scattering angles, due to the beam optics necessary to collide the beam at the desired interaction region.

Thus, the momentum dependence of the TFF is usually studied in single-tag analyses, where only one of the scattered leptons is reconstructed in the detector volume along with the produced hadronic system. The second lepton is expected to escape detection at smallest scattering angles, i. e. along the beam axis. The corresponding momentum transfer is small and the exchanged photon is quasi-real. Thus, the form factor $F(Q_1^2, Q_2^2)$ depends only on a single momentum transfer $F(Q^2)$.

Available measurements of the π^0, η and η' TFF are dominated by the recent measurements at B-factories[11-12]. The TFF has been determined for momentum transfers Q^2 from 4 GeV^2 to 40 GeV^2 and the results triggered a discussion on the applicability of pQCD in this energy range, by the so called Belle-BaBar-puzzle. For $\alpha_\mu^{\mathrm{HLbL}}$, however, these data are less influential. Here, the Q^2-behavior of the TFF at approximately 1.5 GeV^2 is most important[13-14]. At these energies only measurements from the CELLO and CLEO experiments[15-16] are available, which suffer from comparatively low statistics.

The BES Ⅲ experiment can contribute in exactly this region of low momentum transfer and can provide data on the TFF dependence with high statistical accuracy.

1 The BES Ⅲ detector at BEPC Ⅱ

The BES Ⅲ experiment[17] is located at the symmetric e^+e^- collider BEPC Ⅱ, which is operated at the IHEP in Beijing(China). Data can be collected in a center-of-mass energy range from 2.0 GeV to 4.6 GeV. The BES Ⅲ detector setup consists of a helium-based drift chamber surrounding the Beryllium beam pipe, a plastic scintillator time-of-flight system, and a CsI(Tl) electromagnetic calorimeter, which are placed inside the bore of a superconducting solenoidal magnet providing a 1.0 T magnetic field. The flux-return yoke is instrumented with resistive plate counters and serves as muon chamber. The detector covers 93% of the solid angle. Momenta of charged particles and photon energies are measured with a resolution of 0.5% and 2.5% at 1 GeV, respectively.

Data taking has been routinely performed since 2009. In the recent data taking campaigns BES Ⅲ has collected 1.25×10^9 $e^+e^-\to J/\psi$ events, more than 500×10^6 $e^+e^-\to\psi(2S)$ events, 2.9 fb^{-1} at the $\psi(3770)$ peak, and more than 5 fb^{-1} in the center-of-mass region above 4 GeV, which are devoted to studies of the charmonia and charmonium-like states[18-20]. This data set comprises the world's largest samples of J/ψ, $\psi(2s)$, and $\psi(3770)$ mesons. Additional data have been acquired for a τ-mass scan and a high statistics R-scan. Based on these data, the BES Ⅲ collaboration pursues a physics program[21], which focuseson charmonium spectroscopy, charm physics, light hadron spectroscopy, τ physics, and R-measurements.

The investigations in the field of $\gamma\gamma$ physics make use of all larger data sets, whereas the data taken at $\sqrt{s}=3.77$ GeV constitute the largest individual sample. It has been used to study the TFF of π^0, η and η'.

2 Transition form factors of π^0, η and η'

The analysis of the TFF of π^0, η and η' is based on a single-tag technique: Only the decay products of the produced mesons $P=\pi^0$, $\eta\eta'$ and one of the two scattered leptons of the reaction $e^+e^-\to Pe^+e^-$ are measured in the detector. The other lepton is reconstructed from four-momentum conservation and it is required to have a scattering angle smaller than 8°, which corresponds to the radius of the beam pipe at the end of the detector.

The π^0 meson is reconstructed from its decay into two photons. The main source of background in the event selection are QED processes, such as radiative Bhabha scattering. Hard radiative photons in combination with a soft photon from any secondary process easily mimic the invariant mass of a pion. Three conditions are applied on the measured photon pairs to successfully reduce this background: A limit on the helicity angle of the photons, which is the angle between one of the photons in the rest frame of the pion and the direction of motion in the laboratory frame; A threshold on the scattering angle of the pion; A

minimum polar angle difference of the two photons in the laboratory frame. Hadronic background from decays of $\psi(3770)$ into pairs of D mesons, the radiative return to $\psi(2S)$ and J/ψ, and from the $q\bar{q}$ continuum is rejected by a condition, which has been introduced in the BaBar analysis[11], in order to suppress initial state radiation in the signal channels. Since it is based on energy and momentum conservation, it is also efficiently suppressing background from incompletely reconstructed hadronic sources and other two-photon production channels. Remaining event candidates show clear signal peaks, not only of the π^0, but also of the η meson in the invariant mass distribution of the two photons.

In order to extract the TFF of the π^0, remaining background is subtracted bin-by-bin from the differential distribution of momentum transfer. For every bin in Q^2 the invariant mass spectrum of the two photon system is fitted and the number of signal events above the continuous background is counted. The background free Q^2 spectrum is converted to the TFF-distribution by normalizing to the reconstruction efficiency and luminosity and finally dividing out the point-like cross section, by means of a Monte Carlo simulation based on the Wess-Zumino-Witten term[22-23].

The data taken at the $\psi(3770)$ peak statistically only allow for a measurement of the TFF of the π^0 at momentum transfers of $0.3 \leqslant Q^2\ (\mathrm{GeV}^2) \leqslant 3.1$. This corresponds to the kinematical region, which is of importance as input for the calculations on hadronic light-by-light scattering. The statistical accuracy obtained with the analysis scheme described above is unprecedented for $Q^2 \leqslant 1.5\ \mathrm{GeV}^2$; for larger momentum transfers it is still compatible with the CLEO[16] result. The systematics are still under study, where the largest contribution comes from the method of background subtraction. The publication of the result is expected in the near future.

An improved understanding of the contribution of the π^0 TFF to $\alpha_\mu^{\mathrm{HLbL}}$ is, however, only sufficient on the level of the current experimental precision of α_μ. In view of the announced new direct measurements and their planned four-fold improvement in accuracy, it is necessary to include and to improve the understanding of the contributions of η and η'.

A dedicated measurement of the respective TFF has been started, based on the decay modes $\eta \to \pi^0\pi^+\pi^-$ and $\eta' \to \pi^0\pi^+\pi^-$, which result in the same final state, taking into account the subsequent decays of π^0 and η into two photons. The analysis strategy is analogous to the analysis of the π^0 production described above, except for the conditions to suppress radiative Bhabha scattering, which is not of concern in this channel. Hadronic background contributions involve decays of ω and φ mesons into three pions. In the analysis of the η mesons, there is also background from incompletely reconstructed decays of η' mesons, produced in the two-photon collisions. By kinematically fitting the decay systems to the masses of η and η', respectively, background is suppressed completely.

Based on this selection, the TFF can be extracted from data taken at $\sqrt{s} = 3.77$ GeV, for momentum transfers between $0.3 \leqslant Q^2\ (\mathrm{GeV}^2) \leqslant 3.5$. The statistical accuracy is compatible with the published results of the CELLO and CLEO experiments[15-16]. However, it should be noted that in contrast to the previous measurements, here, only one decay channel has been evaluated. Adding more decay channels in the analysis, as well as analyzing the remaining data sets will improve the BES Ⅲ result significantly.

3 Transition form factors of $\pi\pi$

Recently, the BES Ⅲ collaboration started a measurements of $\pi^+\pi^-$ pair production in two-photon collisions. The measurement is not only motivated by its relevance for $\alpha_\mu^{\mathrm{HLbL}}$, especially for the new dispersive calculations. It is also of interest, due to the possibility of extracting parameters of resonances in the two-pion final state and the possibility to study pion rescattering effects at low invariant masses. Previous measurements used untagged measurements, i.e. both scattered leptons escaped detection, and were restricted to invariant masses larger than approximately 500 $\mathrm{MeV/c^2}$. Only a few data points at lower masses

have been published by the MARK Ⅱ experiment[24-26].

The analysis of the $\pi^+\pi^-$ final state at BES Ⅲ follows the single-tag strategy, successfully used in the analysis of single pseudoscalar meson production. The main background contributions stem from the two-photon production of muon pairs, and the radiative Bhabha scattering process, in which the photon couples to a ρ-meson, decaying into two pions.

The QED background of muon production is well understood from the $\gamma\gamma$ physics studies at LEP[27]. Monte Carlo generators are used to produce training samples for the application of an artificial neural network, which was already successfully applied in the measurement of hadronic cross sections, to separate pions from muons[28]. Muon background surviving the condition found with the neural net is subtracted using Monte Carlo distributions.

Background involving the ρ-meson is subtracted by fitting the clearly visible peak in the $\pi^+\pi^-$ invariant mass with the Kühn-Santamaria parameterization[29]. The remaining events allow to study the production of $\pi^+\pi^-$ in bins of the momentum transfer Q^2, the pion invariant mass, and the pion helicity angle $\cos\theta^*$. This is the first measurement in the invariant mass region of $2m_\pi \leqslant M_{\pi\pi}(\mathrm{GeV}) \leqslant 2.0$ and the momentum transfer region of $0.2 \leqslant Q^2(\mathrm{GeV}^2) \leqslant 2.0$ with a full coverage of the helicity angle.

4 Double-tagged measurements

In case of common detector setups at e^+e^- colliders, double-tagged measurements refer to the analysis of events, where both leptons have been scattered into the detector volume, i. e. the scattering angles with respect to the beam axis are in general larger than approximately 20°. Thus, the momentum transfer of each lepton is large. Due to vanishing cross sections for events with the corresponding kinematics, currently, experimental information on TFFs depending on two virtualities $F(Q_1^2, Q_1^2)$ is not available.

First exploratory studies for a double-tagged measurement of the π^0 TFF have been started at BES Ⅲ. The aim is to exploit the large data sets, originally collected for charm physics and charmonium-like spectroscopy, which correspond to almost 8 fb^{-1}. Monte Carlo studies show that a direct measurement of $F(Q_1^2, Q_1^2)$ is possible for $0.5 \leqslant Q_1^2, Q_1^2(\mathrm{GeV}^2) \leqslant 1.5$, which, depending on the reconstruction efficiency, can already have a significant impact on $\alpha_\mu^{\mathrm{HLbL}}$.

The available statistics at BES Ⅲ should at least be sufficient for a comparison between two hadronic models, which was recently suggested by Nyffeler. The momentum transfer dependence of the TFF in VMD and in the LMD + V model[13] differs by a damping factor of Q^2. The difference could be as large as 25% for $F(1\ \mathrm{GeV}^2, 1\ \mathrm{GeV}^2)$, and, thus, be resolved by a measurement.

Another aspect of double-tagged measurements is related to the production mechanism in two-photon collisions. The general term for the cross section can be separated into individual terms depending on the transverse or longitudinal polarization of the individual photons, the relative parallel or perpendicular polarization of the two photons and the helicity of the two-photon system[30]. Another parameter is the dihedral angle of the leptons in the rest frame of the two photons. It can be used to separate multi-meson and tensor contributions to the TFF. Its determination requires knowledge of the four-momentum of both scattered leptons. In single-tag measurements there is, however, a large uncertainty on the azimuthal angle of the untagged lepton. Double-tagged measurements, in turn, suffer from a vanishing cross section.

A way out is the installation of special tagging detectors, which cover small angles. In this way, double-tagged measurements are no longer restricted to events with two large virtualities of the exchanged photons. A first tagging detector has been installed at BES Ⅲ. It is a sampling calorimeter, made from lead an scintillating fibers, which covers polar angles from 1 to 10 m · rad. Its benefits will be tested in the upcoming data taking periods. The tagging detector can also be used to measure photons emitted by initial state radiation. Motivated by the additional use, there are plans to replace the current detector design with crystal calorimeters, which will be installed in both hemispheres of the BES Ⅲ setup.

5 Conclusion

The $\gamma\gamma$ physics program at BES Ⅲ is motivated by the need of new, high precision data on transition form factors of pseudoscalar mesons as input to the calculations of the contribution of hadronic light-by-light scattering to the anomalous magnetic moment of the muon. The measurement of the π^0 TFF results in unprecedented statistical accuracy for momentum transfers in the region of $0.3 \leqslant Q^2\,(\mathrm{GeV}^2) \leqslant 1.5$ and compatible precision with previous measurements for larger Q^2. The results for η and η' are currently limited in statistics by restricting the analysis to only a single decay mode.

The analysis of $\pi^+\pi^-$ in two-photon collisions will provide the first single-tag measurement at low invariant masses and small momentum transfers, with the full coverage of the pion helicity angle. The analysis is being extended to the neutral channels $\pi^0\pi^0$, $\pi^0\eta$ and $\eta\eta$.

In addition to the single-tag studies, first double-tagged investigations have been started. It is the first attempt to obtain a direct and model independent parameterization of the TFF of π^0.

The great potential of the BES Ⅲ experiment, to contribute valuable information on the field of $\gamma\gamma$ physics is currently being extended by the installation of tagging detectors. These add new prospects to the physics program, allowing to measure the scattered leptons with small momentum transfer, which has, so far, escaped detection.

References

[1] GRANGE J, GUARINO V, WINTER P, et al. Muon $g-2$ technical design report[J]. Physics, 2015, 155(1): 372-374..

[2] SHWARTZ B. J-PARC E34 conceptual design report[R]. 2011.

[3] AOYAMA T, HAYAKAWA M, KINOSHITA M, et al. Complete tenth-order QED contribution to the muon $g-2$ [J]. Physical Review Letters, 2012, 109(11): 1253-1306.

[4] GNENDIGER C, STÖCKINGER D, STÖCKINGERKIM H. The electroweak contributions to $(g-2)\mu$ after the Higgs boson mass measurement[J]. Physical Review D, 2013, 88(5): 1201-1205.

[5] DAVIER M, HOECKER A, MALAESCU B, et al. Reevaluation of the Hadronic Contributions to the Muon $g-2$ and to $\alpha(M_Z^2)$[J]. European Physical Journal C, 2011, 71(1): 1-13.

[6] DE RAFAELI E. Hadronic contributions to the muon $g-2$ and low-energy QCD[J]. Physics Letters B, 1994, 322(3): 239-246.

[7] PRADES J, DE RAFAEL E, VAINSHTAIN A. The hadronic light-by-light scattering contribution to the muon and electron anomalous magnetic moments[J]. Advanced Series on Directions in High Energy Physics, 2009, 20: 303-317 arXiv: 0901.0306.

[8] JEGERLEHNER F, NYFFELER A. The muon $g-2$[J]. Physics Reports, 2009, 477(1-3): 1-110.

[9] COLANGELO G, HOFERICHTER M, PROCURA M, et al. Dispersion relation for hadronic light-by-light scattering: theoretical foundations[J]. Journal of High Energy Physics, 2015, 2015(9): 1-77.

[10] PAUK V, VANDERHAEGHEN M. Anomalous magnetic moment of the muon in a dispersive approach[J]. Physical Review D, 2014, 90:113012.

[11] AUBERT B, KARYOTAKIS Y, LEES J P, et al. Measurement of the $\gamma\gamma^* \to \pi^0$ transition form factor[J]. Physical Review D, 2009, 80(5): 141-150.

[12] UEHARA S, WATANABE Y, NAKAZAWA H, et al. Measurement of the $\gamma\gamma^* \to \pi^0$ transition form factor at Belle[J]. Physical Review D, 2012, 86(9): 092007 .

[13] KNECHT M, NYFFELER A. Hadronic light-by-light corrections to the muon $g-2$: The pion-pole contribution [J]. Physical Review D, 2001, 65(7): 133-136.

[14] MASJUAN P. $\gamma\gamma^* \to \pi^0$ transition form factor at low-energies from a model-independent approach[J]. Physical Review D, 2012, 86: 094021.

[15] BEHREND H J, CRIEGEE L, FIELD J H, et al. A measurement of the π^0, η and η' electromagnetic form-factors[J]. Zeitschrift Für Physik C, 1991, 49(3): 401-409.

[16] GRONBERG J, HILL T S, KUTSCHKE R, et al. Measurements of the meson-photon transition form factors of light pseudoscalar mesons at large momentum transfer [J]. Physical Review D, 1997, 57(1): 33-54.

[17] ABLIKIM M, AN Z H, BAI J Z, et al. Design and construction of the BES Ⅲ detector[J]. Nuclear Instruments & Methods in Physics Research A, 2010, 614(3): 345-399.

[18] ABLIKIM M, YANG H X, ZHANG Z P, et al. Determination of the number of J/ψ events with $J/\psi \to$

inclusive $J/\psi\rightarrow$inclusive decays[J]. Chinese Physics C, 2012, 36:915-925.

[19] ABLIKIM M, ACHASOV M N, AMBROSE D J. Determination of the number of ψ' event at BE Ⅲ [J]. Chinese Physics C, 2012, 37(6): 063001.

[20] ABLIKIM M, ACHASOV M N, Aix C, et al. Evidence for $e^+e^-\rightarrow\gamma Xc_{1,2}$ at center-of-mass energies from 4.009 to 4.360 GeV[J]. Chinese Physics C, 2015, 39(4): 41001-41009.

[21] ASNER D M, BARNES T, BIAN J M, et al. Physics at BES-Ⅲ [J]. nternational Journalof Modern Physics A, 2009, 24(S1) arXiv: 0809.1869.

[22] WESS Consequences of anomalous ward identities [J]. Physics Letter B, 1971, 37: 95.

[23] WITTEN E. Global aspects of current algebra[J]. Nuclear Physics B, 1983, 223: 422.

[24] BOYER J, BUTLER F, GIDAL G, et al. Two-photon production of pion pairs[J]. Physical Review D, 1990, 42(5): 1350-1367.

[25] BEHREND H J, CRIEGEE L, FIELD J H, et al. An experimental study of the process $\gamma\gamma\rightarrow\pi^+\pi^-$ [J]. Zeitschrift Für Physik C, 1992, 56(3): 381-390.

[26] MORI T, UEHARA S, WATANABE Y, et al. High statistics study of the f0(980) resonance in $\gamma\gamma\rightarrow\pi^+\pi^-$ production [J]. Physical Review D, 2007, 75(5): 973-974.

[27] BERENDS F A, DAVERVELDT P H, KLEISS R. Monte Carlo simulation of two-photon processes : Ⅱ : Complete lowest order calculations for four-lepton production processes in electron-positron collisions [J]. Computer Physics Communications, 1986, 40(2-3): 285-307.

[28] ABLIKIM M, ACHASOV M N, AI X C, et al. Measurement of the $e^+e^-\rightarrow\pi^+\pi^-$ cross section between 600 and 900 MeV using initial state radiation[J]. Physics Letter B, 2016, 753: 629-638.

[29] KÜHN J H, SANTAMARIA A. τ decays to pions[J]. Zeitschrift Für Physik C, 1990, 48(3): 445-452.

[30] BUDNEV V M, GINZBURG I F, MELEDIN G V, et al. The two-photon particle production mechanism. Physical problems. Applications. Equivalent photon approximation [J]. Physics Report, 1975, 15(4): 181-282.

Article ID:0253-2778(2016)06-0456-06

Hadronic contribution from light by light processes in $(g-2)$ of muon in nonlocal quark model

ZHEVLAKOV A. S.[1], DOROKHOV A. E.[2], RADZHABOV A. E.[3]

(1. *Department of Physics, Tomsk State University, Tomsk* 634050, *Russia*;
2. *Bogoliubov Laboratory of Theoretical Physics, Dubna* 141980, *Russia*;
3. *Institute for System Dynamics and Control Theory SB RAS, Irkutsk* 664033, *Russia*)

Abstract: The hadronic corrections to the muon anomalous magnetic moment α_μ, due to the full gauge-invariant set of diagrams with dynamical quark loop and intermediate pseudoscalar and scalar states light-by-light scattering insertions, are calculated in the framework of the nonlocal chiral quark model. These diagrams correspond to all hadronic light-by-light scattering contributions to α_μ in the leading order of the $1/N_c$ expansion in quark model. The result of the quark loop contribution is $\alpha_\mu^{\mathrm{HLbL,Loop}} = (11.0 \pm 0.9) \cdot 10^{-10}$, and the total result is $\alpha_\mu^{\mathrm{HLbL,N\chi QM}} = (16.8 \pm 1.2) \cdot 10^{-10}$.

Key words: anomalous magnetic moment of muon; nonlocal model; light-by-light; chiral model **CLC number**: O572.3 **Document code**: A doi:10.3969/j.issn.0253-2778.2016.06.002

Citation: ZHEVLAKOV A S, DOROKHOV A E, RADZHABOV A E. Hadronic contribution from light by light processes in $(g-2)$ of muon in nonlocal quark model[J]. Journal of University of Science and Technology of China, 2016, 46(6): 456-461.
ZHEVLAKOV A S, DOROKHOV A E, RADZHABOV A E. 非局域夸克模型中强子 light-by-light 过程对缪子$(g-2)$因子的贡献[J]. 中国科学技术大学学报, 2016, 46(6): 456-461.

非局域夸克模型中强子 light-by-light 过程对缪子$(g-2)$因子的贡献

ZHEVLAKOV A. S.[1], DOROKHOV A. E.[2], RADZHABOV A. E.[3]

(1. 托木斯克国立大学物理系, 托木斯克 634050, 俄罗斯;
2. 理论物理巴格寥夫实验室, 杜布纳 141980, 俄罗斯;
3. 系统动力和控制理论研究院, 伊尔库茨克 664033, 俄罗斯)

摘要:在非局域手征夸克模型框架下,计算了来源于全规范不变性动力学夸克圈图和中间赝标量介子和标量介子态圈图 light-by-lightt 散射过程对缪子反常磁矩 α_μ 的强子修正. 在夸克模型中,这些圈图对应于强子 light-by-light 散射过程对 α_μ 的最低价 $1/N_c$ 的贡献. 夸克圈图贡献的结果是 $\alpha_\mu^{\mathrm{HLbL,Loop}} = (11.0 \pm 0.9) \cdot 10^{-10}$,总贡献结果是 $\alpha_\mu^{\mathrm{HLbL,N\chi QM}} = (16.8 \pm 1.2) \cdot 10^{-10}$.

关键词:缪子反常磁矩; 非局域模型; light-by-light; 手征模型

Received: 2015-11-30; **Revised**: 2016-04-20
Foundation item: Supported by by Russian Science Foundation (14-50-00080), RFBR grant (15-02-03391).
Biography: ZHEVLAKOV A. S. (corresponding author), Professor/PhD. Research field: high energy physics. E-mail: zhevlakov@phys.tsu.ru

0 Introduction

The anomalous magnetic moment (AMM) of lepton and contribution of light by light (LbL) processes has a long history of investigation. After recent experiments on measurement of AMM of muon in Brookhaven National Laboratory (BNL) E821[1] the interest in this topic has returned. Two new experiments on measurement of AMM of muon are under construction in Fermilab[2] and J-PARC[3]. New precision data are demand more accurate calculations.

The most problematic part of the calculation AMM of muon is the segment associated with the strong interaction because most of this contribution is in nonperturbative low energy region. This contribution consist of hadron vacuum polarization (HVP) part (leading in α) and LbL scattering through the nonperturbative QCD vacuum (sub-leading in α). The HVP contribution can be extracted from the experimental data but the contribution of LbL scattering needs to be modeled.

What degrees of freedom (DoF) are relevant to modeling strong interaction at low energy: Mesons or quarks (and gluons)? This question is connected with the confinement problem and is one of the most important tasks in physics of strong interaction. One can separate two different approaches for description of LbL processes. In the first one the only mesonic DoF are used. The second one starts from quark Lagrangian and have mesonic DoF as a bound state.

1 Model

The LbL contribution to AMM of muon is in the low energy region where the perturbative methods of QCD are not applicable.

Nonlocal quark model NχQM is nonlinear realization of Nambu-Jona-Lasinio model. Nonlocality can be motivated by instanton liquid model. The model is formulated in terms of quark degrees of freedom and bound states corresponding to mesons. The circumscribing of the model is made in Refs. [4-5] and here we give a brief description of model properties that is needed for calculation of AMM.

1.1 Lagrangian

The Lagrangian of the $SU(3)$ nonlocal chiral quark model with the $SU(3)\times SU(3)$ symmetry has the form.

$$\mathscr{L} = \bar{q}(x)(i\hat{\partial} - m_c)q(x) + \frac{G}{2}[J_S^a(x)J_S^a(x) + J_{PS}^a(x)J_{PS}^a(x)] - \frac{H}{4}T_{abc}[J_S^a(x)J_S^b(x)J_S^c(x) - 3J_S^a(x)J_{PS}^b(x)J_{PS}^c(x)] \quad (1)$$

where $q(x)$ are the quark fields, $m_c(m_u = m_d \neq m_s)$ is the diagonal matrix of the quark current masses, G and H are the four-and six-quark coupling constants. The second line in the Lagrangian represents the Kobayashi-Maskawa-t′ Hooft determinant vertex with the structural constant

$$T_{abc} = \frac{1}{6}\epsilon_{ijk}\epsilon_{mnl}(\lambda_a)_{im}(\lambda_b)_{jn}(\lambda_c\alpha)_{kl} \quad (2)$$

where λ_a are the Gell－Mann matrices for a $= 1,\cdots,8$ and $\lambda_0 = \sqrt{2/3}I$.

The nonlocal structure of the model is introduced via the nonlocal quark currents

$$J_M^a(x) = \int \mathrm{d}^4x_1\mathrm{d}^4x_2 f(x_1)f(x_2)\bar{q}(x-x_2)\Gamma_M^a q(x+x_2) \quad (3)$$

where $M = S$ for the scalar and $M = PS$ for the pseudoscalar channels, $\Gamma_S^a = \lambda^a$, $\Gamma_{PS}^a = i\gamma^5\lambda^a$ and $f(x)$ is a form factor with the nonlocality parameter Λ reflecting the nonlocal properties of the QCD vacuum.

The model can be bosonized using the stationary phase approximation which leads to the system of gap equations for the dynamical quark masses $m_{d,i}$.

$$m_{d,i} + GS_i + \frac{H}{2}S_jS_k = 0 \quad (4)$$

with $i = u, d, s$ and $j, k \neq i$, and S_i is the quark loop integral

$$S_i = -8N_c\int\frac{d_E^4k}{(2\pi)^4}\frac{f^2(k^2)m_i(k^2)}{D_i(k^2)},$$

where $m_i(k^2) = m_{c,i} + m_{d,i}f^2(k^2)$, $D_i(k^2) = k^2 + m_i^2(k^2)$ is the dynamical quark propagator obtained by solving the Dyson-Schwinger equation, $f(k^2)$ is the nonlocal form factor in the momentum representation. For calculation we use two different form-factors: Gaussian form

$$f(p^2) = \exp(-\frac{p^2}{2\Lambda^2}) \quad (5)$$

monopole form

$$f(p^2) = (1 + \frac{p^2}{\Lambda^2})^{-1} \quad (6)$$

where Λ is the cutoff parameter. The model have five parameters which can be fitted on physical observables. In order to investigate the sensitivity of the model to the change in model parameters the dynamical mass of light quark varies between 200-350 MeV with corresponding refit of other parameters. This region corresponds to the more or less physical range of dynamical quark mass.

1.2 Meson propagator

The quark-meson vertex functions and the meson masses can be found from the solution of Bethe-Salpeter equation Fig. 1. For the separable interaction[5] the quark-antiquark scattering matrix in each (PS or S) channels becomes

$$\boldsymbol{T} = \dot{\boldsymbol{T}}(p^2)\delta^4(p_1 + p_2 - (p_3 + p_4))\prod_{i=1}^{4} f(p_i^2) \quad (7a)$$

$$\dot{\boldsymbol{T}}(p^2) = i\gamma_5\lambda_k(\frac{1}{-\boldsymbol{G}^{-1} + \prod(p^2)})_{ki} i\gamma_5\lambda_l \quad (7b)$$

where p_i are the momenta of external quark lines, $\boldsymbol{G}$ and $\prod(p^2)$ are the corresponding matrices of the four-quarkcoupling constants and the polarization operators of mesons($p = p_1 + p_2 = p_3 + p_4$). The meson masses can be found from the zeros of determinant $\det(\boldsymbol{G}^{-1} - \prod(-M^2)) = 0$. The $\dot{\boldsymbol{T}}$-matrix for the system of mesons in each neutral channelcan be expressed as

$$\dot{\boldsymbol{T}}_{ch}(p^2) = \sum_{M_{ch}} \frac{\bar{V}_{M_{ch}}(P^2) \otimes V_{M_{ch}}(P^2)}{-(P^2 + M_{ch}^2)}) \quad (8)$$

where M_M are the meson masses, and $V_M(P^2)$ are the vertex functions ($\bar{V}_M(p^2) = \gamma^0 V_M^+(P^2)\gamma^0$). The sum in Eq. (8) is over the full set of light mesons: ($M_{PS} = \pi^0, \eta, \eta'$) in the pseudoscalar channel and ($M_S = a_0(980), f_0(980), \sigma$) in the scalar one.

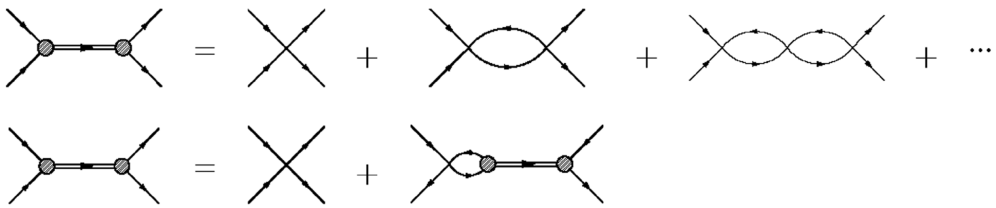

Fig. 1 The set of diagram with four-quarks interaction vertex can be represented by pure four-quarks vertex and sum of diagram that will be associated with meson exchange

Details about the vertex of interaction of mesons with quarks, meson propagator, etc. can be found in Refs. [4, 6-7].

1.3 Interaction with external photons

The next step for description LbL processes is to introduce in the nonlocal chiral Lagrangian(Eq. (1)) the gauge-invariant interaction with an external photon field $A_\mu(z)$ by Schwinger factor(Eq. (9)). In the result we obtain infinite series of vertexes quark – antiquark interactions with photons.

$$q(y) \to Q(x,y) = p\exp\{i\int_x^y dz^\mu A_\mu(z)\}q(y) \quad (9)$$

The scheme, based on the rules that the derivative of the contour integral does not depend on the path shape

$$\frac{\partial}{\partial y^\mu}\int_x^y dz^\nu F_\nu(z) = F_\mu(z),\ \delta^{(4)}(x-y)\int_x^y dz^\nu F_\nu(z) = 0,$$

was suggested in Ref. [8] and applied to nonlocal models in Ref. [9]. The actual form of the vertexes shown in Fig. 2 can be found in Ref. [10].

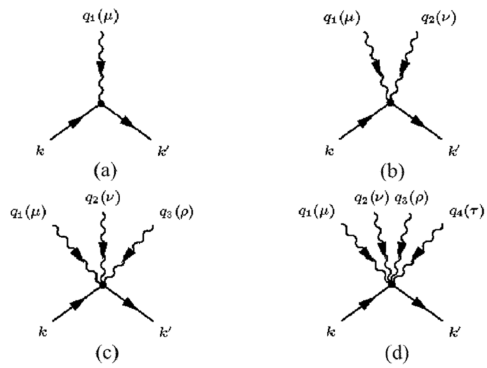

Fig. 2 The quark-photon vertex $\Gamma_\mu^{(1)}(q)$, $\Gamma_{\mu\nu}^{(2)}(q_1, q_2)$, $\Gamma_{\mu\nu\rho}^{(3)}(q_1, q_2, q_3)$, $\Gamma_{\mu\nu\rho\tau}^{(4)}(q_1, q_2, q_3, q_4)$

1.4 Box diagram

In effective quark model under consideration there are two different parts which correspond to contact contribution or contribution with the intermediate meson.

Using quark-antiquark interactions vertexes with one, two, three or four photons, see Fig. 3 (The numbers in front of the diagrams are the combinatoric factors), we can build five types of diagrams.

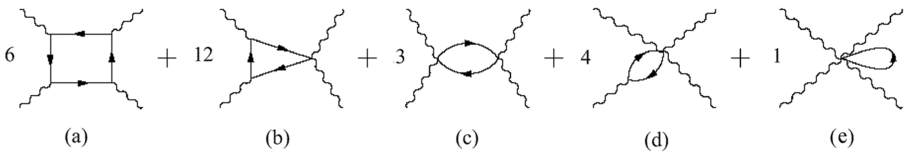

Fig. 3　The box diagram and the diagrams with nonlocal multiphoton interaction vertices that give the contributions to $\prod_{\mu\nu\lambda\rho}(q_1, q_2, q_3)$

The contribution of the box diagram with the local vertices, Fig. 3(a), is the dot (olive) line(Loc); the box diagram, Fig. 3(a), with the nonlocal parts of the vertices is the dash line(NL_1); the triangle, Fig. 3(b), and loop, Fig. 3(c), diagrams with the two-photon vertices is the dash-dot line(NL_2); the loop with the three-photon vertex, Fig. 3(d), is the dot-dot line(NL_3); the loop with the four-photon vertex, Fig. 3(e), is the dash-dot-dot line(NL_4); the sum of all contributions (Total) is the solid line. At zero all contributions are finite. Only the sum of all diagrams is gauge invariant and corresponds to contact (or quark loop) contribution.

2 LbL in AMM of muon

The contribution of light by light process to AMM of muon has the form:

$$a_\mu^{\mathrm{LbL}} = \frac{e^6}{48m_\mu}\int\frac{\mathrm{d}^4q_1}{(2\pi)^4}\int\frac{\mathrm{d}^4q_2}{(2\pi)^4}\times \frac{\prod_{\rho\mu\nu\lambda\sigma}(q_2, -q_3, q_1)T^{\rho\mu\nu\lambda\sigma}(q_1, q_2, p)}{q_1^2q_2^2q_3^2((p+q_1)^2-m_\mu^2)((p+q_2)^2-m_\mu^2)} \tag{10}$$

where the tensor $T^{\rho\mu\nu\lambda\sigma}$ is the Dirac trace

$$T^{\rho\mu\nu\lambda\sigma}(q_1, q_2, p) = \mathrm{Tr}((\hat{p}+m_\mu[\gamma^\rho,\gamma^\sigma](\hat{p}+m_\mu)\times \gamma^\mu(\hat{p}-\hat{q}_2+m_\mu)\gamma^\nu(\hat{p}+\hat{q}_1+m_\mu)\gamma^\lambda).$$

Taking the Dirac trace, the tensor $T^{\rho\mu\nu\lambda\sigma}$ becomes a polynomial in the momenta p, q_1, q_2.

After that, it is convenient to convert all momenta into the Euclidean space, and we will use the capital letters P, Q_1, Q_2 for the corresponding counterparts of the Minkowskian vectors p, q_1, q_2, e. g. $P^2 = -p^2 = -m_\mu^2$, $Q_1^2 = -q_1^2$, $Q_2^2 = -q_2^2$. Then Eq. (10) becomes

$$\left.\begin{aligned} a_\mu^{\mathrm{LbL}} &= \frac{e^6}{48m_\mu}\int\frac{\mathrm{d}_E^4Q_2}{(2\pi)^4}\int\frac{\mathrm{d}_E^4Q_2}{(2\pi)^4}\frac{1}{Q_1^2Q_2^2Q_3^2}\frac{T^{\rho\mu\nu\lambda\sigma}\prod_{\rho\mu\nu\lambda\sigma}}{D_1D_2}\\ D_1 &= (P+Q_1)^2 = m_\mu^2 = 2(P\cdot Q_1)+Q_1^2,\ x\\ D_2 &= (P-Q_2)^2 = m_\mu^2 = 2(P\cdot Q_2)+Q_2^2 \end{aligned}\right\} \tag{11}$$

Since the highest order of the power of the muon momentum P in $T^{\rho\mu\nu\lambda\sigma}$ is two * and $\prod_{\rho\mu\nu\lambda\sigma}$ is independent of P, the factors in the integrand of Eq. (11) can be rewritten as

$$\frac{T^{\rho\mu\nu\lambda\sigma}\prod_{\rho\mu\nu\lambda\sigma}}{D_1D_2} = \sum_{a=1}^{6}A_a\widetilde{\prod}_a \tag{12}$$

with the coefficients

$$\left.\begin{aligned} A_1 &= \frac{1}{D_1},\ A_2 = \frac{1}{D_2},\ A_3 = \frac{(P\cdot Q_2)}{D_1}\\ A_4 &= \frac{(P\cdot Q_2)}{D_2},\ A_5 = \frac{1}{D_1D_2},\ A_6 = 1 \end{aligned}\right\} \tag{13}$$

where all P-dependence is included in the A_a factors, while $\widetilde{\prod}_a$ are P-independent.

Then, one can average over the direction of the muon momentum P (as was suggested in Ref. [11] for the pion-exchange contribution)

$$\int\frac{\mathrm{d}_E^4Q_1}{(2\pi)^4}\int\frac{\mathrm{d}_E^4Q_2}{(2\pi)^4}\frac{A_a}{Q_1^2Q_2^2Q_3^2}\cdots = \frac{1}{2\pi^2}\int_0^\infty\mathrm{d}Q_1\int_0^\infty\mathrm{d}Q_2\int_{-1}^{1}\mathrm{d}t\ \sqrt{1-t^2}\,\frac{Q_1Q_2}{Q_3}\langle A_a\rangle\cdots \tag{14}$$

where the radial variables of integration $Q_1 \equiv |Q_1|$ and $Q_2 \equiv |Q_2|$ and the angular variable $t = (Q_1\cdot Q_2)/(|Q_1|\,|Q_2|)$ are introduced. The averaged A_a factors

was introduced in Ref. [11].

3 Density function

For investigation of the dependence of contribution from photon legs virtuality one can watch for "density function". This is the function which corresponds to the LbL contribution to AMM before integration over intermediate photons virtualities.

$$\rho^{\mathrm{LbL}}(Q_1,Q_2)=\frac{Q_1Q_2}{2\pi^2}\sum_{a=1}^{6}\int_{-1}^{1}\mathrm{d}t\,\frac{\sqrt{1-t^2}}{Q_3^2}\langle A_a\rangle\widetilde{\Pi}_a \quad (15)$$

The volume under 3D-density function is full contribution to AMM of muon. In Fig. 4, this function is shown for the nonlocal model in leading $1/N_c$ order.

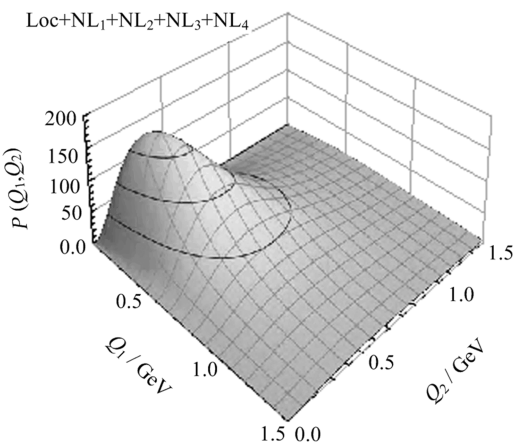

Fig. 4 The 3D density $\rho(Q_1,Q_2)$ defined in Eq. (15)

One can see that contribution is mainly localized in a range of virtualities of photons around 1 GeV, as shown in Fig. 5. Different curves correspond to the contributions of topologically different sets of diagrams drawn in Fig. 3.

In Fig. 5, the slice of $\rho^{\mathrm{HLbL}}(Q_1,Q_2)$ in the diagonal direction $Q_2=Q_1$ is presented together with the partial contributions from the diagrams of different topology. One can see, that the $\rho^{\mathrm{HLbL}}(0,0)=0$ is due to a nontrivial cancellation of different diagrams of Fig. 3. This important result is a consequence of gauge invariance and the spontaneous violation of the chiral symmetry, and represents the low energy theorem analogous to the theorem for the Adler function at zero momentum. Another interesting feature is that the large Q_1, Q_2 behavior is dominated by the box diagram with

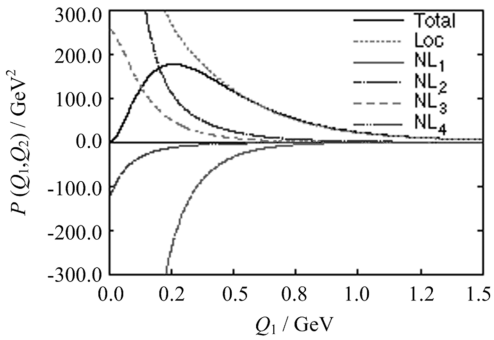

Fig. 5 The 2D slice of the density $\rho(Q_1,Q_2)$ at $Q_2=Q_1$

local vertices and quark propagators with momentum-independent masses in accordance with the perturbative theory. All these are very important characteristics of the NχQM, interpolating the well-known results of the chiral perturbative theory at low momenta and the operator product expansion at large momenta. Earlier, similar results were btained for the two-point [12] and three-point[13] correlators.

4 Conclusion

The contribution to AMM of muon from LbL process in NχQM corresponds to contributions from contact term and term with intermediate pseudoscalar and scalar channels. The contact term contribution is

$$a_\mu^{\mathrm{HLbL,Loop}}=(11.0\pm0.9)\cdot10^{-10} \quad (16)$$

and the total contribution is estimated as

$$a_\mu^{\mathrm{HLbL}}=16.8(1.25)\cdot10^{-10} \quad (17)$$

where the error bar is the band in the region of physical dynamical mass.

In Fig. 6, one can see that it is important, at least in the framework of quark model, to take into account not only diagrams with intermediate mesons but also the contact term (or quark loop) contribution. The solid curve is total contribution, the others dashed curves: contact terms in Fig. 3 and meson exchange Refs. [6-7], respectively.

In comparison with other model calculations, our results are quite close to the recent results obtained in Refs. [14-15]. The specific feature of our model and Dyson-Schwinger approach[14] is that due to nonlocal interaction kernel the quarks become dynamical ones

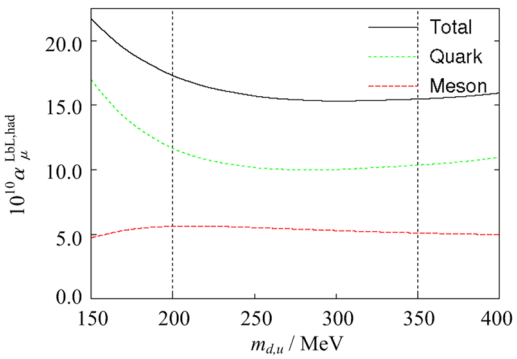

Fig. 6　The contribution of muon AMM from LbL depending on the dynamical mass of quark $m_{d,u}$ in zero order on $1/N_c$

with momentum-dependent mass. The predictions of the NχQM for the different contributions to the muon $g-2$ are in agreement with Ref. [14] within 10%.

The next step of calculations is to extend the quark model in order to estimate subleading in $1/N_c$ terms. This subleading contribution from diagrams with the meson loop has a negative sign[16].

To solve the puzzle of LbL contribution, we should to better understand the physics of strong interaction at a long distance. In principle one can do this with more accurate measurement of meson form factors.

References

[1] BENNETT G W, BOUSQUET B, BROWN H N, et al. Final report of the E821 muon anomalous magnetic moment measurement at BNL[J]. Physical Review D, 2006, 73(7): 072003(1-41).

[2] VENANZONI G. Latest on the muon $(g-2)$ from experiment[J]. Physics, 2012, 349: arXiv:1203.1501.

[3] SAITON. A novel precision measurement of muon $(g-2)$ and EDM at J-PARC[C]// Proceedings of American Institute Physics Conference. Kyoto, Japan: AIP Publishing, 2012, 1467: 45-56.

[4] SCARPETTINI A, GÓMEZ D, SCOCCOLA N N. Light pseudoscalar mesons in a nonlocal SU(3) chiral quark model[J]. Physical Review D, 2004, 69: 114018 (1-14).

[5] ANIKIN I V, DOROKHOV A E, TOMIO L. Pion structure in the instanton liquid model[J]. Physics of Particles and Nuclear, 2000, 31 (5): 509-537.

[6] DOROKHOV A E, RADZHABOV A E, ZHEVLAKOV A S. The pseudoscalar hadronic channel contribution of the light-by-light process to the muon $(g-2)$ μ within the nonlocal chiral quark model [J]. European Physical Journal C, 2011, 71(7): 1702 -1713.

[7] DOROKHOV A E, RADZHABOV A E, ZHEVLAKOV A S. The light-by-light contribution to the muon $(g-2)$ from lightest pseudoscalar and scalar mesons within nonlocal chiral quark model [J]. European Physical Journal C, 2012, 72(11): 2227 (1-12).

[8] MANDELSTAM S. An extension of the Regge formula [J]. Annals of Physics. 1962, 19(2): 254-261.

[9] TERNING J. Gauging nonlocal Lagrangians[J]. Physical Review D, 1991, 44(3): 887-897.

[10] DOROKHOV V, VANDERHAEGHEN M. Anomalous magnetic moment of the muon in a dispersive approach [J]. European Physical Journal C, 2015, 75 (9): 417 (1-11).

[11] JEGERLEHNERF, NYFFELER A. The muon $g-2$[J]. Physics Reports, 2009, (1-3): 477(1-131).

[12] DOROKHOV A E. Adler function and hadronic contribution to the muon $g-2$ in a nonlocal chiral quark model[J]. Physical Review D, 2004, 70(9): 094011 (1-21).

[13] DOROKHOV A E. VAṼ correlator within the instanton vacuum model[J]. European Physical Journal C, 2005, 42(3): 309(1-16).

[14] GOECKE T, FISCHER C S, WILLIAMS R. Erratum: Hadronic light-by-light scattering in the muon $g-2$: A Dyson-Schwinger equation approach[J]. Physical Review D, 2011, 83: 094006 (1-2).

[15] GREYNAT D, DE RAFAEL E. Hadronic contributions to the muon anomaly in the constituent chiral quark model [J]. Journal of High Energy Physics, 2012, (7): 020 (1-33).

[16] KINOSHITA T, N Ⅱ Ć B, OKAMOTO Y. Hadronic contributions to the anomalous magnetic moment of the muon [J]. Physical Review D, 1985, 31 (8): 2108-2119.

Article ID:0253-2778(2016)06-0462-08

η transition form factor: A combined analysis of space- and time-like experimental data through rational approximants

ESCRIBANO R.[1,2]

(1. *Departament de Física, Universitat Autònoma de Barcelona, Grup de Física Teòrica E*-08193 *Bellaterra, Spain*;
2. *Institut de Física d'Altes Energies, The Barcelona Institute of Science and Technology, Campus UAB, E*-08193 *Bellaterra, Spain*)

Abstract: A combined analysis of the space- and time-like experimental data for the η transition form factor is performed in a model-independent way by means of rational approximants. The recent measurement of the e^+e^- invariant mass spectrum of the $\eta \to e^+e^-\gamma$ decay provided by the A2 Collaboration allowed us to extract the most precise and up-to-date slope and curvature parameters of the form factor. The impact of this new analysis on the η-η' mixing parameters and the $VP\gamma$ couplings is also discussed.

Key words: η transition form factor; space- and time-like data analysis; rational approximants; slope and curvature parameters; η-η' mixing; $V \to P\gamma$ radiative decays

CLC number: O572.3 **Document code**: A doi:10.3969/j.issn.0253-2778.2016.06.003

Citation: Escribano R. η transition form factor: A combined analysis of space- and time-like experimental data through rational approximants[J]. Journal of University of Science and Technology of China, 2016,46(6):462-469.
Escribano R. η 跃迁形状因子:合理近似的类时和类空实验数据的综合分析[J]. 中国科学技术大学学报,2016,46(6): 462-469.

η 跃迁形状因子:合理近似的类时和类空实验数据的综合分析

ESCRIBANO R.[1,2]

(1. 巴塞罗那自治大学,E-08193,西班牙;2. 巴塞罗那科学与技术研究所,E-08193,西班牙)

摘要:通过合理的近似,用类时和类空实验数据对 η 的跃迁形状因子进行了模型无关的综合分析. 最近 A2 合作组提供的衰变道不变质量谱的测量使我们能够提取最新、最精确的形状因子斜率和曲率参数, 并讨论了新分析对混合参数的影响和 $VP\gamma$ 耦合.

关键词:η 跃迁形状因子; 类时和类空数据分析;合理近似; 斜率和曲率参数; 合 辐射衰变

0 Introduction

The pseudoscalar transition form factors (TFFs) describe the effect of the strong interaction on the $\gamma^*\gamma^*P$ vertex, where $P = \pi^0, \eta, \eta', \eta_c \cdots$, and is represented by $F_{P\gamma^*\gamma^*}(q_1^2, q_2^2)$, a function of the

Received:2015-11-30;**Revised**:2016-04-20

Foundation item: Supported in part by the the Ministerio de Ciencia e Innovación (FPA2011-25948), the Ministerio de Economía y Competitividad (CICYT-FEDER-FPA 2014-55613-P, SEV-2012-0234), the Secretaria d´Universitats i Recerca del Departament d'Economia i Coneixement de la Generalitat de Catalunya(2014 SGR 1450), the Spanish Consolider-Ingenio 2010 Programme CPAN(CSD2007-00042).

Biography: Escribano R(corresponding author), Professor/PhD. Research field: high energy physics. E-mail: rafel.escribano@ifae.es

photon virtualities q_1^2, and q_2^2. From the experimental point of view, one can study such TFFs from both space- and time-like energy regions. The time-like region of the TFF can be accessed at meson facilities either through the double Dalitz decay processes $P\to l^+l^-l^+l^-$, which give access to both photon virtualities (q_1^2, q_2^2) in the range $4m_l^2 < (q_1^2, q_2^2) < (m_P - 2m_l)^2$, or the single Dalitz decay processes $P\to l^+l^-\gamma$, which contains a single virtual photon with transferred momentum in the range $4m_l^2 < q_1^2 < m_P^2$, thus simplifying the TFF to $F_{P\gamma^*\gamma^*}(q_1^2, 0) \equiv F_{P\gamma^*\gamma^*}(q^2)$. To complete the time-like region, e^+e^- colliders access to the values $q^2 > m_P^2$ through the $e^+e^-\to P\gamma$ annihilation processes. The space-like region of the TFFs are accessed in e^+e^- colliders by the two-photon-fusion reaction $e^+e^-\to e^+e^-P$, where at the moment the measurement of both virtualities is still an experimental challenge. The common practice is then to extract the TFF when one of the outgoing leptons is tagged and the other is not, that is, the single-tag method. The tagged lepton emits a highly off-shell photon with transferred momentum $q_1^2 \equiv -Q^2$ and is detected, while the other, untagged, is scattered at a small angle with $q^2 \simeq 0$. The form factor extracted from the single-tag experiment is then $F_{P\gamma^*\gamma^*}(-Q^2, 0) \equiv F_{P\gamma^*\gamma}(Q^2)$.

At low-momentum transfer, the TFF can be described by the expansion

$$F_{P\gamma^*\gamma}(Q^2) = F_{P\gamma\gamma}(0)\left(1 - b_P\frac{Q^2}{m_P^2} + c_P\frac{Q^4}{m_P^4} + \cdots\right) \quad (1)$$

where $F_{P\gamma\gamma}(0)$ is the normalization, the low-energy parameters (LEPs) b_P and c_P are the slope and the curvature of the TFF, respectively, and m_P is the pseudoscalar meson mass. $F_{P\gamma\gamma}(0)$ can be obtained either from the measured two-photon partial width of the meson P or, in the case of π^0, η and η', from the prediction of the axial anomaly in the chiral limit of QCD.

The slope parameter has been extensively discussed from both theoretical analyses[1-5] and experimental measurements[6-12]. With respect to the experimental determinations, the values for the slope are usually obtained after a fit to data using a normalized, single-pole term with an associated mass Λ_P, i. e.

$$F_{P\gamma^*\gamma}(Q^2) = \frac{F_{P\gamma\gamma}(0)}{1 + Q^2/\Lambda_P^2} \quad (2)$$

The A2 Collaboration reported $b_\eta = 0.59(5)$ [12], the most precise experimental determination up to date. The curvature was for the first time reported in Ref. [3] with the value $c_\eta = 0.37(10)_{\text{stat}}(7)_{\text{sys}}$.

Several attempts to describe the η TFF are available in the literature at present[2, 4-5, 13-27] but none of them tries for a unique description of both space- and time-like experimental data, specially at low energies. In Ref. [28], it was suggested for the π^0 case that a model-independent approach to the space-like TFF can be achieved using a sequence of rational functions, the Padé approximants (PAs), to fit the data. Later on, in Ref. [3], the same method was applied to the η and η' TFFs. More recently, the A2 Collaboration reported a new measurement of the $\eta\to e^+e^-\gamma$ Dalitz decay process with the best statistical accuracy up to date[12]. A comparison with different theoretical approaches was also performed. In particular, the results from Ref. [3], based on space-like data, were extrapolated to the time-like region and agreed perfectly with their measurement. Triggered by these new A2 results, we explore in the present work a combined description of both space- and time-like regions of the η TFF within our method of rational approximants. This will provide, for the first time, a determination of the energy dependence of the η TFF in both regions together with a unified extraction of its LEPs.

Our approach makes use of PAs as fitting functions to all the experimental data. PAs are rational functions $P_M^N(Q^2)$ (ratio of a polynomial $T_N(Q^2)$ of order N and a polynomial $R_M(Q^2)$ of order M) constructed in such a way that they have the same Taylor expansion as the function to be approximated up to order $\mathcal{O}(Q^2)^{N+M+1}$ [29]. Since PAs are built in our case from the unknown low-energy parameters (LEPs) of the TFF, once the fit to the experimental data is done, the reexpansion of the PAs yields the desired

coefficients. The advantage of PAs over Taylor expansions is their ability to enlarge the domain of convergence. However, to prove the convergence of a given PA sequence is a difficult task and only for certain classes of functions can this be done rigorously. In practice, the success of PAs in the description of experimental data can only be seen a posteriori in the sense that the pattern of convergence can be shown but unfortunately not proven mathematically. We refer the interested reader to Refs. [30-31] for details on this technique.

1 η transition form factor: a space- and time-like description

To extract the η TFF low-energy parameters b_η and c_η (slope and curvature, respectively) from the available data, we start with a $P_1^L(Q^2)$ sequence. However, according to Ref. [32], the pseudoscalar TFFs behave as $1/Q^2$ for $Q^2 \to \infty$, which means that, for any value of L, one will obtain in principle a good fit only up to a finite value of Q^2 but not for $Q^2 \to \infty$. Therefore, it would be desirable to incorporate this asymptotic-limit information in the fits to $Q^2 F_{\eta\gamma^*\gamma}(Q^2)$ by considering also a $P_N^N(Q^2)$ sequence.

Experimental data from the space-like region is obtained from CELLO, CLEO, and BABAR Collaborations[7-8, 33], together with the time-like experimental data from NA60 and A2 Collaborations[9-10, 12]. We also include the value $\Gamma_{\eta\to\gamma\gamma} = 0.516(18)$ keV[34] (which is basically dominated by the recent KLOE-2 measurement[35]) in our fits.

We start fitting with a $P_1^L(Q^2)$ sequence. We reach $L = 7$, shown in Fig. 1 as a green-dashed line. The smaller plot in Fig. 1 is a zoom into the time-like region. The obtained LEPs are shown in Fig. 2 together with our previous results (empty orange) when only space-like data were included in our fits[3]. The stability observed for the LEPs with the $P_1^L(Q^2)$ sequence is remarkable, and the impact of the inclusion of time-like data is clear since it not only allows us to reach higher precision on each PA but also to enlarge our PA sequence by 2 elements. The stability of the result is also clearer and reached earlier, reduces our systematic error, and shows the ability of our method to extract, for the first time, the LEPs from a combined fit to all the available data.

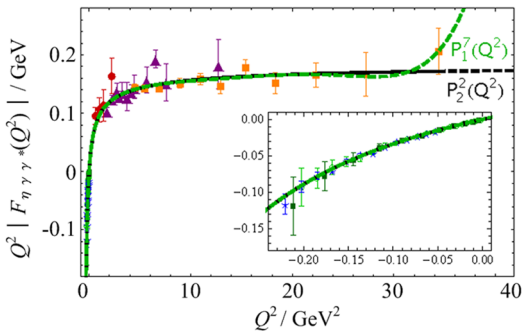

Fig. 1 η-TFF best fits

In Fig. 1, The gray-dashed line shows our best $P_1^L(Q^2)$ fit and the black line our best $P_N^N(Q^2)$ fit. Experimental data points in the space-like region are from CELLO (circles)[7], CLEO (triangles)[8], and BABAR (squares)[33] Collaborations. Experimental data points in the time-like region are from NA60 (stars)[9], A2 2011 (dark squares)[10], and A2 2013 (empty circles)[12]. The inner plot shows a zoom into the time-like region.

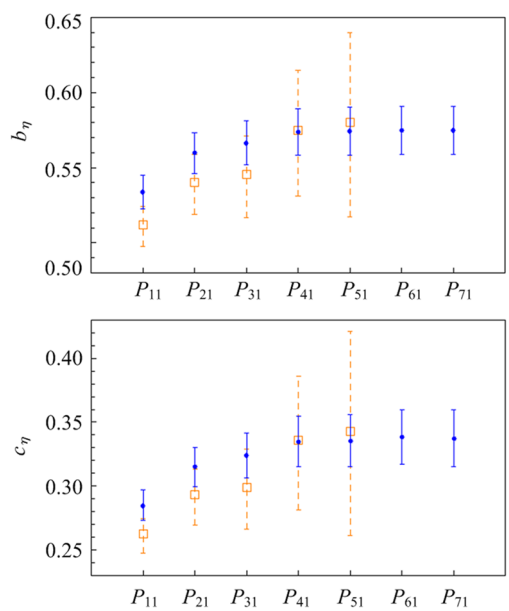

Fig. 2 Slope and curvature predictions for the η TFF using the $P_1^L(Q^2)$ up to $L = 7$ (solid line)

Previous results considering only space-like data

from Ref. [3] are also shown (empty squares) as a way to stress the role of the time-like data in our fits. Only statistical errors are shown.

To reproduce the asymptotic behavior of the TFF, we have also considered the $P_N^N(Q^2)$ sequence. The results obtained are in very nice agreement with our previous determinations. The best fit is shown by the black-solid line in Fig. 1. We reach $N=2$. Since these approximants contain the correct high-energy behavior built-in, they can be extrapolated up to infinity (black-dashed line in Fig. 1) and then predict the leading $1/Q^2$ coefficient:

$$\lim_{Q^2\to\infty} Q^2 F_{\eta\gamma^*\gamma}(Q^2) = 0.177^{+0.020}_{-0.009}\ \text{GeV} \qquad (3)$$

This prediction, although larger than in our previous work[3], still cannot be satisfactorily compared with the BABAR time-like measurement at $q^2 = 112\ \text{GeV}^2$, $F_{\eta\gamma^*\gamma}(112\ GeV^2) = 0.229(30)(8)\ \text{GeV}$[36]. The impact of such discrepancy in the η-η' mixing is discussed in the next section.

Our combined weighted average results, taking into account both types of PA sequences, give

$$\left.\begin{aligned} b_\eta &= 0.576(11)_{\text{stat}}(4)_{\text{sys}} \\ c_\eta &= 0.339(15)_{\text{stat}}(5)_{\text{sys}} \end{aligned}\right\} \qquad (4)$$

where the second error is systematic (around 0.7 and 1.5% for b_P and c_P, respectively.

Eq. (4) can be compared with $b_\eta = 0.60(6)_{\text{stat}}(3)_{\text{sys}}$ and $c_\eta = 0.37(10)_{\text{stat}}(7)_{\text{sys}}$ using space-like data exclusively[3]. As expected, not only statistical results have been improved but also systematics, both by an order of magnitude, yielding the most precise slope determination ever.

Our slope is compared with experimental determinations from Refs. [6-12] together with theoretical extraction from Refs. [1-5, 37-38] in Fig. 3.

One should notice that all the previous collaborations used a VMD model fit to extract the slope. In order to be consistent when compared with our results, a systematic error of about 40% should be added to the experimental determinations based on space-like data[3, 28], and a systematic error of about 5% should be added to the experimental determinations based on time-like data.

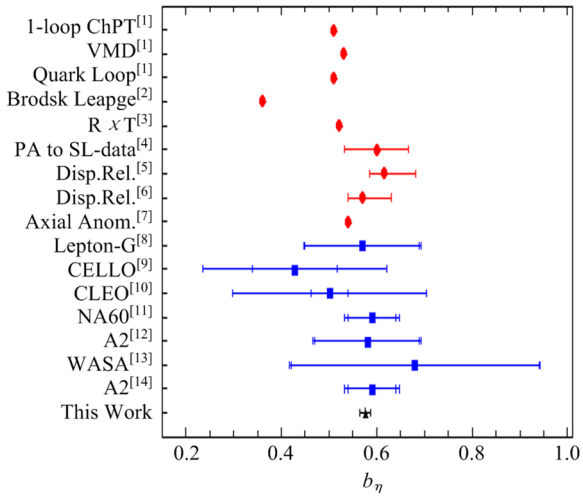

Fig. 3　Slope determinations for η TFF

When comparing different theoretical extractions of the slope of the η TFF with our result in Fig. 3, we find a pretty good agreement with the exception of the results in Ref. [2] that reported $b_\eta = 0.546(9)$ and $b_\eta = 0.521(2)$ using Resonance Chiral theory with one- or two-octet ansätze. The disagreement is between 2 and 5 standard deviations. Ref. [2] uses Resonance Chiral theory, which is based in large-N_c arguments, to extract LEPs. Going from large-N_c to $N_c = 3$ imposes a systematic error[31, 39-40]. Since Ref. [2] considered two approximations for fitting the η TFF (with one and two octets), one could consider the difference between them as a way to estimate such error[3, 42]. In such a way, the η TFF slope would read $b_\eta = 0.53(1)$, at 2.5 standard deviation from our result.

Eventually, we want to comment on the effective single-pole mass determination Λ_P from Eq. (2). Using $b_P = m_P^2/\Lambda_P^2$ and the values in Eq. (4), we obtain $\Lambda_\eta = 0.722(7)\ \text{GeV}$ or $\Lambda_\eta^{-2} = 1.919(39)\ \text{GeV}^{-2}$.

The fits shown in Fig. 1 use the experimental value of the two - photon decay width as an experimental datum to be fitted. Such fit could be repeated without including that decay. In such a way, we reach again a $P_1^7(Q^2)$ and a $P_2^2(Q^2)$ as our best PA with the advantage now that the value $F_{\eta\gamma\gamma}(0)$ is a prediction of our fits. We find $F_{\eta\gamma\gamma}(0)|_{\text{fit}} = 0.250$

(38) GeV^{-1} for the $P_1^7(Q^2)$ and $F_{\eta\gamma\gamma}(0)|_{\rm fit}=0.248$ (28) GeV^{-1} for the $P_2^2(Q^2)$, which translates into $\Gamma_{\eta\gamma\gamma}|_{\rm fit}=0.43(13)$ keV and $\Gamma_{\eta\gamma\gamma}|_{\rm fit}=0.42(10)$ keV, respectively. Compared with the experimental value $\Gamma_{\eta\gamma\gamma}|_{\rm exp}=0.516(18)$ keV such predictions are at 0.66 and 0.94 standard deviation each.

2 Reanalysis of η-η' mixing parameters

In this section we briefly summarize the main elements to extract the mixing parameters exclusively from our fits to the form factor data. As was done in Ref. [3], we analyze η-η' mixing using the quark-flavor basis. In this basis, the η and η' decay constants are parametrized as

$$\begin{pmatrix} F_\eta^q & F_\eta^s \\ F_{\eta'}^q & F_{\eta'}^s \end{pmatrix} = \begin{pmatrix} F_q\cos\phi_q & -F_s\sin\phi_s \\ F_q\sin\phi_q & F_s\cos\phi_s \end{pmatrix} \tag{5}$$

where $F_{q,s}$ are the light-quark and strange pseudoscalar decay constants, respectively, and $\phi_{q,s}$ the related mixing angles. Several phenomenological analyses find $\phi_q\simeq\phi_s$, which is also supported by large-N_c ChPT calculations where the difference between these two angles is seen to be proportional to an OZI-rule violating parameter and hence small[43-44].

Within this approximation, the asymptotic limits of the TFFs take the form

$$\left.\begin{aligned} \lim_{Q^2\to\infty} Q^2F_{\eta\gamma^*\gamma}(Q^2) &= 2(\hat{c}_qF_\eta^q+\hat{c}_sF_\eta^s) = \\ & 2(\hat{c}_qF_q\cos\phi-\hat{c}_sF_s\sin\phi) \\ \lim_{Q^2\to\infty} Q^2F_{\eta'\gamma^*\gamma}(Q^2) &= 2(\hat{c}_qF_{\eta'}^q+\hat{c}_sF_{\eta'}^s) = \\ & 2(\hat{c}_qF_q\sin\phi+\hat{c}_sF_s\cos\phi) \end{aligned}\right\} \tag{6}$$

and their normalization at zero

$$\left.\begin{aligned} F_{\eta\gamma\gamma}(0) &= \frac{1}{4\pi^2}\left(\frac{\hat{c}_qF_{\eta'}^s-\hat{c}_sF_{\eta'}^q}{F_{\eta'}^sF_\eta^q-F_{\eta'}^qF_\eta^s}\right) = \\ & \frac{1}{4\pi^2}\left(\frac{\hat{c}_q}{F_q}\cos\phi-\frac{\hat{c}_s}{F_s}\sin\phi\right) \\ F_{\eta'\gamma\gamma}(0) &= \frac{1}{4\pi^2}\left(\frac{\hat{c}_qF_\eta^s-\hat{c}_sF_\eta^q}{F_\eta^qF_{\eta'}^s-F_\eta^sF_{\eta'}^q}\right) = \\ & \frac{1}{4\pi^2}\left(\frac{\hat{c}_q}{F_q}\sin\phi+\frac{\hat{c}_s}{F_s}\cos\phi\right) \end{aligned}\right\} \tag{7}$$

with $\hat{c}_q=5/3$ and $\hat{c}_s=\sqrt{2}/3$.

Experimental information provides $|F_{\eta\gamma\gamma}(0)|_{\rm exp}=0.274$ (5) GeV^{-1} and $|F_{\eta'\gamma\gamma}(0)|_{\rm exp}=0.344$ (6) GeV^{-1} and for the asymptotic value of the η TFF we take the value shown in Eq. (3) with symmetrical errors, $\lim_{Q^2\to\infty} Q^2F_{\eta\gamma^*\gamma}(Q^2)=0.177$ (15) GeV. With these values, the mixing parameters are predicted to be

$$\left.\begin{aligned} F_q/F_\pi &= 1.07(1),\ F_s/F_\pi = 1.39(14) \\ \phi &= 39.3(1.2)^\circ \end{aligned}\right\} \tag{8}$$

with $F_\pi=92.21(14)$ MeV[34]. The uncertainties are dominated by the error from the asymptotic value prediction.

The mixing parameters obtained with our fits are precise enough to be competitive with the standard approaches with the advantage of using much less input information.

3 A prediction for the $VP\gamma$ couplings

In this section, we extend our analysis to the vector-pseudoscalar electromagnetic form factors. In particular, we are interested in the couplings of the radiative decays of lowest-lying vector mesons into η or η', i.e., $V\to(\eta,\eta')\gamma$, and of the radiative decays $\eta'\to V\gamma$, with $V=\rho,\ \omega,\ \phi$.

We follow closely the method presented in Refs. [44-45], and make use of the equations in Appendix A in Ref. [44] to relate the form factors with the mixing angle and the decay constants in the flavor basis. To account for the $\pi-\omega$ mixing we use $\phi_V=3.4^\circ$. The form factors, saturated with the lowest-lying resonance and then assuming vector meson dominance, can be expressed by

$$F_{VP\gamma}(0,0) = \frac{f_V}{m_V}g_{VP\gamma} \tag{9}$$

where $g_{VP\gamma}$ are the couplings we are interested in, and f_V are the leptonic decay constants of the vector mesons and are determined from the experimental decay rates via

$$\Gamma(V\to e^+e^-) = \frac{4\pi}{3}\alpha^2\frac{f_V^2}{m_V}c_V^2 \tag{10}$$

with c_V is an electric charge factor of the quarks that make up the vector, $c_V=(\frac{1}{\sqrt{2}},\frac{\sin\theta_V}{\sqrt{6}},\frac{\cos\theta_V}{\sqrt{6}})$ for $V=\rho,\ \omega,\ \phi$ respectively. Here $\theta_V=\phi_V+\arctan(1/\sqrt{2})$.

Experimentally we find

$$\left.\begin{aligned} f_{\rho^0} &= (221.2 \pm 0.9)\ \text{MeV} \\ f_{\omega} &= (179.9 \pm 3.1)\ \text{MeV} \\ f_{\phi} &= (239.0 \pm 3.8)\ \text{MeV} \end{aligned}\right\} \quad (11)$$

using $\Gamma(\rho \to e^+e^-) = 7.04(6)$ keV, $\Gamma(\omega \to e^+e^-) = 0.60(2)$ keV, and $\Gamma(\phi \to e^+e^-) = 1.27(4)$ keV from Ref. [34].

The couplings in this flavor basis are:

$$\left.\begin{aligned} g_{\rho\eta\gamma} &= \frac{3m_\rho}{4\pi^2 f_{\rho^0}} \frac{\cos\phi}{\sqrt{2}F_q},\ g_{\rho\eta'\gamma} = \frac{3m_\rho}{4\pi^2 f_{\rho^0}} \frac{\sin\phi}{\sqrt{2}F_q} \\ g_{\omega\eta\gamma} &= \frac{m_\omega}{4\pi^2 f_\omega}\left(\cos\phi_V \frac{\cos\phi}{\sqrt{2}F_q} - 2\sin\phi_V \frac{\sin\phi}{\sqrt{2}F_s}\right) \\ g_{\omega\eta'\gamma} &= \frac{m_\omega}{4\pi^2 f_\omega}\left(\cos\phi_V \frac{\sin\phi}{\sqrt{2}F_q} + 2\sin\phi_V \frac{\cos\phi}{\sqrt{2}F_s}\right) \\ g_{\phi\eta\gamma} &= \frac{m_\phi}{4\pi^2 f_\phi}\left(\sin\phi_V \frac{\cos\phi}{\sqrt{2}F_q} + 2\cos\phi_V \frac{\sinsφ}{\sqrt{2}F_s}\right) \\ g_{\phi\eta'\gamma} &= \frac{m_\phi}{4\pi^2 f_\phi}\left(\sin\phi_V \frac{\sin\phi}{\sqrt{2}F_q} - 2\cos\phi_V \frac{\cos\phi}{\sqrt{2}F_s}\right) \end{aligned}\right\} \quad (12)$$

where we have assumed $\phi_q = \phi_s = \phi$. Tab. 1 collects our predictions in its second column. Corrections due to $\phi_q \neq \phi_s$ to these formulae can be found in Appendix A, Eq. (A.5) of Ref. [44].

Tab. 1　Summary of $VP\gamma$ couplings

parameter	prediction	experoment
$g_{\rho\eta\gamma}$	1.50(4)	1.58(5)
$g_{\rho\eta'\gamma}$	1.18(5)	1.32(3)
$g_{\omega\eta\gamma}$	0.57(2)	0.45(2)
$g_{\omega\eta'\gamma}$	0.55(2)	0.43(2)
$g_{\phi\eta\gamma}$	−0.83(11)	−0.69(1)
$g_{\phi\eta'\gamma}$	0.98(14)	0.72(1)
$R_{J/\Psi} = \frac{\Gamma(J/\Psi \to \eta'\gamma)}{\Gamma(J/\Psi \to \eta\gamma)}$	4.74(55)	4.67(20)

The decay widths of $P \to V\gamma$ and $V \to P\gamma$ are

$$\left.\begin{aligned} \Gamma(P \to V\gamma) &= \frac{\alpha}{8} g^2_{VP\gamma}\left(\frac{m_P^2 - m_V^2}{m_P}\right) \\ \Gamma(V \to P\gamma) &= \frac{\alpha}{24} g^2_{VP\gamma}\left(\frac{m_V^2 - m_P^2}{m_V}\right) \end{aligned}\right\} \quad (13)$$

The experimental decay widths from Ref. [34] allow us to extract an experimental value for $g_{VP\gamma}$, which are collected in the last column in Tab. 1, experimental determinations are from Ref. [34].

Our predictions compare well with the experimental determinations, see Tab. 1, specially considering the simplicity of the approach. The differences are always below 2 standard deviations, excepting the ω couplings. Our prediction for the ratio of J/Ψ decays is in that respect remarkable.

4　Conclusion

In the present work, the η transition form factor has been analyzed for the first time in both space- and time-like regions at low and intermediate energies, making use of a model-independent approach based on the use of rational approximants of Padé type. The model independence of our approach is achieved trough a detailed and conservative evaluation of the systematic error associated with it. The new set of experimental data on the $\eta \to e^+e^-\gamma$ reaction provided by the A2 Collaboration in the very low-energy part of the time-like region allows for a much better determination of the slope and curvature parameters of the form factor, as compared to the predictions obtained in our previous work only using space-like data, which constitute the most precise values up-to-date of these low-energy parameters. Our method is also able to predict for the first time the third derivative of the form factor. In addition, the new analysis has served to further constrain its values at zero momentum transfer and infinity. We have seen that our results, in particular for the case of the slope parameter, are quite insensitive to the values used in the fits for the two-photon decay width of the η, thus showing that the collection of space- and time-like experimental data is more than enough to fix a value for the normalization of the form factor compatible with current measurements. We have also seen that the role played by the high-energy space-like data is crucial to getting accurate predictions for the low-energy parameters of the form factor and its asymptotic value. As a consequence of these new results, we have fully reanalyzed the η-η' mixing parameters this time also considering renormalisation-scale dependent effects of the singlet decay constant F_0. The new values obtained are

already competitive with standard results with the advantage of requiring much less input information. Related to this, we have also obtained predictions for the $VP\gamma$ couplings which are in the ballpark of present-day determinations.

In summary, the method of Padé approximants has been shown to be very powerful for fixing the low-energy properties of the η transition form factor, making their predictions more accurate and well-established. This fact opens the door to a more exhaustive analysis of the single Dalitz decay processes $P\to l^+ l^- \gamma$, with $P=\pi^0$, η, η' and $l=e$, μ, the double Dalitz ones $P\to l^+ l^- l^+ l^-$ (in all possible kinematically allowed configurations)[46], and the rare lepton-pair decays $P\to l^+ l^-$ (see the $\pi^0\to e^+ e^-$ application in Ref. [47]), which are usually discussed only in terms of monopole approximations. Indeed, when this work was being concluded the BES Ⅲ Collaboration reported a first observation of the $\eta'\to ze^+e^-\gamma$ process measuring the branching ratio and extracting the η' transition form factor[48]. This new measurement may put our approach with its back to the wall. However, a very preliminary analysis of this recent data in comparison with our prediction for this form factor in the time-like region exhibits a nice agreement but reveals the necessity of going beyond the vector meson dominance model used in the experimental analysis[49].

References

[1] AMETLLER L, BIJNENS J, BRAMON A, et al. Transition form factors in π^0, η, and η' couplings to $\gamma\gamma^*$ [J]. Physical Review D, 1992, 45(3): 986-989.

[2] CZYŽH, IVASHYN S, KORCHIN A, et al. Two-photon form factors of the π^0, η, and η' mesons in the chiral theory with resonances[J]. Physical Review D, 2012, 85(9): 094010(1-11).

[3] ESCRIBANOR, MASJUAN P, SANCHEZ-PUERTAS P. η, and η' transition form factors from rational approximants[J]. Physical Review D, 2014, 89(3): 034014(1-15).

[4] HANHART C, KUPSC A, MEISSNER U G, ET AL. Dispersive analysis for $\eta\to\gamma\gamma^*$ [J]. European Physical Journal C, 2013, 73(12): 2668(1-11).

[5] KLOPOT Y, OGANESIAN A, TERYAEV O. Axial anomaly and vector meson dominance model[J]. JETP Letters, 2014, 99(12): 679-684.

[6] DJHELYADINR I, GOLOVKIN S V, KACHANOV V A, et al. Investigation of the electromagnetic structure of the η meson in the decay $\eta\to\mu^+\mu^-\gamma$[J]. Physics Letters B, 1980, 94(4): 548-550.

[7] BEHREND H J, CRIEGEE L, FIELD J H, et al. A measurement of the π^0, η, and η' electromagnetic form factors[J]. Zeitschrift Für Physik C, 1991, 49(3): 401-409.

[8] GRONBERG J, HILL T S, KUTSCHKE R, et al. Measurements of the meson-photon transition form factors of light pseudoscalar mesons at large momentum transfer [J]. Physical Review D, 1998, 57(1): 33-54.

[9] ARNALDI R, BANICZ K, CASTON J, et al. Study of the electromagnetic transition form-factors in $\mu^+\mu^-\gamma$ and $\omega\to\mu^+\mu^-\pi^0$ decays with NA60[J]. Physics Letters B, 2009, 677(5): 260-266.

[10] BERGHÄUSER H, METAG V, STAROSTIN A, et al. Determination of the η-transition form factor in the $\gamma p\to p\eta\to p\gamma e^+e^-$ reaction[J]. Physics Letters B, 2011, 701(5): 562-567.

[11] HODANAM, MOSKAL P. Study of the $\eta\to e^+e^-\gamma$ decay using WASA-at-COSY detector system[C]// EPJ Web Conference. EDP Sciences, 2012, 37: 09017.

[12] AGUAR-BARTOLOMÉP, ANNAND P, ARENDS J R M, et al. New determination of the η transition form factor in the Dalitz decay $\eta\to e^+e^-\gamma$ with the Crystal Ball/TAPS detectors at the Mainz Microtron[J]. Physical Review C, 2014, 89(4): 044608.

[13] KROLL P. The form factors for the photon to pseudoscalar meson transitions - an update[J]. European Physics Journal C, 2011, 71: 1623(1-33).

[14] DOROKHOV A E, RADZHABOV A E, ZHEVLAKOV A S. The pseudoscalar hadronic channel contribution of the light-by-light process to the muon $(g-2)$ μ within the nonlocal chiral quark model [J]. European Physics Journal C, 2011, 71(7): 1702(1-12).

[15] BRODSKY S J, CAO F G, DE TERAMOND G F. Evolved QCD predictions for the meson-photon transition form factors[J]. Physical Review D, 2011, 84(3): 033001(1-34).

[16] BRODSKY S J, CAO F G, DE TERAMOND G F. Meson transition form factors in light-front holographic QCD[J]. Physical Review D, 2011, 84(7): 2437-2452.

[17] KLOPOTY N, OGANESIAN A G, TERYAEV O V. Axial anomaly and mixing: from real to highly virtual photons [J]. Physical Review D, 2011, 84(5): 412-419.

[18] WU X G, HUANG T. Constraints on the light pseudoscalar meson distribution amplitudes from their meson-photon transition form factors[J]. Physical Review D, 2011, 84(7): 443-444.

[19] NOGUERA S, SCOPETTA S. The eta-photon transition

form factor[J]. Physical Review D, 2012, 85: 054004.

[20] BALAKIREVA I, LUCHA W, MELIKHOV D. Pion elastic and $(\pi 0, \eta, \eta') \to \gamma\gamma^*$ transition form factors in a broad range of momentum transfers [J]. Physical Review D, 2012, 85(2012) 036006(1-7).

[21] MELIKHOV D, STECH B. On the $\gamma^* \gamma \to \pi(\eta, \eta')$ transition form factors [J]. Physical Review D, 2012, (5): 051901(1-4).

[22] KROLL P, PASSEK-KUMERICKI K. The $\eta(\eta')$ gamma transition form factor and the gluon-gluon distribution amplitude [J]. Journal of Physics G, 2012, 40(7): 75005-75021.

[23] MELIKHOV D, STECH B. Universal behavior of the $\gamma^* \gamma \to (\pi^0, \eta, \eta')$ transition form factors [J]. Physics Letters B, 2012, 718(2): 488-491.

[24] GENG C Q, Lih C C. Erratum: Pseudoscalar transition form factors within the light-front quark model [J]. Physical Review C, 2013, 87(3): 039901.

[25] KLOPOT Y, OGANESIAN A, TERYAEV O. Transition form factors and mixing of pseudoscalar mesons from anomaly sum rule [J]. Physical Review D, 2013, 87: 036013.

[26] BIJNENS J, BRAMON A, CORNET F. Pseudoscalar decays into two photons in chiral perturbation theory[J]. Physical Review Letters, 1988, 61(113): 1453-1456.

[27] BIJNENS J, BRAMON A, CORNET F. Chiral perturbation theory for anomalous processes [J]. Zeitschrift Für Physik C, 1990, 46(4): 599-607.

[28] MASJUAN P. $\gamma^* \gamma \to \pi^0$ transition form factor at low-energies from a model-independent approach [J]. Physical Review D, 2012, 86: 094021(1-9).

[29] BAKERG A, GRAVES-MORRIS P. Padé Approximants, Encyclopedia of Mathematics and its Applications [M]. Cambridge University Press, 1996.

[30] MASJUAN P, PERIS S, SANZ-CILLERO J J. Vector meson dominance as a first step in a systematic approximation: The pion vector form factor[J]. Physical Review D, 2008, 78(7): 074028(1-12).

[31] MASJUAN P. Rational approximations in quantum chromodynamics [J]. Eprint Arxiv, 2010: arXiv: 1005.5683.

[32] LEPAGE G P, Brodsky S J. Exclusive processes in quantum chromodynamics: Evolution equations for hadronic wavefunctions and the form factors of mesons [J]. Physical Review D, 1980, 22: 2157.

[33] DEL AMO SANCHEZ P, LEES J P, POIREAU V, et al. Measurement of the $\gamma\gamma^* \to \eta$ and $\gamma\gamma^* \to \eta'$ transition form factors [J]. Physical Review D, 2011, 84(38): 1821-1824.

[34] OLIVE K A, AGASHE A, AMSLER C, et al. Review of particle physics [J]. Chinese Physics C, 2014, 38: 090001.

[35] BABUSCI D, BADONI D, BALWIERZ-PYTKO I, et al. Measurement of η meson production in $\gamma\gamma$ interactions and $\Gamma(\eta \to \gamma\gamma)$ with the KLOE detector[J]. Journal of High Energy Physics, 2013, 119(1): 1301(1-23).

[36] AUBERT B, BARATE M, BONA D, et al. Measurement of the η and η' transition form factors at $q^2 = 112$ GeV^2 [J]. Physical Review D, 2006, 74(1): 012002(1-14).

[37] BRODSKY S J, LEPAGE G P. Large-angle two-photon exclusive channels in quantum chromodynamics [J]. Physical Review D, 1981, 24(7): 1808-1817.

[38] KUBIS B, PLENTER J. Anomalous decay and scattering processes of the eta meson[J]. European Physical Journal C, 2015, 75(6): 1-12.

[39] MASJUAN P, PERIS S. A rational approach to resonance saturation in large-N_c QCD [J]. Journal of High Energy Physics, 2007, (5): 1285-1291.

[40] MASJUAN P, PERIS S. A rational approximation to $<VV-AA>$ and its $\mathcal{O}(p^6)$ low-energy constant [J]. Physics Letters B, 2008, 663(1): 61-65.

[41] MASJUAN P, ARRIOLA E R, BRONIOWSKI W. Meson dominance of hadron form factors and large-N_c phenomenology[J]. Physical Review D, 2013, 87(1): 014005(1-16).

[42] MASJUAN P, VANDERHAEGHEN M. Ballpark prediction for the hadronic light-by-light contribution to the muon $(g-2)_\mu$ [J]. Journal of Physics G, 2015, 42(12): 10-12.

[43] FELDMANN T, KROLL P, STECH B. Mixing and decay constants of pseudoscalar mesons [J]. Physical Review D, 1998, 58(11): 398-399.

[44] ESCRIBANOR, FRÈRE J M. Study of the η-η' system in the two mixing angle scheme[J]. Journal of High Energy Physics, 2005, (6): arXiv:hep-ph/0501072.

[45] BALL P, FRÈRE J M, TYTGAT M. Phenomenological evidence for the gluon content of η and η' [J]. Physics Letters B, 1996, 365(1-4): 367376.

[46] ESCRIBANO R, GONZÀLEZ-SOLÍSR S. A data-driven model-independent approach to π^0, η and η' single and double Dalitz decays[J]. 2015: arXiv:1511.04916.

[47] MASJUAN P, SANCHEZ-PUERTAS P. Phenomenology of bivariate approximants: The $\pi^0 \to e^+ e^-$ case and its impact on the electron and muon g-2 [J]. Blood, 2015, 98(10): 3169-3171.

[48] ABLIKIM M, ACHASOV M N, AI X C, et al. Observation of the Dalitz decay $\eta' \to \gamma e^+ e^-$ [J]. Physical Review D, 2015, 92: 012001(1-11).

[49] ESCRIBANO R, GONZÀLEZ-SOÍLSR S, MASJUAN P, et al. The η' transition form factor from space- and time-like experimental data [J]. European Physical Journal C, 2015, 75(9): 1-16.

Article ID:0253-2778(2016)06-0470-06

$\sin^2\theta_W$ theory and new physics

LEE Hye-Sung

(*Center for Theoretical Physics of the Universe*, *IBS*, *Daejeon* 34051, *Korea*)

Abstract: After briefly discussing the importance of the precise measurement of the weak mixing angle, the implication of the dark Z on the low-Q^2 parity tests is discussed. The dark Z is a very light (roughly, MeV-GeV scale) gauge boson, which couples to the electromagnetic current as well as the weak neutral current.

Key words: parity test; dark force; dark photon; dark Z

CLC number: O572.3 **Document code**: A doi:10.3969/j.issn.0253-2778.2016.06.004

Citation: LEE H S. $\sin^2\theta_W$ theory and new physics[J]. Journal of University of Science and Technology of China, 2016, 46(6): 470-475.

LEE H S. $\sin^2\theta_W$ 理论与新物理[J]. 中国科学技术大学学报,2016,46(6): 470-475.

$\sin^2\theta_W$ 理论与新物理

LEE Hye-Sung

(理论物理中心, 大田市 34051,韩国)

摘要:简要介绍弱混合角的精确测量的重要意义后,讨论了在低能区宇称检验中的暗Z粒子的意义. 暗Z粒子是一种非常轻(大致在 MeV 到 GeV 的尺度)的规范玻色子,能够在耦合电磁流的同时耦合弱中性流.

关键词:宇称检验; 暗作用力; 暗光子; 暗Z粒子

0 Introduction

In this article, we emphasize the importance of the low-Q^2 parity test for the new physics searches. We illustrate our point with a specific example called the dark parity violation[1-4], which means the parity violation induced by a dark gauge boson. This presentation shares some parts with Ref. [5], although updates and complementary descriptions are provided.

Let us briefly look back on the history of the $\sin^2\theta_W$ physics. It is well documented in the review[6], and we will go over only some part of it very briefly. In 1961, Glashow introduced the $SU(2)_L \times U(1)_L$ symmetry, which has a mixing between two neutral gauge bosons[7]. In 1967, Weinberg added the Higgs mechanism with a Higgs doublet and a vacuum expectation value, establishing the mass relation $m_W = m_Z\cos\theta_W$ with the weak mixing angle θ_W[8]. He also predicted the weak neutral current mediated by the Z boson. In 1973, the neutral current was discovered in the neutrino scattering experiments at the CERN Gargamelle detector[9]. Whether the $SU(2)_L \times U(1)_Y$ is a correct theory to describe this neutral current was not clear then though. One of the features of the

Received: 2015-11-30; **Revised**: 2016-04-20

Foundation item: Supported in part by the IBS(IBS-R018-D1).

Biography: LEE Hye-Sung(corresponding author), Professor/PhD. Research field: high energy physics. E-mail: hlee@ibs.re.kr

$SU(2)_L \times U(1)_Y$ was the mixing term in the weak neutral current interaction, proportional to $\sin^2\theta_W$, and the parity test measuring this $\sin^2\theta_W$ can possibly test the standard model(SM).

In 1978, SLAC E122 experiment using the polarized electron beam and the deuteron target measured the parity violation asymmetry, which gave $\sin^2\theta_W \approx 0.22(2)$, agreeing to the SM[10]. It is noticeable that this establishment of the $SU(2)_L \times U(1)_Y$ by the SLAC parity test in 1978 occurred much earlier than the direct discovery of the W/Z boson resonances at the CERN SPS experiments in 1983[11-12]. In 1979, after only one year of the SLAC parity test, Glashow, Salam, and Weinberg received the Nobel prize in physics.

The lessons we can learn from this history include: ① the parity test(by the precise measurement of $\sin^2\theta_W$) can be a critical way to search for a new gauge interaction; ② its finding may precede the direct discovery of a gauge boson by the bump search.

Fig. 1 taken from Ref. [4] shows the running of the $\sin^2\theta_W$ in the SM and the current experimental constraints. While the current data are more or less consistent with the SM prediction with the given error bars, more precise measurements in the future experiments (red bars) may reveal potential new physics effects that were elusive for the current constraints.

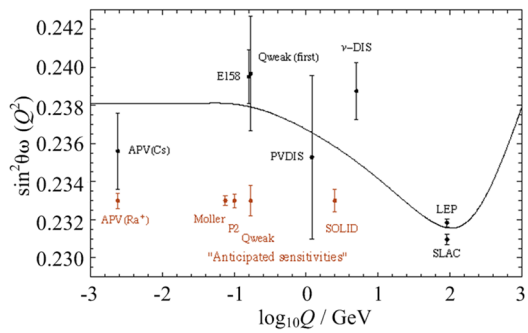

Fig. 1 The running of the $\sin^2\theta_W$

In Fig. 1, the running of the $\sin^2\theta_W$ with the momentum transfer Q in the SM and the current experimental constraints taken from Ref. [4]. The red bars show the anticipated sensitivities in the future parity tests.

1 Dark Photon vs. Dark Z

The dark gauge boson (we use Z' for its notation) is a hypothetical particle with a very small mass and a small coupling to the SM particles. While the heavy Z' (typically TeV scale) has been a traditional target of discovery [13], the light Z' (typically MeV-GeV scale) is a recently highlighted subject with a growing interest[14]. For such a light particle to survive all experimental constraints, it should have extremely small couplings to the SM particles.

There are number of dark force models in the literature, but we consider only two of them. Both models commonly assume the kinetic mixing between the $U(1)_Y$ and the $U(1)_{\text{dark}}$[15]. The SM particles have zero charges under the new gauge group $U(1)_{\text{dark}}$, yet the gauge boson Z' of the $U(1)_{\text{dark}}$ can still couple to the SM fermions through the mixing with the SM gauge bosons.

One model is the dark photon[16], which couples only to the electromagnetic current at the leading order. Another is a relatively new model, the dark Z [1], which couples to the electromagnetic current as well as the weak neutral current. Their interactions are given by

$$\mathscr{L}_{\text{dark }\gamma} = -\varepsilon e J^{\mu}_{EM} Z'_{\mu} \quad (1)$$

$$\mathscr{L}_{\text{dark }Z} = -[\varepsilon e J^{\mu}_{EM} + \varepsilon_Z (g/2\cos\theta_W) J^{\mu}_{NC}] Z'_{\mu} \quad (2)$$

with $J^{\text{EM}}_{\mu} = Q_f \bar{f}\gamma_\mu f$ and $J^{\text{NC}}_{\mu} = (T_{3f} - 2Q_f \sin^2\theta_W)\bar{f}\cdot\gamma_\mu f - (T_{3f})\bar{f}\gamma_\mu\gamma_5 f$. ε and ε_Z are the parametrization of the effective γ-Z' mixing and Z-Z' mixing, respectively.

The difference of the two models comes from how the Z' gets a mass or the details of the Higgs sector. Because of the Z coupling, the Z' in the dark Z model inherits some properties of the Z boson such as the parity violating nature. In a rough sense, the dark photon is a heavier version of the photon, and the dark Z is a lighter version of the Z boson.

Because of the new coupling, some experiments that are irrelevant to the dark photon searches are relevant to the dark Z searches[1-4, 17-20]. They include

the low $-Q^2$ parity test, which will be discussed later in this article.

2 Bump hunt

There are many ongoing and proposed searches for the dark force in the labs around the world[14]. A particularly attractive feature about the dark force is that it is one of the rare new physics scenarios that can be tested/discovered at the low-energy experiments, which are typically built for nuclear or hadronic physics. Of course, it is possible because the dark force carrier Z' is very light (MeV-GeV scale).

Fig. 2 in Ref. [21] shows the parameter space of the dark photon with the current bounds. The bounds come from the electron[22-23] and muon[24-26] anomalous magnetic moments, fixed target experiments[27-28], beam dump experiments[29], meson decays[30-35], and e^+e^- collision ($e^+e^-\to\gamma+l^+l^-$) experiments[36-37]. Except for the anomalous magnetic moments, the searches are all based on the dilepton searches from the Z', that is the bump hunt.

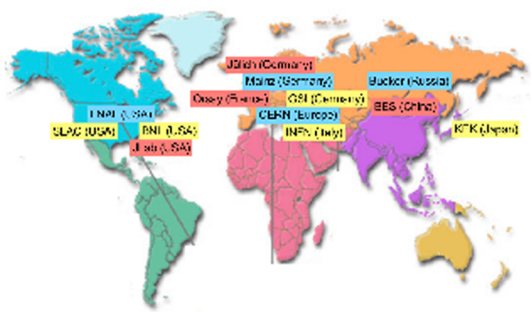

Fig. 2 Dark force searches all around the world

If we put some of these experimental efforts on the map (Fig. 2), we can see the search is practically a global activity. Quite obviously, we are going through a very exciting time with so many contemporary searches to find a new fundamental force of nature.

3 Low-energy parity test

Now, we discuss the low-energy parity test[1-4] as another means to search for the dark force. The presence of the dark Z modifies the effective lagrangian of the weak neutral current scattering,

$$\mathscr{L}_{\text{eff}} = -\frac{4G_F}{\sqrt{2}} J^{\mu}_{\text{NC}}(\sin^2\theta_W) J^{\text{NC}}_{\mu}(\sin^2\theta_W) \tag{3}$$

$$G_F \to \left(1+\delta^2\frac{1}{1+Q^2/m_{Z'}^2}\right)G_F \tag{4}$$

$$\sin^2\theta_W \to \left(1-\varepsilon\delta\frac{m_Z}{m_{Z'}}\frac{\cos\theta_W}{\sin\theta_W}\frac{1}{1+Q^2/m_{Z'}^2}\right)\sin^2\theta_W \tag{5}$$

where Q is the momentum transfer between the two neutral currents, and δ is a reparametrization of the ε_Z with $\varepsilon_Z = (m_{Z'}/m_Z)\delta$. One salient feature is that these shifts are sensitive only to the low-Q^2 (low momentum transfer). Thus, the dark Z effectively changes the weak neutral current scattering, including the effective $\sin^2\theta_W$, which describes the parity violation, but only for the low momentum transfer.

Fig. 3 (from Ref. [3] with a slight modification) shows an example of how the effective $\sin^2\theta_W$ changes with Q in the presence of a dark Z for $m_{Z'}=100$ Mev, 200 Mev cases. Although there are some details in the figure, the important point is that the deviations appear only in the low Q values, roughly $Q \leqslant m_{Z'}$. They never appear in the high Q values relevant to the high-energy experiments, which tells us that we need low-energy experiments to see the dark Z mediated scattering effects.

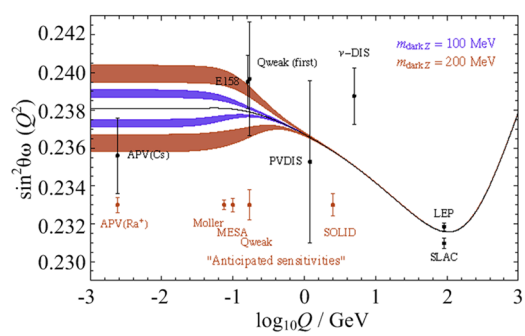

Fig. 3 Effective $\sin^2\theta_W$ running taken from Ref. [3]

In Fig. 3, dark Z of 100 MeV and 200 MeV were taken. Note that the deviations appear only in the low-Q^2 regime ($Q^2 \leqslant m_{Z'}^2$).

In this region, non-perturbative QCD contributions to the SM value become important. They have traditionally been determined utilizing dispersion relations[38-39]. Recently, first-principle lattice QCD

determinations of the leading-order hadronic effects have also become available[40-41].

For the low-Q^2 parity tests, one can use the atomic parity violation in Cs[42-44], Ra^+ ion[45-46] or the low-Q^2 polarized electron scattering experiments SLAC E158[47], JLAB Qweak[48], JLAB Møller[49] and Mainz P2 [50]. The possible deviations due to the dark Z can be large enough to be observed with the future experiments.

For the intermediate scale Z' of $m_{Z'} \approx \mathcal{O}(10)$ Gev, the deep inelastic scattering experiments such as JLAB PVDIS[51] and JLAB SOLID[52] may also be sensitive. In fact, as Fig. 4 (The NuTeV anomaly can be addressed by this intermediate scale dark Z) taken from Ref. [4] shows, the intermediate scale Z' can address the NuTeV ($< Q > \approx 5$ Gev) anomaly[53].

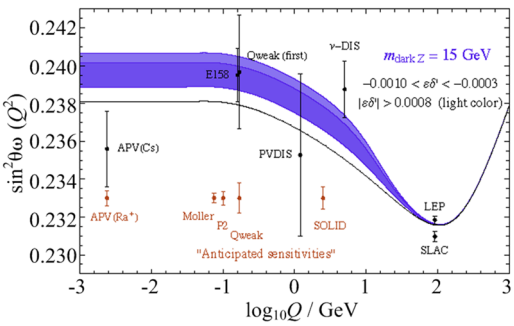

Fig. 4 The 15 GeV dark Z case taken from Ref. [4]

4 Conclusion

The parity test by precise measurement of the $\sin^2\theta_W$ has been important in studying new gauge interactions. Especially, it critically helped establishing the $SU(2)_L \times U(1)_Y$ electroweak theory. There is a growing interest in the dark gauge interaction (mediated by a light Z' gauge boson) around the world partly because many existing low-energy facilities can join the searches. While most searches of the light Z' are based on the direct bump searches, the parity tests in the low-Q^2 (such as the atomic parity violation, polarized electron scattering, deep inelastic scattering) are important and complementary searches for the dark force. The latter are also independent of the Z' decay branching ratios.

If the history may repeat, the dark force evidence from the low-Q^2 parity test might precede the discovery of a new resonance just like what happened in the electroweak interaction case.

References

[1] DAVOUDIASL, LEE H S, MARCIANO W J. "Dark" Z implications for parity violation, rare meson decays, and Higgs physics[J]. Physical Review D, 2012, 85(11): 115019(1-13).

[2] DAVOUDIASLH, LEE H S, MARCIANO W J. Muon anomaly and dark parity violation[J]. Physical Review Letters, 2012, 109(3): 031802(1-5).

[3] DAVOUDIASLH, LEE H S, MARCIANO W J. Muon $g-2$, rare kaon decays, and parity violation from dark bosons[J]. Physical Review D, 2014, 89(9)98-105.

[4] DAVOUDIASL H, LEE H S, MARCIANO W J. Low Q^2 weak mixing angle measurements and rare higgs decays [J]. Physical Review D, 2015, 92(5): 055005(1-5).

[5] KLOPOTH S. Parity violation by a dark gauge boson[J]. Eprint Arxiv, 2014: arXiv:1410.8435.

[6] KUMARK S, MANTRY S, MARCIANO W J, et al. Low energy measurements of the weak mixing angle [J]. Annual Review of Nuclear and Particle Science, 2013, 63(6): 237-267.

[7] GLASHOW S L. Partial-symmetries of weak interactions [J]. Nuclear Physics, 1961, 22(4): 579-588.

[8] WEINBERG S. A model of leptons[J]. Physical Review Letters, 1967, 19: 1264-1266.

[9] HASERT F J, KABE S, KRENZ W, et al. Observation of neutrino-like interactions without muon or electron in the Gargamelle neutrino experiment[J]. Physcs Letters B, 1973, 46(1): 138-140.

[10] PRESCOTT C Y, ATWOOD W B, COTTRELL R L A, et al. Parity non-conservation in inelastic electron scattering [J]. Physics Letters B, 1978, 77(3): 347-352.

[11] BANNER M, BATTISTON R, BLOCH P, et al. Observation of single isolated electrons of high transverse momentum in events with missing transverse energy at the CERN $\bar{p}p$ collider[J]. Physics Letters B, 1983, 122(5-6): 476-485.

[12] ARNISON G, ASTBURY A, AUBERT B, et al. Experimental-observation of lepton pairs of invariant mass around 95 GeV/c^2 at the cern sps collider[J]. Physics Letters B, 1983, 126: 398-410.

[13] LANGACKER P. The physics of heavy Z' gauge bosons

[J]. Review of Modern Physics, 2009, 81(3): 1199-1228.

[14] ESSIG R, JAROS J A, WESTER W, et al. Dark sectors and new, light, weakly-coupled particles[J]. Eprint Arxiv, 2013: arXiv:1311.0029.

[15] HOLDOM B. Two $U(1)$'s and ε charge shifts[J]. Physics Letters B, 1986, 166(2): 196-198.

[16] ARKANI-HAMEDN, FINKBEINER D P, SLATYER T R, ET AL. A theory of dark matter[J]. Physical Review D, 2009, 79(1): 015014(1-22).

[17] DAVOUDIASLH, LEE H S, LEWIS I et al. Higgs decays as a window into the dark sector[J]. Physical Review D, 2013, 88(1): 392-426.

[18] DAVOUDIASL H, MARCIANO W J, RAMOS R, et al. Charged higgs discovery in the W plus "Dark" vector boson decay mode[J]. Physics, 2014, 89(1): 1858-1871.

[19] KONG K, LEE H S, PARK M. Dark decay of the top quark[J]. Physical Review D, 2014, 89(7): 539-560.

[20] KIM D, LEE H S, PARK M. Invisible dark gauge boson search in top decays using a kinematic method[J]. Journal of High Energy Physics, 2015, 134(3): 1-2 (arXiv:1411.0668).

[21] SOFFER A. Searches for light scalars, pseudoscalars, and gauge bosons[J]. Physics, 2015: arXiv:1507.02330.

[22] DAVOUDIASL H, LEE H S, MARCIANO W J. Dark side of higgs diphoton decays and muon $g-2$[J]. Physical Review D, 2012, 86(9): 095009(1-7).

[23] ENDO M, HAMAGUCHI K, MISHIMA G. Constraints on hidden photon models from electron $g-2$ and hydrogen spectroscopy[J]. Physical Review D, 2012, 86(9): 579-599.

[24] GNINENKO S N, KRASNIKOV N V. The muon anomalous magnetic moment and a new light gauge boson [J]. Physics Letters B, 2001, 513(1-2): 119-122.

[25] FAYET P. U-boson production in e^+e^- annihilations, ψ and γ decays, and light dark matter[J]. Physical Review D, 2007, 75(11): 115017(1-18).

[26] POSPELOV M. Secluded $U(1)$ below the weak scale[J]. Physical Review D, 2009, 80(9): 281-287.

[27] ABRAHAMYAN S, AHMED Z, ALLADA K, et al. Search for a new gauge boson in electron-nucleus fixed-target scattering by the APEX experiment[J]. Physical Review Letters, 2011, 107(19): 191804(1-5).

[28] MERKEL H, ACHENBACH P, GAYOSO C A, et al. Search for light massive gauge bosons as an explanation of the $(g-2)\mu$ anomaly at MAMI[J]. Physical Review Letters, 2014, 112: 221802(arXiv:1404.5502).

[29] ANDREASS, NIEBUHR C, RINGWALD A. New limits on hidden photons from past electron beam dumps[J]. Physical Review D, 2012, 86(9): 095019(arXiv:1209.6083).

[30] BJORKEN J D, ESSIG R, SCHUSTER P, et al. New fixed-target experiments to search for dark gauge forces [J]. Physical Review D, 2009, 80(7): 264-284.

[31] BABUSCI D, BADONI D, BALWIERZ-PYTKO I, et al. Limit on the production of a light vector gauge boson in phi meson decays with the KLOE detector[J]. Physics Letters B, 2013, 720(1-3): 111-115.

[32] AGAKISHIEV G, BALANDA A, BELYAEV A, et al. Searching a dark photon with HADES[J]. Physics Letters B, 2014, 731(2): 265-271(arXiv:1311.0216).

[33] ADARE A, AFANASIEV S, AIDALA C, et al. Search for dark photons from neutral meson decays in p^+p and d^+Au collisions at $\sqrt{s_{NN}}=200$ GeV[J]. Physical Review C, 2015, 91(3): 031901(arXiv:1409.0851).

[34] GUNJI T. Dark Photon Searches at ALICE[R]. Presented at Dark Interactions 2014 Workshop at Brookhaven National Laboratory, USA.

[35] BATLEY J R, KALMUS G, LAZZERONI C, et al. Search for the dark photon in π^0 decays[J]. Physics Letters B, 2015, 746: 178-185(arXiv:1504.00607).

[36] BABUSCI BALWIERZ-PYTKO I, BENCIVENNI G, et al. Search for light vector boson production in $e^+e^-\to\mu^+\mu^-\gamma$ interactions with the KLOE experiment[J]. Physics Letters B, 2014, 736: 459(arXiv:1404.7772).

[37] LEESJ P, POIREAU V, TISSERAND V, et al. Search for a dark photon in e^+e^- collisions at BABAR[J]. Physical Review Letters, 2014, 113(20): 201801(arXiv:1406.2980).

[38] ERLER J, RAMSEY-MUSOLF M J. Weak mixing angle at low energies[J]. Physical Review D, 2005, 72: 073003 (arXiv:hep-ph/0409169).

[39] JEGERLEHNER F. Electroweak effective couplings for future precision experiments[J]. Eprint Arxiv, 2011, 31: arXiv:1107.4683.

[40] BURGER F, JANSEN K, PETSCHLIES M, et al. Leading hadronic contributions to the running of the electroweak coupling constants from lattice QCD[J]. Journal of High Energy Physics, 2015, 11(11): 1-23(arXiv: 1505.03283).

[41] FRANCIS A, GÜLPERS V, HERDOÍZA G, et al. Study of the hadronic contributions to the running of the QED coupling and the weak mixing angle[J]. Physics, 2015,

110: 101-103(arXiv:1511.04751).

[42]GILBERT S L, NOECKER M C, WATTS R N, et al. Measurement of parity nonconservation in atomic cesium [J]. Physical Review Letters, 1985, 55(24): 2680 (doi.org/10.1103/PhysRevLett.55.2680).

[43]WOOD C S, BENNETT S C, CHO D, et al. Measurement of parity nonconservation and an anapole moment in cesium[J]. Science, 1997, 275(5307): 1759-1763.

[44]BENNETTS C, WIEMAN C E. Erratum: Measurement of the 6s→7s transition polarizability in atomic cesium and an improved test of the standard model [J]. Physical Review Letters, 1999, 82(12): 2484-2487.

[45]PORTELA M N, DIJCK E A, MOHANTY A, et al. Ra^+ ion trapping: Toward an atomic parity violation measurement and an optical clock[J]. Applied Physics B, 2014, 114: 173-182.

[46]JUNGMANN K P. Symmetries and fundamental interactions-selected topics [J]. Hyperfine Interactions, 2014, 227(1): 5-16.

[47]ANTHONY P L, ARNOLD R G, ARROYO C, et al. Precision measurement of the weak mixing angle in Moller scattering[J]. Physical Review Letters, 2005, 95(8): 081601(hep-ex/0504049).

[48]ANDROIC D, ARMSTRONG D S, ASATURYAN A, et al. First determination of the weak charge of the proton [J]. Physical Review Letters, 2013, 111(14): 141803 (arXiv:1307.5275).

[49]MAMMEI J. The MOLLER Experiment [J]. Physics, 2012, 35(4): 203(arXiv:1208.1260).

[50]AULENBACHER K. Opportunities for parity violating electron scattering experiments at the planned MESA facility[J]. Hyperfine Interactions, 2011, 200(1): 3-7.

[51]WANG D, PAN K, SUBEDI R, et al. Measurement of parity violation in electron-quark scattering[J]. Nature, 2014, 506(7486): 67-70.

[52]REIMER P E. Parity violating deep inelastic scattering [J]. Nuovo Cimento C, 2012, 35(4): 209-213.

[53]ZELLER G P, Mcfarland K S, ADAMS T, et al. Precise determination of electroweak parameters in neutrino-nucleon scattering[J]. Physical Review Letters, 2002, 88(9): 386-389.

Article ID:0253-2778(2016)06-0476-05

Perspectives of a precise measurement of the charge asymmetry in muon pair production at BelleⅡ

FERBER T.[1], SHWARTZ B.[2,3](for the Belle/BelleⅡ collaboration)

(1. *Department of Physics and Astronomy, The University of British Columbia, Vancouver, BC*;
2. *Budker Institute of Nuclear Physics, Novosibirsk* 630090, *Russia*; 3. *Novosibirsk State University, Novosibirsk* 630090, *Russia*)

Abstract: Forward-backward asymmetry in the muon pairs production in electron-positron annihilation is caused by the interference of the photon and Z-boson already at leading order. A high precise measurement of the value of this asymmetry, A_{FB}, at the SuperB-factory will provide stringent limitations on the New Physics effects. Even though $A_{FB} \approx 0.01$ at 10 GeV center-of-mass energy of B-factory operation, a huge statistics expected at the BelleⅡ experiment will provide an opportunity to obtain high precision. This report briefly describes perspectives as well as obstacles on the way to achieve the precise results.

Key words: electron-positron collider; muon pair production; forward-backward asymmetry; detector; Monte-Carlo simulation

CLC number: O572.3 **Document code**: A doi:10.3969/j.issn.0253-2778.2016.06.005

Citation: FERBER T, SHWARTZ B, (for the Belle/BelleⅡ collaboration). Perspectives of a precise measurement of the charge asymmetry in muon pair production at BelleⅡ[J]. Journal of University of Science and Technology of China, 2016,46(6): 476-480.
FERBER T, SHWARTZ B,(代表 Belle/BelleⅡ合作组). BelleⅡ上缪子成对产生过程中电荷不对称性精确测量的展望[J]. 中国科学技术大学学报,2016, 46(6): 476-480.

BelleⅡ上缪子成对产生过程中电荷不对称性精确测量的展望

FERBER T.[1], SHWARTZ B.[2,3](代表 Belle/BelleⅡ合作组)

(1. 英属哥伦比亚大学天文物理系, 温哥华,加拿大;
2. 俄罗斯布德克尔核物理研究所, 新西伯利亚 630090, 俄罗斯;
3. 国立新西伯利亚理工大学, 新西伯利亚 630090, 俄罗斯)

摘要:由于光子和 Z 玻色子在领头阶即已存在干涉,导致电子-正电子在淹没产生缪子对的过程中前后不对称. 超级 B 工厂对这个不对称值(A_{FB})的精确测量会严格限制新物理学效应. 即使在 B 工厂运行在 10 GeV 质心能量, 测得 $A_{FB} \approx 0.01$. 我们也期待 BelleⅡ实验巨大统计量的高精度结果. 本文简要描述了研究前景以及要得到精确结果面临的困难.

关键词:正负电子对撞机; 缪子对产生; 前后不对称性; 探测器; 蒙特卡洛模拟

Received:2015-11-30;**Revised**:2016-04-20

Biography:FERBER T, PhD. Research field: electro-positron annihilation into hadrons. E-mail: ferber@physics.ubc.ca
Corresponding author:SHWARTZ B, Professor/PhD. E-mail: shwartz@inp.nsk.su

0 Introduction

The standard model (SM) of the electro-weak interactions was tested in many experiments and no clear discrepancies have found. However, at present an intensive quest for such discrepancies which can indicate a new physics are continuing. One of the SM effects is a forward-backward asymmetry in the process $e^+e^- \to \mu^+\mu^-$ induced by the interference of diagrams with the virtual photon and Z-boson:

$$A_{FB} = \frac{N(\theta^+ > 90°) - N(\theta^+ < 90°)}{N(\theta^+ > 90°) + N(\theta^+ < 90°)} \quad (1)$$

where θ^+ is an angle between positive muon momentum and positron beam direction in the center-of-mass frame and N is a number of events. Experimental measurements of A_{FB} are presented in Fig. 1[1]. The data can be found in the review[2] and references therein. All results are in good agreement with the SM calculation. However, the accuracy of these measurements is not very high and new measurements with a precision of about 1% could be quite useful.

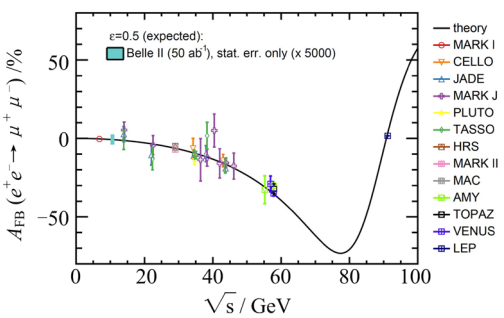

Fig. 1　Measured forward-backward asymmetry

The $\mu^+\mu^-$ production differential cross section is expressed by the formula:

$$\frac{d\sigma}{d\cos\theta^+} = \frac{\pi\alpha^2(s)}{2s}\left[F_1(1+\cos^2\theta^+) + 2F_2\cos\theta^+\right] \quad (2)$$

where $s = 4E_{CM}^2$.

$$\left.\begin{aligned} F_1 &= 1 - 2\chi g_V^2\cos\delta_R + \chi^2(g_V^2+g_A^2) \\ F_2 &= 2\chi g_A^2\cos\delta_R + 4\chi^2 g_V^2 g_A^2 \\ \chi &= \frac{G_F}{2\sqrt{2}\pi\alpha(s)}\frac{sM_Z^2}{\sqrt{(M_Z^2-s)^2+M_Z^2\Gamma_Z^2}} \\ \tan\delta_R &= M_Z\Gamma_Z/(M_Z^2-s) \end{aligned}\right\} \quad (3)$$

where G_F is the Fermi constant and g_V, g_A are the vector and axial coupling constants of the neutral current weak interactions. Then the asymmetry is $A_{FB} = 3F_2/4F_1$. The g_V and g_A constants can be expressed via fundamental parameters of SM as:

$$g_V = \sqrt{\rho_l}(T_{3L}^l - 2Q_l\sin^2\theta_W) \approx \frac{1}{2}2\sin^2\theta_W g_A = \sqrt{\rho_l}T_{3L}^l \approx \frac{1}{2} \quad (4)$$

where $T_{3L}^l = -1/2$ is third component of the charged lepton weak isospin, Q_l is lepton charge and θ_W is the weak mixing angle. Parameter ρ_l is close to 1 and summarises the high-order electro-weak corrections and hypothetical New Physics effects. Since for charged leptons $g_V = (1/2 - 2\sin^2\theta_W) \approx 0$ charge asymmetry contribution, F_2 is practically insensitive to the θ_W. However, a precise A_{FB} measurement can be used to a search of a New Physics.

When $s \ll M_Z^2$ the asymmetry (in the Born leading order) can be written as:

$$A_{FB} = \frac{3F_2}{4F_1} \approx \frac{3}{16\sqrt{2}}\frac{G_F s}{\pi\alpha(s)} \quad (5)$$

For the Belle Ⅱ energy range, $\sqrt{s} \approx 10$ GeV, which results in $A_{FB} \approx -0.008$.

1 Belle Ⅱ experiment

The KEKB B-factory[3], energy-asymmetric collider with the world's highest luminosity, 2×10^{34} $cm^{-2}s^{-1}$, was in operation from 1999 until 2010. Experiments with the Belle detector[4] in the energy range of 10-11 GeV collected an integrated luminosity exceeding 1000 fb^{-1}. This huge data sample provided a number of important results concerning the CP symmetry violation in the quark sector, heavy quarkonium spectroscopy, tau lepton decays and two-photon physics. The total number of $e^+e^- \to \mu^+\mu^-$ events is about 10^9 that can provide a statistical uncertainty of $\sigma A_{FB}/A_{FB} \sim 1\%$. However an achievement of the comparable systematic uncertainties, caused by the apparatus effects as well as background asymmetry, is quite a difficult task.

At present the new SuperKEKB collider and the Belle Ⅱ detector are under construction at KEK[5]. This new experiment will continue and widen that began at the previous experiments. The instantaneous

luminosity of this collider will exceed the previous one by about 40 times, amounting to 8×10^{35} cm^{-2} s^{-1}. However, high luminosity is unavoidably accompanied by high event rate and background. Then the detector should be drastically upgraded. A schematic view of the Belle Ⅱ detector (top half) in comparison to the previous Belle detector (bottom half) is presented in Fig. 2.

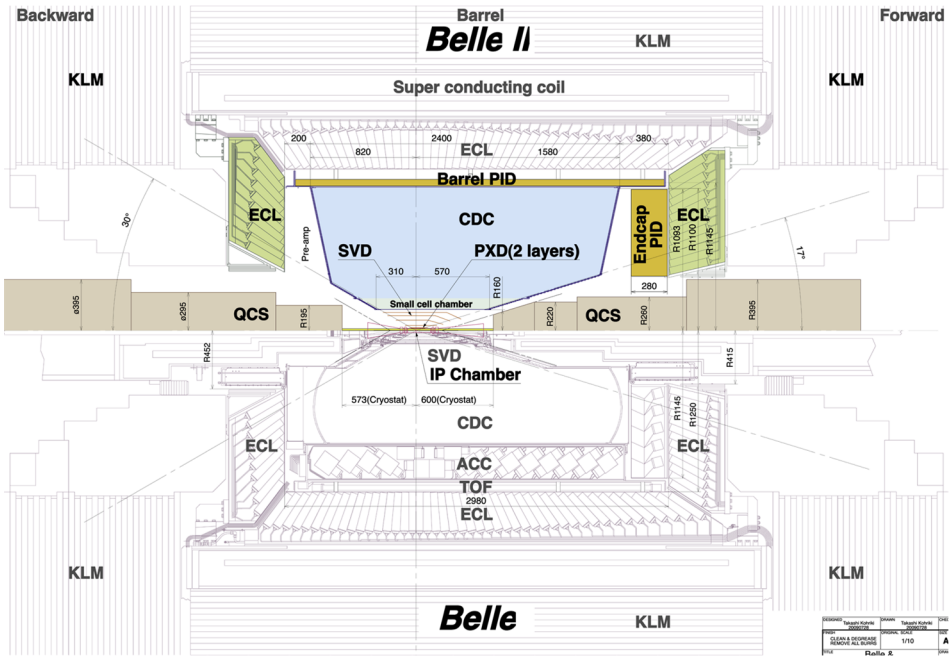

Fig. 2 Schematic view of the Belle Ⅱ detector (top half)

In Fig. 2, schematic view of the Belle Ⅱ detector (top half) in comparison to the previous Belle detector (bottom half). Belle and Belle Ⅱ: SVD -silicon vertex detector, CDC -central drift chamber, ECL -electromagnetic crystal calorimeter, KLM -K-long and muon detector; Belle: ACC -aerogel Cherenkov counters, TOF -time-of-flight system; Belle Ⅱ: PXD -pixel vertex detector, Barrel PID-Cherenkov time-of-propagation counters, Endcap PID-aerogel RICH detector.

The vertex detector, central drift chamber and particle identification system will be replaced completely. The KLM will be partially upgraded. The ECL scintillation crystals and mechanical structure is kept from the previous experiments. However, the calorimeter electronics will be replaced by a more modern one.

Although the SM was confirmed in the previous A_{FB} measurements, achieved accuracies still leave certain room for the New Physics (NP). Thus, a search for NP, i. e. phenomena which are not described by the SM, becomes the most important task for the Belle Ⅱ experiment. With an integrated luminosity of about 50 ab^{-1}, which should be reached with SuperKEKB, statistical uncertainties in the value A_{FB} reduce to 0.1%. High statistics will help to reduce the systematics uncertainties by the detail study of the $\mu^+ \mu^-$ angular distribution, careful study of the background processes and detector asymmetry effects.

To estimate the Belle Ⅱ capability for the discussed asymmetry a MC simulation of the studied process including the weak interaction contribution was done. The Belle software was used in this study. A set of the straight forward selections were applied to the detected events.

(Ⅰ) Number of good tracks: 2.

(Ⅱ) Acollinearity: $\psi_{CM} < 10°$.

(Ⅲ) $E_{CM}/(\sqrt{s}/2) > 0.75$ (for both tracks).

(Ⅳ) $|\cos(\theta^+_{CM})| < 0.75$.

(Ⅴ) Particle identification.

Here ψ_{CM}, E_{CM}, $\cos(\theta^+_{CM})$ are acollinearity, particle energy and positron polar angle respectively.

After these selections the tracking acceptance is about 70% and the detection efficiency after particle identification selection becomes about 45%.

Main background processes and corresponding contaminations to $\mu^+\mu^-$ are $e^+e^-\to e^+e^-\mu^+\mu^-$ ($\sim 1\times10^{-3}$), $e^+e^-\to\tau^+\tau^-\to(\mu^+\bar{\nu}_\tau\nu_\mu)(\mu^-\bar{\nu}_\mu\nu_\tau)$ ($\sim 5\times10^{-4}$) and Bhabha scattering, $e^+e^-\to e^+e^-$, due to electron misidentification ($\lesssim 10^{-4}$). Backgrounds from the cosmic rays as well as from the $e^+e^-\to uu/dd/ss/cc$ and $e^+e^-\to e^+e^-e^+e^-$ are negligible.

The main theoretical uncertainty comes from the higher order contributions: An interference of the initial state and final state radiation (see Fig. 3) as well as two double internal photon lines diagrams (see Fig. 4).

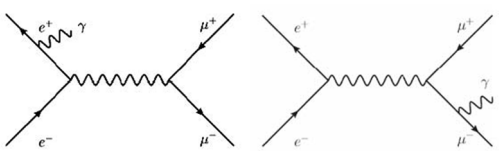

Fig. 3　Feynman diagrams corresponding to the initial and final state radiation

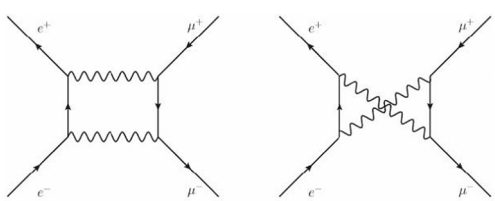

Fig. 4　Box diagrams providing small FB asymmetry

The asymmetry provided by these contributions calculated with the KKMC code is shown in Fig. 5. As seen from the figure the main contribution comes from the interference of the initial and final state radiation diagrams. It decreases with the increase of the acollinearity angle and has the opposite sign in comparison with the electro-weak induced asymmetry.

The value of this QED FB asymmetry is about 10^{-2} at the accolinearity cut of 10° that is approximately the same as that induced by electroweak

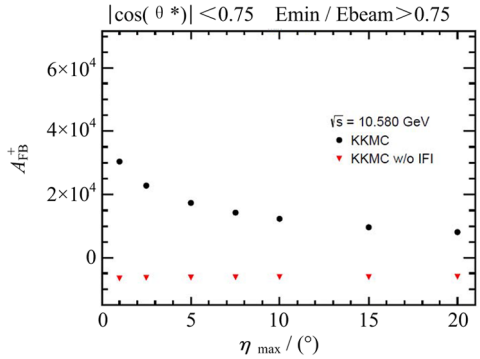

Fig. 5　A_{FB} with and without QED interference contribution

interactions. Then the QED asymmetry should be calculated with high accuracy. One can expect to achieve a required precision in the QED induced A_{FB} taking into account the detector acceptance using. The QED asymmetry can be studied using the existing MC generators KKMC 4.19[6] and PHOKHARA 9.1[7]. Very large experimental statistics which can be collected at SuperKEKB will provide a possibility of a careful checks on both the QED as well as apparatus asymmetries by detailed fits of the angular distributions for the different cuts on acollinearity. The detector induced asymmetry will be revealed by a study of the other QED processes.

Effects of the New Physics can be described by three parameters[8]: S, T and U. A difference between measured and theoretical values of the ρ parameter obtained from low energy asymmetry measurements can be expressed as $\Delta\rho = \alpha(M_Z^2)\,T$ where $\alpha(M_Z^2) = 1/128.945$ is the running electromagnetic coupling constant at Z-boson mass. At the accuracy in $\sigma(A_{FB})/A_{FB}\sim 10^{-3}$ T parameter uncertainty becomes ~ 0.1 which is comparable to the existing accuracy obtained from other experiment. It should be noted that in this case the limits on T are obtained independently of other parameters, S and U.

2　Conclusion

(Ⅰ) Belle Ⅱ provides a unique environment for a

precision electroweak measurement far from the Z pole

(Ⅱ) The $\mu^+\mu^-$ FB asymmetry study is complementary to measurements of the parity violation at low energy.

(Ⅲ) For precise calculations of the high order QED contributions to the FB asymmetry the theoretical input is highly needed.

(Ⅳ) Existing Belle data is used now to study detector related uncertainties as well as to optimize Belle Ⅱ triggers and Belle Ⅱ Monte Carlo simulation.

(Ⅴ) The Belle Ⅱ experiment starts data taking in 2017 and 50 ab^{-1} is expected by the end of 2023.

References

[1] FERBER T. Towards a precision measurement of the muon pair asymmetry in e^+e^- annihilation at Belle and Belle Ⅱ [J]. International Journal of Modern Physics, 2016, 40(1):1660078.

[2] MNICH J. Experimental tests of the standard model in $e^+e^-\to f\bar{f}$ at the Z resonance[J]. Physics Reports, 1996, 271(4):181-266.

[3] KUROKAWA S, KIKUTANI E. Overview of the KEKB accelerators [J]. Nuclear Instruments & Methods in Physics Research A, 2003, 499(1): 1-7.

[4] ABASHIAN A, GOTOW K, MORGAN N, et al. The Belle detector[J]. Nuclear Instruments & Methods in Physics Research A, 2002, 479: 117-232.

[5] ABE T, ADACHI I, ADAMCZYK K, et al. Belle Ⅱ technical design report[R]. KEK Report 2010-1, 2010.

[6] JADACH S, WARD B F L, WAS Z. The precision Monte Carlo event generator *KK* for two-fermion final states in e^+e^- collisions[J]. Computer Physics Communications, 2000, 130(3): 260-325.

[7] CAMPANARIO F, CZYŻ H, GLUZA J, et al. Complete QED NLO contributions to the reaction $e^+e^-\to\mu^+\mu^-\gamma$ and their implementation in the event generator PHOKHARA [J]. Journal of High Energy Physics, 2014, 1402: 114.

[8] ERLER J, FREITAS A. Electroweak model and constraints on new physics[J]. Chinese Physics C, 2014, 2(9):139-160.

Article ID:0253-2778(2016)06-0481-07

Measuring the weak mixing angle with the P2 experiment at MESA

BERGER N.[1], AULENBACHER K.[1,2], BAUNACK S.[1], BECKER D.[1], DIEFENBACH J.[1,2], GERICKE M.[3], GERZ K.[1], HERBERTZ R.[1], KUMAR K.[4], MAAS F.[1,2], MOLITOR M.[1], PIÑEIRO D. R.[1,2], SOROKIN I.[1], SOUDER P.[5], SPIESBERGER H.[6], TYUKIN A.[1], TYUKIN V.[1], ZIMMERMANN M.[1]

(1. *PRISMA Cluster of Excellence and Institute of Nuclear Physics, Johannes Gutenberg University, Mainz, Germany*;
2. *Helmholtz Institue, Mainz, Germany*; 3. *Department of Physics and Astronomy, University of Manitoba, Winnipeg, Canada*;
4. *Department of Physics and Astronomy, Stony Brook University, Stony Brook, USA*; 5. *Physics Department, Syracuse University, Syracuse, USA*;
6. *PRISMA Cluster of Excellence and Institute of Physics, Johannes Gutenberg University, Mainz, Germany*)

Abstract: The P2 experiment in Mainz aims to measure the weak mixing angle $\sin^2\theta_W$ in electron- proton scattering to a precision of 0.13%. In order to suppress uncertainties due to proton structure and contributions from box graphs, both a low average momentum transfer Q^2 of $4.5\times10^{-3}\mathrm{GeV}^2/c^2$ and a low beam energy of 155 MeV are chosen. In order to collect the enormous statistics required for this measurement, the new Mainz energy recovery superconducting accelerator(MESA) is being constructed. These proceedings describe the motivation for the measurement, the experimental and accelerator challenges and plans to tackle them.

Key words: weak mixing angle; parity violation; electron scattering

CLC number: O572.3 **Document code**: A doi:10.3969/j.issn.0253-2778.2016.06.006

Citation: BERGER N, AULENBACHER K, BAUNACK S, et al. Measuring the weak mixing angle with the P2 experiment at MESA[J]. Journal of University of Science and Technology of China, 2016,46(6): 481-487.
BERGER N, AULENBACHER K, BAUNACK S, 等. MESA P2 实验对弱混合角的测量[J]. 中国科学技术大学学报,2016,46(6): 481-487.

MESA P2 实验对弱混合角的测量

BERGER N.[1], AULENBACHER K.[1,2], BAUNACK S.[1], BECKER D.[1], DIEFENBACH J.[1,2], GERICKE M.[3], GERZ K.[1], HERBERTZ R.[1], KUMAR K.[4], MAAS F.[1,2], MOLITOR M.[1], PIÑEIRO D. R.[1,2], SOROKIN I.[1], SOUDER P.[5], SPIESBERGER H.[6], TYUKIN A.[1], TYUKIN V.[1], ZIMMERMANN M.[1]

(1. 德国约翰内斯堡大学核物理学院卓越研究中心, 美因茨, 德国;2. 亥姆霍兹公司, 美因茨, 德国;
3. 曼尼托巴大学天文物理学系, 温尼伯格 加拿大;4. 石溪大学天文物理学系, 石溪, 美国;
5. 锡拉丘兹大学物理系, 锡拉丘兹, 美国; 6. 德国约翰内斯堡大学物理学院卓越研究中心, 美因茨, 德国)

Received:2015-11-30; **Revised**:2016-04-20

Foundation item: Supported the Cluster of Excellence PRISMA and the Collaborative Research Center 1044, both Funded Through the Deutsche Forschungsgemeinschaft (DFG).

Biography: BERGER N(corresponding author), Professor/PhD. Research field: high energy physics. E-mail: niberger@uni-mainz.de

摘要:美因茨的 P2 实验致力于通过电子-质子散射将弱混合角$\sin^2\theta_W$的测量精确度提高到 0.13%. 为了压低由于质子结构和箱图贡献的不确定性,选择了低平均四动量转移 Q^2(4.5 × 10^{-3} GeV^2/c^2)和低束流能量(155 MeV). 为了达到实验要求的巨大统计量,新的美因茨能量恢复超导加速器(MESA)正在建设中. 本文描述了测量的动机、实验和加速器面临的挑战以及解决问题的方案.

关键词:弱混合角; 宇称破缺; 电子散射

0 Introduction

The weak mixing angle $\sin^2\theta_W$ is one of the fundamental parameters of the standard model(SM) of elementary particle physics. It has been measured with great precision at the Z resonance[1], where the determinations from LEP and SLD are marginally consistent. Due to quantum corrections, the effective weak mixing angle is a scale dependent quantity and measurements at different scales become important both for testing the SM and searching for effects of new physics beyond the SM in the running[2-3].

Measurements at lower scales were obtained in neutrino nucleon scattering[4], deep inelastic electron scattering[5], parity violating electron scattering on electrons[6] and protons[7] and atomic parity violation in Caesium[8]. These measurements were sufficient to establish the running of $\sin^2\theta_W$, more precision is however required for a stringent test of the SM and searches for new physics. The final result from the Qweak experiment is eagerly awaited and should improve on the published result[7] by a factor of three to four. More precise determinations require new experimental approaches, such as the proposed Møller[9] and deep inelastic (SOLID[10]) scattering experiments at JLAB and the P2 experiment in Mainz, which will be described in the following. An overview of current and planned experiments together with the theory prediction[11] for the running of $\sin^2\theta_W$ is shown in Fig. 1.

A precise determination of the weak mixing angle at low scales is sensitive to contributions of new physics beyond the SM which can change the running of $\sin^2\theta_W$ via contributions of new gauge bosons, additional fermions, mixing terms[12] or the exchange of very heavy particles which can be parametrized as four-fermion contact interactions[2]. In the last case, P2 will be sensitive to scales up to 49 TeV, comparable to the experiments at the large hadron collider after collecting 300 fb^{-1} of integrated luminosity.

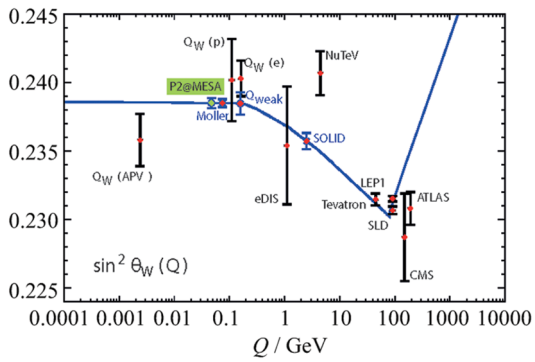

Fig. 1 Scale dependence of $\sin^2\theta_W$ together with completed and planned experimental measurements

1 Requirements

The P2 experiment aims to determine $\sin^2\theta_W$ with a precision of 0.13% by performing a measurement of the parity violating asymmetry A_{PV} in electron-proton scattering. This asymmetry between the cross-sections for left- and righthanded electrons σ_L and σ_R is determined by the weak charge of the proton Q_W:

$$A_{PV} = \frac{\sigma_L - \sigma_R}{\sigma_L + \sigma_R} = \frac{G_F Q^2}{4/2\alpha}(Q_W + F(Q^2)) \quad (1)$$

where G_F is the Fermi constant, the fine structure constant and Q^2 the squared four-moment transfer, setting the scale. Contributions stemming from the fact that the proton is not a point-like particle are collected in $F(Q^2)$ and are small for low values of Q^2, thus motivating an experiment at low momentum transfer. Further hadronic uncertainties come from box graphs such as the one shown in Fig. 2. These uncertainties with a weak dependence on the momentum transfer do however, increase steeply with rising center-of-mass

energy[13-14], favouring a low beam energy.

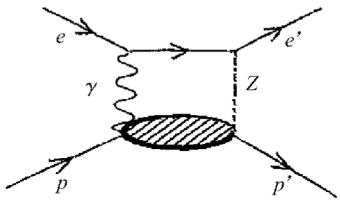

Fig. 2 γ-Z box graph for electron-proton scattering

The weak mixing angle is related to Q_W via

$$Q_W = 1 - 4\sin^2\theta_W \quad (2)$$

which implies by propagation of uncertainty that a 0.13% measurement of $\sin^2\theta_W$ requires a 1.5% measurement of Q_W, which also corresponds to the target uncertainty in the asymmetry. Due to the small weak charge of the proton and the small Q^2, the expected asymmetry is only 33 ppb, thus requiring a measurement with 0.44 ppb precision. The statistical uncertainty scales with the number of scattered electrons as $\frac{1}{\sqrt{N}}$, which in turn requires the observation of $\mathcal{O}(10^{18})$ electrons. For sociological reasons, the total measurement time is limited to 10 000 hours, which requires observing $\mathcal{O}(10^{11})$ signal electrons per second.

These very high rates can be achieved by directing a 150 μA electron beam onto a 60 cm long liquid hydrogen target, producing a luminosity of 2.4×10^{39} $s^{-1}cm^{-2}$.

The aim of determining $\sin^2\theta_W$ with a precision of 0.13% is thus extremely challenging for the accelerator and detector systems. The following sections outline how the MESA accelerator, the polarisation measurement and the P2 experiment intend to tackle these challenges.

2 The MESA accelerator

In order to accommodate the very long running time and demanding stability requirements of the P2 experiment, a new accelerator, the Mainz energy-recovery superconducting accelerator (MESA[15]) is being built.

With a maximum extracted beam energy of 155 MeV, MESA is small enough to fit into the existing halls that have become available with the completion of the A4 parity violating electron scattering program at the Mainz Microtron MAMI. P2 and the MAGIX spectrometer (see the contribution of *A*. Denig to this conference for details on the MESA program beyond the P2 experiment) will be housed in a new hall as part of the recently funded centre for fundamental physics. Fig. 3 shows the overall layout of accelerator and experiments (indicating existing and new halls at the institute of nuclear physics in Mainz).

P2 requires a highly polarized (> 85%), high intensity (150 μA) beam of 155 MeV electrons with excellent availabiliy (> 4000 h/year). The beam helicity will be flipped several thousand times a second. The main challenge is to reduce any helicity correlated changes in beam intensity, energy, position and angle to less than 0.1 ppb. Here we can profit from the extensive experience in beam stabilization gained at the Mainz Microtron MAMI. Tab. 1 compares the values for helicity correlated beam fluctuations achieved at MAMI with the requirements for P2 at MESA. Whilst the energy stability already fulfills the demands, improvements of one to two orders of magnitude have to be achieved for position, angle and intensity; new digital feedback electronics for beam stabilization are currently being designed and tested at MAMI.

Tab. 1 Helicity correlated beam fluctuations

Beam Quantity	Achieved at MAMI	Contribution to $\delta(A_{PV})$	Required for MESA
Energy	0.04 eV	<0.1ppb	fulfilled
Position	3 nm	5 ppb	0.13 nm
Angle	0.5 rad	3 ppb	0.06 nrad
Intensity	14 ppb	4 ppb	0.36ppb

The MESA lattice design is finalized, the superconducting RF cavities have been ordered and civil construction on the new hall will start 2016. We plan to start installing the accelerator in 2018 and have beam available for P2 before 2020.

3 Polarimetry

P2 requires a knowledge of the beam polarisation

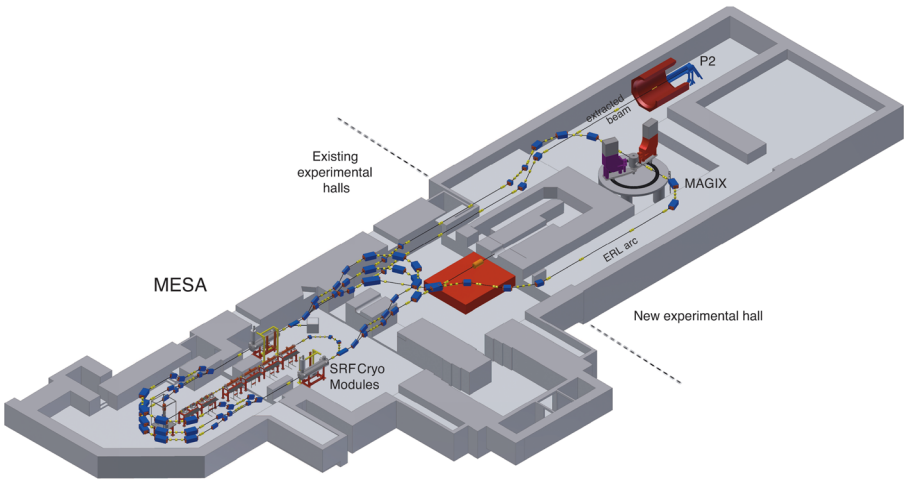

Fig. 3 Layout of the MESA accelerator and experiments

of better than 0.5%. We aim to achieve this precision via two paths[16], namely an invasive double Mott polarimeter at the electron source and a hydro-Møller polarimeter, which can be operated at the same time as and is placed right in front of the main experiment.

3.1 Double Mott polarimeter

The asymmetry of Mott scattering in thin foils can be used to determine the beam polarization, it however requires a precise knowledge of the analyzing power of the scattering foils which introduces a large uncertainty into the measurement. Double Mott scattering[17] in two foils allows to determine the effective analyzing power within the setup, thus reducing the associated uncertainty which makes it a suitable choice for precise source polarimetry at MESA. A prototype of the double-Mott polarimeter is currently tested with the MESA source prototype in operation in Mainz.

3.2 Hydro-Møller polarimeter

We plan to determine the beam polarization at the final energy with a hydro-Møller polarimeter[18] right in front of the main experiment. Here the asymmetry in Møller scattering of the beam electrons with the electrons in fully polarized atomic hydrogen is used. The hydrogen is polarized using a 7-8 T solenoid magnet. In order to avoid hydrogen recombination, the gas is kept at cryogenic temperatures and the walls of the vessel are coated with superfluid helium. Operating this cryogenic setup with a high intensity electron beam passing through the center is certainly challenging. The cryostat/magnet for this setup is currently under construction.

4 The P2 experiment

For a given electron beam energy, the scattering angle θ determines the momentum transfer Q^2. At low Q^2, the uncertainty of the asymmetry measurement is dominated by statistics and helicity correlated beam fluctuations. At large Q^2, uncertainties in the proton form factors become dominant. For our setup, the best accuracy can be reached with a central scattering angle of 35° at an angular acceptance of 20° (as shown in Fig. 4).

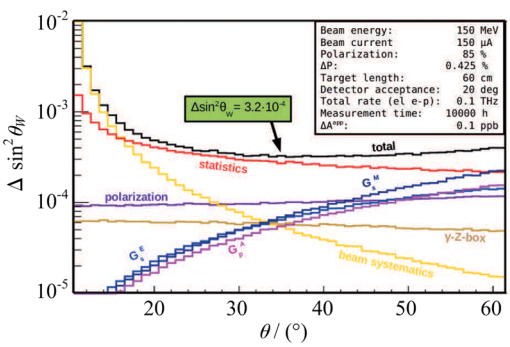

Fig. 4 Contributions to the uncertainty

In Fig. 4, contributions to the uncertainty of the $\sin^2\theta_W$ measurement at fixed beam energy, intensity and run time in dependence of the central scattering angle. G_E^S, G_M^S and G_P^A refer to the uncertainties stemming from the electric and magnetic strange form

factor and the axial form factor of the proton respectively.

As the very high intensity beam produces several thousand Bremsstrahlung photons for every electron scattered into the angular range of interest as well as a large amount of Møller scattered electrons with low transverse momentum, a magnetic spectrometer is required in order to guide signal electrons to detectors whilst at the same time shielding them from photon and Møller backgrounds. The detectors in turn face the challenge of reliably detecting more than 100 GHz of scattered electrons. The following sections will describe the spectrometer design, the development of integrating Cherenkov detectors as well as a pixellated tracking detector for a precise determination of the momentum transfer Q^2.

4.1 Spectrometer

For the spectrometer design, the main choice is between a toroidal (as used in the Qweak experiment) and a solenoidal magnetic field. The advantages of a toroidal setup, such as zero field in the target region and easy access to instrumentation are compromised by the fact that the coils are necessarily inside of the spectrometer acceptance, typically leading to a loss of about half the signal electrons and consequently a doubling of the measurement time, which is unrealistic in the context of P2.

We have thus decided to employ a solenoidal design and studied possible placements of the target, shielding and detectors for several existing solenoids, e. g. from the ZEUS experiment at HERA[19] or the FOPI experiment at GSI[20]. We have shown using both ray-tracing in the magnet field maps and full Geant4 based simulations that with a careful optimization of the shape and placement of lead shields, sufficient signal-to-background ratios can be achieved in the integrating detectors. A possible view of the setup is shown in the rendering in Fig. 5 (showing the solenoid coil, target, lead shielding and integrating detectors as well as a hunky physicist for scale).

4.2 Integrating detectors

Individually counting hundreds of GHz of electrons is extremely challenging, but not actually required for P2. Instead, we opt for an integrating measurement, where the electrons produce Cherenkov light in bars of fused silica (quartz), which is detected with photomultipliers operated at low gain. The current of these photomultipliers is integrated over one helicity period and read out with high precision (22 bit) analog-to-digital converters.

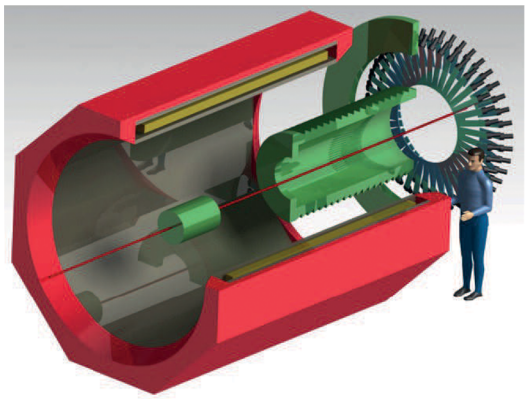

Fig. 5 Rendering of a possible P2 setup

We are currently testsing different types and polishing finishes as well as wrappings of quartz bars with the MAMI beam and have found both a performance sufficient for P2 as well as an excellent agreement of the light yield at different incident angles with Geant4 based simulations.

The switchable gain photomultiplier base is currently under development in Mainz; for the integrating ADC a joint development with the Møller experiment is ongoing at the University of Manitoba.

4.3 Tracking detectors

In order to determine the average momentum transfer $< Q^2 >$ of the scattered electrons creating signals in the integrating detectors, a tracking detector is required. The high rates at MESA, the precision requirements and the low momenta of the scattered electrons (making multiple coulomb scattering in the tracker material the dominating uncertainty in the momentum measurement) call for a fast, high granularity sensor with very little material. We choose to employ high-voltage monolithic active pixel senors (HV-MAPS[21-25]) as the detector technology. These sensors, manufactured in a commercial CMOS

technology, apply a "high" voltage of around 90 V between deep n-wells and the substrate, leading to very fast charge collection from a thin depletion layer. The thin charge collection zone allows for thinning of the sensors to just 50 μm. The sensor is segmented into 80 by 80 μm pixels. The CMOS process used allows for integrating both analog and digital electronics directly on the sensor; the output are zero suppressed hit addresses and timestamps on a fast differential link. In the development of the sensors for P2, we closely collaborate with the Mu3e, ATLAS and Panda experiments.

From these thin sensors, we plan to build a tracking detector with four planes (shown in Fig. 6, consisting of four planes of HV-MAPS sensors). The arrangement in two double planes combines a good momentum and angular resolution in a multiple scattering dominated regime with ease of reconstruction in a high multiplicity environment. We are currently studying tracking algorithms that also perform well in the non-uniform field close to the edge of the magnet and are at the same time robust and fast enough to allow for on-line track finding and fitting, possibly on highly parallel architectures such as graphics processing units (GPUs).

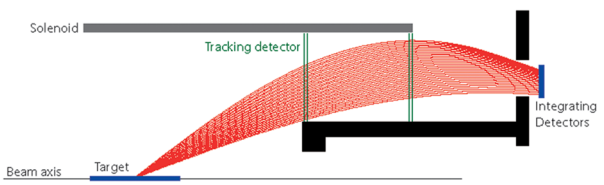

Fig. 6 Schematic view of the P2 tracking detector

5 Conclusion

The P2 experiment aims to measure $\sin^2\theta_W$ at low momentum transfer with unprecedented accuracy, which both improves the precision on one of the fundamental parameters of the standard model and allows to search for new physics. The new MESA accelerator in Mainz will provide a stable, very high intensity electron beam combined with precision polarimetry. P2 will measure the parity violating asymmetry in electron- proton scattering using a solenoid spectrometer with integrating Cherenkov detectors combined with a thin pixel tracker. Accelerator commissioning is scheduled to start in 2018 and a first P2 data taking for 2020. Beyond the $\sin^2\theta_W$ measurement, P2 can also be used to study parity violation with different target materials, giving access e. g. to neutron skins. The MESA accelerator also has a wide physics program beyond P2, described elsewhere in these proceedings.

References

[1] SCHAEL S, BARATE R, BRUNELIERE R, et al. Precision electroweak measurements on the Z resonance [J]. Physics Reports. 2006, 427(5-6): 257-454.

[2] ERLER J, KURYLOV A, RAMSEY-MUSOLF M J. The weak charge of the proton and new physics[J]. Physical Review D, 2003, 68(1): 462-467.

[3] ERLER J, RAMSEY-MUSOLF M J. Low energy tests of the weak interaction [J]. Progress in Particle Nuclear Physics, 2004, 54(2): 351442.

[4] ZELLER G P, MCFARLAND K S, ALTON A, et al. Precise determination of electroweak parameters in neutrino-nucleon scattering[J]. Physical Review Letters, 2001, 88(9): 386-389.

[5] AKTAS A, ANDREEV V, ANTHONIS T, et al. A determination of electroweak parameters at HERA [J]. Physics Letters B, 2006, 632(1): 35-42.

[6] ANTHONY P L, ARNOLD R G, ARROYO C, et al. Observation of parity nonconservation in møller scattering [J]. Physical Review Letters, 2004, 92(18):181602.

[7] ANDROIC D. First determination of the weak charge of the proton[J]. Physical Review Letters, 2013, 111(14): arXiv:1307.5275.

[8] WOOD C S, BENNETT S C, CHO D, et al. Measurement of parity nonconservation and an anapole moment in cesium[J]. Science, 1997, 275953070: 1759-1763.

[9] BENESCH P, BRINDZA R D, CARLINI J P, et al. The MOLLER experiment: An ultra-precise measurement of the weak mixing angle using Møller scattering[J]. EPrint Arxiv, 2014: arXiv:1411.4088.

[10] CHEN J P, GAO H, HEMMICK T K, et al. A white paper on SoLID(Solenoidal lardge intensity device)[J]. EPrint Arxiv, 2014: arXiv:1409.7741.

[11] ERLER J, RAMSEY-MUSOLF J. Weak mixing angle at low energies [J]. Physical Review D, 2004, 72(7): arXiv:hep-ph/0409169.

[12] DAVOUDIASL H, LEE H S, MARCIANO W J. Muon

$g-2$, rare kaon decays, and parity violation from dark Bosons[J]. Physical Review D, 2014, 89(9)98-105.

[13]GORCHTEIN M, HOROWITZ C J, RAMSEY-MUSOLF M J. Model-dependence of the γZ dispersion correction to the parity-violating asymmetry in elastic *ep* scattering[J]. Physical Review C 84, 2011, 84(1): 015502(arXiv: 1102.3910).

[14]GORCHTEIN M, SPIESBERGER H, ZHANG X. How strange is pion electroproduction? [J]. Physical Letters B, 2016, 752: 135-145.

[15]AULENBACHER K. The MESA accelerator[C]// AIP Conference Proceedings. Cambridge, USA: 2013, 1563: 5-12.

[16]AULENBACHER K, ALEXANDER I, TIOUKINE V. The polarimetry chain for the P2 experiment[J]. Nuovo Cimento C, 2012, 186: 035N04.

[17]GELLERICH A, KESSLER J. Precision measurement of the Sherman asymmetry function for electron scattering from gold[J]. Physical Review A, 1991, 43(1): 204-216.

[18]BARTOLOMÉ P A, AULENBACHER K, TYUKIN V. Møller polarimetry with polarized atomic hydrogen at MESA[C]// AIP Conference Proceedings. 1553, 243-246.

[19]ACERBI E, ALESSANDRIA F, BACCAGLIONI G, et al. The Zeus thin superconducting solenoid[J]. Proceedings of International Conference on Magnet Technology. Zürich, Switzerland, 1985: 163-166.

[20]RITMAN J, HERMANN N, BEST D, et al. On the transverse momentum distribution of strange hadrons produced in relativistic heavy ion collisions[J]. Nuclear Physics Proceedings, 1995, 44(S): 708-715.

[21]PERIĆ /I. A novel monolithic pixelated particle detector implemented in high-voltage CMOS technology[J]. Nuclear Instruments and Methods in Physics Research Section A, 2007, 582: 876-885.

[22]PERIĆ I, FISCHER P, KREIDL C, et al. High-voltage pixel detectors in commercial CMOS technologies for ATLAS, CLIC and Mu3e experiments[J]. Nuclear Instruments and Methods in Physics Research Section A, 2013, 731(18): 131-136.

[23]SHRESTHA S (Mu3e Collaboration). The high-voltage monolithic active pixel sensor for the Mu3e experiment[C]// Proceedings of Technology and Instrumentation in Particle Physics. Amsterdam, 2014: 047(1-9).

[24]AUGUSTIN H, BERGER N, BRAVAR S, et al. The MuPix high voltage monolithic active pixel sensor for the Mu3e experiment[J]. Journal of Instrumentation, 2015, 10(3): C03044(1-8).

[25]PERIĆ I, EBER R, EHRLER F, et al. Overview of HVCMOS pixel sensors[J]. Journal of Instrumentation, 2015, 10(5): C05021 (1-8).

Article ID:0253-2778(2016)06-0488-06

Dalitz decay studies at BEPCⅢ

WANG Dayong(for BEPCⅢ Collaboration)

(*School of Physics and State Key Lab. of Nucl. Phys. and Tech.*, *Peking University*, *Beijing* 100871, *China*)

Abstract: EM Dalitz decays could be sensitive and provide very rich information about meson structures, and they play an important role in constraining the uncertainties to $(g-2)_\mu$. BEPCⅢ has performed and published several Dalitz decays, including $\eta'\to\gamma e^+e^-$, $J/\psi\to Pe^+e^-$ ($P=\eta',\eta$ and π^0), $\eta'\to\omega e^+e^-$ etc. These processes are all observed and measured for the first time, furthering our knowledge about meson structures and meson interactions. Many more related work is ongoing and there will be more results to come, which will further test the theory against the measurements and could be sensitvie to the new physics beyond the standard model.

Key words: BEPCⅢ; Dalitz decay; meson structure; vector meson dominance

CLC number: O572.3 **Document code**: A doi:10.3969/j.issn.0253-2778.2016.06.007

Citation: WANG Dayong(for BEPCⅢ Collaboration). Dalitz decay studies at BEPCⅢ[J]. Journal of University of Science and Technology of China, 2016,46(6): 488-493.
王大勇(代表BEPCⅢ合作组). 北京谱仪Ⅲ实验上的达利兹衰变研究[J]. 中国科学技术大学学报, 2016,46(6): 488-493.

北京谱仪Ⅲ实验上的达利兹衰变研究

王大勇(代表BEPCⅢ合作组)

(北京大学核物理与核技术国家重点实验室,北京大学物理学院)

摘要:电磁达利兹衰变过程对介子结构非常敏感,可以提供了解介子结构的丰富信息,在约束$(g-2)_\mu$的不确定度方面也发挥着重要作用.近期,北京谱仪Ⅲ研究和发表了对几个重要达利兹衰变的测量结果,包$\eta'\to\gamma e^+e^-$, $J/\psi\to Pe^+e^-$ ($P=\eta',\eta/\pi^0$), $\eta'\to\omega e^+e^-$等.对这些过程的研究都是世界上的首次发现和测量,深化了我们对于介子结构和介子相互作用的理解.更多的相关工作仍在进行之中,预期它们将会进一步促进测量和理论的比较,也会对超出标准模型的新物理有一定的敏感度.

关键词:北京谱仪Ⅲ; 达利兹衰变; 介子结构; 矢量介子为主模型

0 Introduction

BEPCⅡ is the only currently running τ-charm factory working at the C. M. energy range of 2.0~4.6 GeV, located at Institute of High Energy Physics, Beijing. This energy range has a lot of unique features which benet greatly the rich physics programs:

(Ⅰ) It is rich of resonances, including many

Received:2015-11-30; **Revised**:2016-04-20

Foundation item: Supported by National Natural Science Foundation of China (U1232105), Ministry of Science and Technology (2015CB856700).

Biography: WANG Dayong (corresponding author), Professor/PhD. Research field: high energy physics. E-mail: dayong.wang@pku.edu.cn

charmonia and charmed mesons.

(Ⅱ) Pairs of particles, such as τ, D, D_s, charmed baryons etc are copiously produced with unique threshold characteristics.

(Ⅲ) This energy region is in the transition between perturbative and non-perturbative in terms of QCD.

(Ⅳ) Dierent types of hadrons, conventional or exotic, can demonstrate their structures and interactions through processes of their productions, decays, transitions and behaviors under various probes.

The BEPC Ⅲ detector has a geometrical acceptance of 93% of 4π and consists of four main components: ① A small-celled, helium-based main draft chamber (MDC) with 43 layers, which provides measurements of ionization energy loss (dE/dx). The average single wire resolution is 135 μm, and the momentum resolution for charged particles with momenta of 1 GeV/c in a 1 T magnetic field is 0.5%. ② An electromagnetic calorimeter (EMC) made of 6240 CsI (Tl) crystals arranged in a cylindrical shape (barrel) plus two end caps. For 1.0 GeV photons, the energy resolution is 2.5% in the barrel and 5% in the end caps, and the position resolution is 6 mm in the barrel and 9 mm in the end caps. ③ A time-of-flight system for particle identication (PID) composed of a barrel part made of two layers with 88 pieces of 5 cm thick, 2.4 m long plastic scintillators in each layer, and two end caps with 96 fan-shaped, 5 cm thick plastic scintillators in each end cap. The time resolution is 80 ps in the barrel and 110 ps in the endcaps, corresponding to a $2\sigma K/\pi$ separation for momenta up to about 1.0 GeV/c. ④ A muon chamber system (MUC) made of about 1000 m^2 of resistive plate chambers arranged in nine layers in the barrel and eight layers in the end caps, and incorporated in the return iron of the superconducting magnet. The position resolution is about 2 cm. More details of the detector are described in Ref. [1].

In general, the clean environments and high luminosity at BEPC Ⅲ are very helpful to study the structure and interaction of hadrons. BEPC Ⅲ has accumulated 1.3 Billion J/Ψ's, 0.5 Billion Ψ's and 2.9 fb^{-1} at $\Psi(3773)$, all of which are the largest data sets in the world. There are also very huge samples of light mesons from decays of these charmonia, such as η, η', π^0, K etc. By simple estimation based on the branching ratios, there would be about 7.1 M η' s and 1.9 M η' s from the two most abundant channels in the J/Ψ sample, which provide ideal samples for studying their Dalitz decays.

1 Dalitz decay of mesons and experimental techniques

Meson Dalitz decays are very sensitive EM probes to study the structures and the interactions of mesons[2]. The information of meson transition form factors (TFF) etc can be retrieved from these processes to test various models of mesons. These TFFs can also help to reduce the uncertainties caused by the light-by-light hadronic contributions to the calculations of $(g-2)_\mu$, which has seen 3.6σ discrepancies with the experimental measurements[3-4].

There are a pair of electron and positron in the final states of meson Dalitz decays, which could be easily polluted by the converted electron-positron pairs from phontons interacting with detector materials. Thus it is crucial to exclude the gamma conversion events as much as possible in order to establish the meson Dalitz decays experimentally.

At BEPC Ⅲ, a photon conversion nder is developed, with the algorithm based on the information of common vertex position on the tranverse plane. It is described in Ref. [5].

Fig. 1 shows the performance of vetoing gamma conversions, with the process $J/\psi \to \eta'\gamma$, $\eta' \to \gamma\pi^+\pi^-$. The conversion mostly takes place at beam pipe and the innerMDC wall. The algorithm can reconstruct the conversion vertex quite well and data-MC consistency is good.

2 First observation of $\eta' \to \gamma e^+ e^-$

BEPC Ⅲ measured the Dalitz decay $\eta' \to \gamma e^+ e^-$ for the first time. The results are published at Ref. [6]. The dierential decay width, are normalized to the radiative decay width $\Gamma(\eta' \to \gamma\gamma)$ to reduce the

common systematic errors. The measured ratio is $R_{\eta'} = (2.13 \pm 0.09(\text{stat}) \pm 0.07(\text{sys})) \times 10^{-2}$. This corresponds to a branching fraction $BR(\eta' \to \gamma e^+ e^-) = (4.69 \pm 0.20(\text{stat}) \pm 0.23(\text{sys})) \times 10^{-4}$. The first errors are statistic and the second ones are systematic.

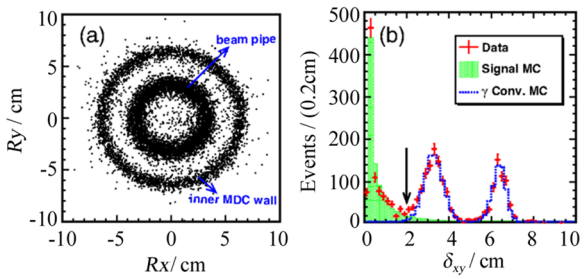

Fig. 1 Veto of γ conversions at BEPCⅢ

In Fig. 1(a), Ry vs Rx distributions for the simulated γ conversion events. In Fig. 1(b), δxy distributions, in which the shaded histogram shows the MC-simulated signal events. The symbol " + " with error bars are data. The dotted histogram shows the background from the γ-conversion events. In Fig. 1(b), the solid arrow indicates the requirement on δxy.

The ratio $R_{\eta'}$ can be described clearly in theory. It is formulated with the calculable QED part for a point meson, then times the TFF. The latter is described byphenomeno logical models, and can be experimentally determined from dierences between the measured dilepton invariant mass spectrum and the QED calculation. In the vector meson dominance (VMD) model[2], it is assumed that interactions between a virtual photon and hadrons are dominated by a superposition of neutral vector meson states. So we could retrieve the TFF information from the measurements. Fig. 2 shows the eciency-corrected signal yields versus mass of electron positron pairs from $\eta' \to \gamma e^+ e^-$, with the QED shape superimposed for comparison. The discrepancy between QED and data, which reflects the TFF, is evident in the high $M(ee)$ region.

In Fig. 2, the black crosses are data and the gray shaded histogram indicates the pointlike QED result.

The most common TFF model uses only the first

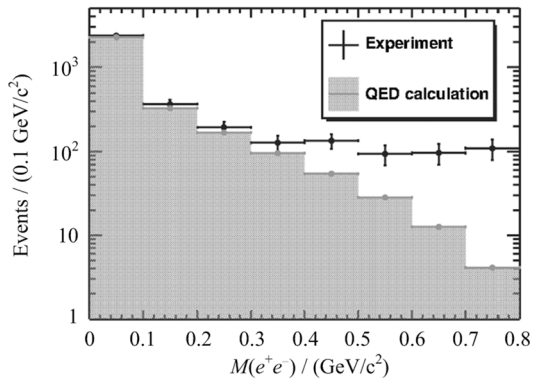

Fig. 2 Eciency-corrected signal yields versus mass of electron positron pairs from $\eta' \to \gamma e^+ e^-$

term in the dispersion relation. The results of a least-squares fit with this single-pole model are shown in Fig. 3. The parameters of the form factors thus determined are in agreement with the result obtained in the process of $\eta \to \gamma \mu^+ \mu^-$ as measured in Ref. [7].

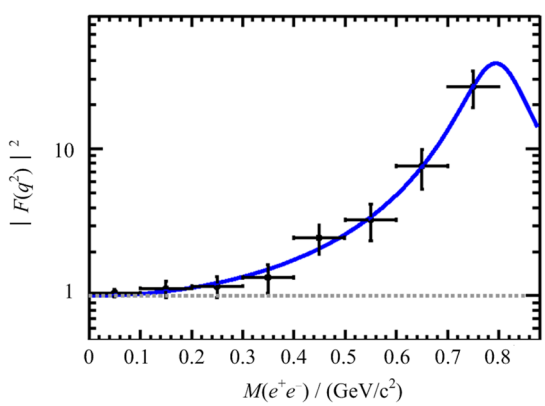

Fig. 3 The single-pole form factor fitting of $\eta' \to \gamma e^+ e^-$

In Fig. 3, The black crosses are data, where the statistical and systematic uncertainties are combined; the gray solid curve shows the fit results. The gray dotted line shows the pointlike case for comparison.

3 First observation of $J/\psi \to Pe^+e^-$ ($P = \eta', \eta$ and π^0)

In the previous measurements from other experiments, only Dalitz decays of light mesons are studied. In order to shed light on some of the puzzles observed in these measurements, it would be interesting to search for and study the Dalitz decay of heavy quarkonium.

The theoretical and experimental investigations of the EM Dalitz decays of the light vector mesons motivate us to study the rare charmonium decays $J/\psi \to Pe^+e^-$, which should provide useful information on the interaction of the charmonium states with the electromagnetic field. The huge J/ψ sample at BEPC Ⅲ provides a good chance for this. BEPC Ⅲ made this measurement and provided experimental information on these decays for the first time[8].

BEPC Ⅲ studied the processes of $J/\psi \to Pe^+e^-$, and established this decay pattern for three dierent pseudoscalar mesons: η, η', and π^0 in the major decay modes. Fig. 4 shows the mass distributions of the pseudoscalar meson candidates in $J/\psi \to Pe^+e^-$. All the modes are established experimentally for the first time.

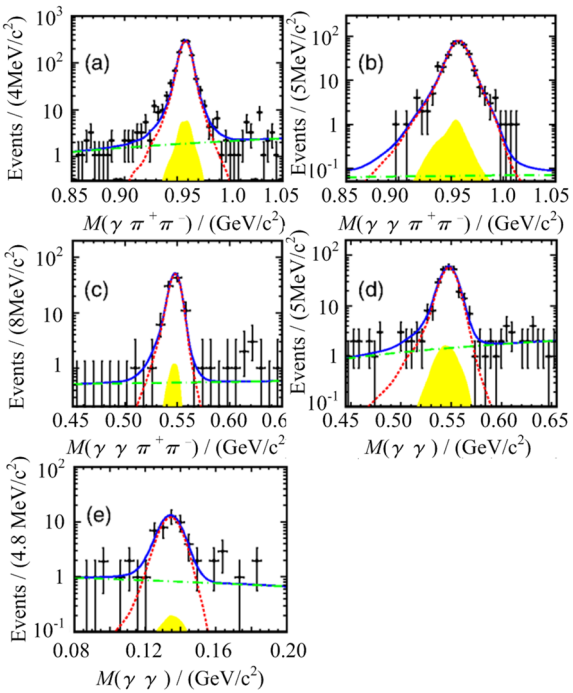

Fig. 4　Mass distributions of the pseudoscalar meson candidates in $J/\psi \to Pe^+e^-$

In Fig. 4, the subplots (a) to (e) are from dierent pseudoscalar states and their subsequent decay channels as inidcated. The black dots with error bars are data, the small dashed lines represent the signal, the long dotted-dashed curves show the nonpeaking back-ground shapes, and the gray shaded components are the shapes of the peaking backgrounds from the $J/\psi \to Pe^+e^-$ decays. Total ts are shown as the solid lines.

The branching fractions of these processes are determined. The BR are measured to be $B(J/\psi \to \eta' e^+e^-) = (5.81 \pm 0.16 \pm 0.31) \times 10^{-5}$, $B(J/\psi \to \eta e^+e^-) = (1.16 \pm 0.07 \pm 0.06) \times 10^{-5}$ and $B(J/\psi \to \pi^0 e^+e^-) = (7.56 \pm 1.32 \pm 0.50) \times 10^{-7}$, respectively.

The measurements for $J/\psi \to \eta' e^+e^-$ and $J/\psi \to \eta e^+e^-$ decay modes are consistent with the theoretical prediction in Ref. [9]. The theoretical prediction for the decay rate of $J/\psi \to \pi^0 e^+e^-$ based on the VMD model is about 2.5 standard deviations from the measurement in this analysis, which may indicate that further improvements of the QCD radiative and relativistic corrections are needed.

Direct information on the form factor is obtained by studying the efficiency-corrected signal yields for each given $M(e^+e^-)$ bin. Fig. 5 shows the form factor obtained for $J/\psi \to \eta' e^+e^-$. The crosses are data, and the fit is shown as the solid curve. The dotted-dashed curve indicate the prediction of the simple pole model, where the form factor is parametrized by the simple pole approximation with the pole mass at 3.686 GeV/c^2.

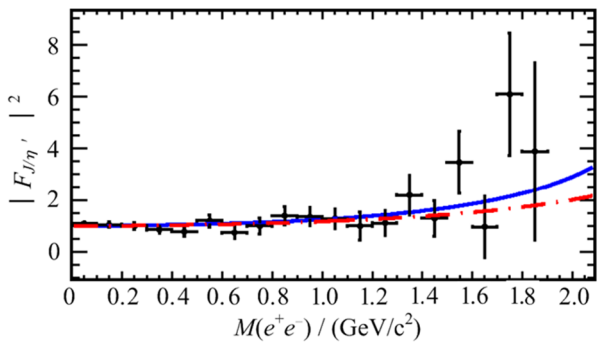

Fig. 5　Form factor for $J/\psi \to \eta' e^+e^-$

In Fig. 5, the crosses are data, the dotted-dashed curve is the prediction of the simple pole model with the pole mass of 3.686 GeV/c^2, and the fit is shown by the solid curve.

4　Measurement of $\eta' \to \omega e^+e^-$

With a sample of 1.31 billion J/ψ events

collected with the BEPC Ⅲ detector, we have also analyzed the decays $\eta'\to\gamma\omega$ and $\eta'\to\omega\ e^+e^-$, via $J/\psi\to\eta'\gamma$. The results are published in Ref. [10].

Similar to the study of $\eta'\to\gamma\ e^+\ e^-$, the process $\eta'\to\omega\ e^+\ e^-$ has to be measured with respect to the normalization process of $\eta'\to\omega\gamma$. With the optimized event selections, the decay $\eta'\to\omega\gamma$ is observed in the dis tribution of $M(\pi^0\pi^+\pi^-\gamma)$ versus $M(\pi^0\pi^+\pi^-)$ shown in Fig. 6. The concentration of events in the central region indicate the existence of $\eta'\to\omega\gamma$, which serves as normalization.

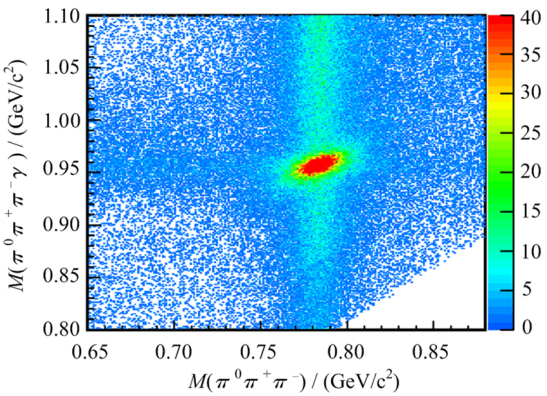

Fig. 6 2D distribution of the invariant masses $M(\pi^0\pi^+\pi^-\gamma)$ vs $M(\pi^0\pi^+\pi^-)$ from $\eta'\to\omega e^+e^-$ data

To improve the mass resolution, as well as to better handle the background in the vertical band around the ω mass region and horizontal band around the η' mass region, we determine the signal yield from the distribution of the difference between $M(\pi^0\pi^+\pi^-e^+e^-)$ and $M(\pi^0\pi^+\pi^-)$. The backgrounds in the vertical and horizontal bands do not peak in the signal region, which is demonstrated by the inclusive MC sample, as shown by the histogram in Fig. 7.

The dots with error bars are data, the histogramshows the MC simulation of inclusive J/ψ decays. The solid curve represents the fit results, and the dashed curve is the background determined by the fit.

To determine the $\eta'\to\omega\ e^+e^-$ yield, an unbinned maximum likelihood fit on the distribution of $M(\pi^0\pi^+\pi^-e^+e^-)-M(\pi^0\pi^+\pi^-)$, as shown in Fig. 8, is performed. The signal component is modeled

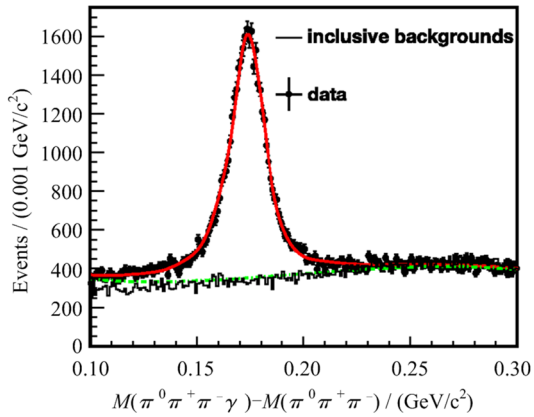

Fig. 7 Distribution of the mass difference $M(\pi^0\pi^+\pi^-e^+e^-)-M(\pi^0\pi^+\pi^-)$ from $\eta'\to\omega e^+e^-$

by the MC simulated signal shape convoluted with a Gaussian function to account for the difference in the mass resolution between data and MC simulation. The shape of the dominant non-resonant background is derived from the MC simulation, and its magnitude is fixed taking into account the decay branching fraction from the PDG[11]. The remaining background contributions are described with a 2nd-order Chebychev polynomial. The fit shown in Fig. 8 has a statistical significance of 8σ, which is determined by the change of the log-likelihood value and of the number of degrees of freedom in the fit with and without the signal included.

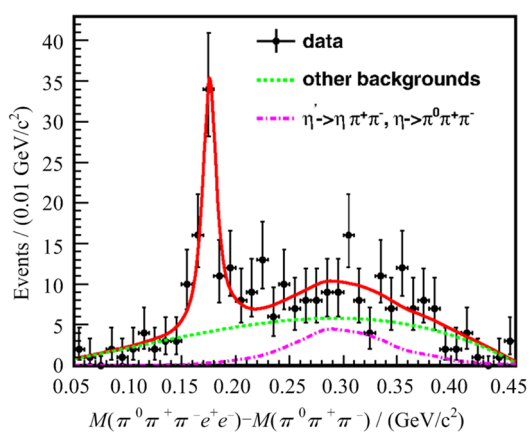

Fig. 8 Fitting results from $\eta'\to\omega e^+e^-$ on the distribution of $M(\pi^0\pi^+\pi^-e^+e^-)-M(\pi^0\pi^+\pi^-)$

In Fig. 8, the crosses show the distribution of data. The dash-dotted line represents the $\eta'\to$

$\eta\pi^+\pi^-$ component, and the dotted curve shows the background except $\eta'\to\eta\pi^+\pi^-$.

So for the first time, the decay of $\eta'\to\omega e^+e^-$ is observed with a statistical significance of 8σ, and its branching fraction is measured to be $B(\eta'\to\omega e^+e^-) = (1.97 \pm 0.34(\text{stat}) \pm 0.17(\text{syst})) \times 10^4$, which is consistent with theoretical prediction, 2.0×10^{-4}[12]. The branching fraction of $\eta'\to\omega\gamma$ is determined to be $B(\eta'\to\omega\gamma) = (2.55 \pm 0.03(\text{stat}) \pm 0.16(\text{syst})) \times 10^{-2}$, which is in good agreement with the world average value in Ref. [11] and the most precise measurement to date.

5 Conclution

In summary, EM Dalitz decays could be sensitive and provide very rich information about meson structures, and plays an important role in constraining the uncertainties to $(g-2)_\mu$. BEPC Ⅲ has performed and published several Dalitz decays, including $\eta'\to\gamma e^+e^-$, $J/\psi\to P e^+e^-$ ($P=\eta'$, η' and π^0), $\eta'\to\omega e^+e^-$ etc. These processes are all observed and measured for the first time. They have furthered our knowledge about meson structures and meson interactions. Many more related work is ongoing. There will be more results to come, and they will further test the theory against the measurements and could be sensitvie to the new physics beyond the standard model.

References

[1] ABLIKIM M, AN Z H, BAI J Z, et al. Design and construction of the BEPC Ⅲ detector [J]. Nuclear Instruments & Methods in Physics Research A, 2010, 614(3): 345-399.

[2] LANDSBERG L G. Electromagnetic decays of light mesons[J]. Physics Reports, 1985, 128(6): 301-376.

[3] DAVIER M, HOECKER A, MALAESCU B, et al. Reevaluation of the hadronic contributions to the muong-2 and to $\alpha(M_Z^2)$[J]. European Physical Journal C, 2011, 71: 1515-1527.

[4] MILLER J P, DE RAFAEL E, ROBERTS B L, et al. Muon(g-2): Experiment and theory [J]. Annual Review of Nuclear & Particle Science, 2012, 62: 237-264.

[5] XU M, ACHASOV M N, AI X C, et al. A photon conversion finder at BEPC Ⅲ [J] Chinese Physics C, 2012, 36(8): 742-749.

[6] ABLIKIM M, ACHASOV M N, AI X C, et al. Measurement of matrix elements for the decays $\eta\to\pi^+\pi^-\pi^0$ and $\eta/\eta'\to\pi^0\pi^0\pi^0$ [J]. Physics Review D, 2015, 92(1): 012001(1-12).

[7] DZHELYADIN R I, GOLOVKIN S V, KONSTANTINOV A S, et al. Study of the electromagnetic transition formfactor in $\omega\to\pi^0\mu^+\mu^-$ decay [J]. Physics Letters B, 1981, 102(4): 296-298.

[8] ABLIKIM M, ACHASOV M N, AI X C, et al. Observation of electromagnetic Dalitz decays $J/\psi\to Pe^+e^-$ [J]. Physical Review D, 2014, 89(9): 092008(1-10).

[9] FU J L, LI H B, QIN X S, et al. Study of the electromagnetic transitions $J/\psi\to Pl^+l^-$ and probe dark photon [J]. Modern Physics Letters A, 2012, 27: 1250223.

[10] RODRIGUEZ C L, MORSCHER M, PATTABIRAMAN B, et al. Erratum: Binary black hole mergers from globular clusters: Implications for advanced LIGO[J]. PHysical Review Letters, 2016, 116(2): 029901.

[11] OLIVE K K A, AGASHE K, AMSLER C, et al. Review of particle physics[J]. Chinese Physics C, 2014, 38(9): 1-1232.

[12] FAESSLER A, FUCHS C, KRIVORUCHENKO M I. Dilepton spectra from decays of light unflavored mesons [J]. Physical Review C, 2000, 61: 035206.

第46卷第6期 中国科学技术大学学报 Vol. 46, No. 6
2016年6月 JOURNAL OF UNIVERSITY OF SCIENCE AND TECHNOLOGY OF CHINA Jun. 2016

Article ID:0253-2778(2016)06-0494-08

Combined study of the η and η' mesons: Phenomenology, chiral extrapolation of lattice QCD and effective field theory

GUO Zhihui[1,2]

(1. *Department of Physics, Hebei Normal University, Shijiazhuang* 050024, *China*)
(2. *State Key Laboratory of Theoretical Physics, Institute of Theoretical Physics, CAS, Beijing* 100190, *China*)

Abstract: A comprehensive phenomenological study is carried out of the decay processes with the η or η' in the initial/final states within the effective field theory approach. Two primary types of processes are analyzed: The ones only with light-flavor hadrons and those involving the J/ψ. The couplings from the effective Lagrangian, together with the η-η' mixing parameters from the two-mixing-angle scheme, are fitted to a large number of experimental data, including the various decay widths and the form factors. With the phenomenological mixing parameters and the lattice simulation data of the masses and decay constants of the light pseudoscalar mesons as inputs, a next-to-next-to-leading order study is performed of the η-η' mixing system in $U(3)$ chiral perturbation theory. Updated values of the relevant low energy constants are obtained.

Key words: chiral Lagrangian; η and η' mixing

CLC number: O572.3 **Document code**: A doi:10.3969/j.issn.0253-2778.2016.06.008

Citation: GUO Zhihui. Combined study of the η and η' mesons: Phenomenology, chiral extrapolation of lattice QCD and effective field theory[J]. Journal of University of Science and Technology of China, 2016,46(6): 494-501.
郭志辉. 物理的唯象学和格点手征延拓研究[J]. 中国科学技术大学学报,2016,46(6): 494-501.

物理的唯象学和格点手征延拓研究

郭志辉[1,2]

(1. 河北师范大学物理科学与信息工程学院, 河北石家庄, 050024)
(2. 中国科学院理论物理所,理论物理国家重点实验室, 北京, 100190)

摘要:首先在有效场论框架下对η和η'唯象学进行了全面的研究,主要包括两种类型的衰变过程:一种是只含有轻味强子的过程; 另一种是有J/ψ参与的反应过程. 通过拟合大量相关的衰变宽度和形状因子的实验数据,我们确定了有效拉氏量中自由参数的取值,同时也给出了双混合角机制下的η-η'混合参数. 结合通过实验数据定出的混合参数以及格点量子色动力学数值模拟给出的轻赝标介子质量和衰变常数,我们在$U(3)$手征微扰理论框架下对η-η'混合进行了次次领头阶的分析,并给出了更新的低能耦合常数的数值.

关键词:手征有效场论; η-η'混合

Received:2015-11-30; **Revised**:2016-04-20

Foundation item: Supported by National Natural Science Foundation of China (U1232105), Ministry of Science and Technology (2015CB856700).

Biography: GUO Zhihui (corresponding author), Professor/PhD. Research field: high energy physics. E-mail: zhguo@mail.hebtu.edu.cn

0 Introduction

The light-flavor η and η' mesons provide a valuable window to study many important nonperturbative properties of Quantum Chromodynamics (QCD), including the spontaneously chiral symmetry breaking, the mechanism of explicit breaking of $SU(3)$-flavor symmetry and the $U(1)_A$ anomaly of strong interactions.

There are many experimental collaborations that have measured or planned to measure the physical processes with the η or η' mesons, with high precision and high statistics, such as BES Ⅲ[1-2], Jefferson Lab[3-4], KLOE[5], CELSIUS/WASA[6], CBELSA/TAPS[7] and CMD-2[8]. On the other hand, lattice QCD simulations have greatly progressed on the η and η' mesons and many precise simulation data have been released[9-13].

We have performed a thorough analysis of the radiative decay processes involving the η or η' and light-flavor vector resonances within the framework of resonance chiral theory ($R\chi T$) in Ref.[14]. In the following sections, we extend the discussions to study the decay processes of $J/\psi \to VP$, $P\gamma^{(*)}$, with V denoting the light-flavor vectors and P the light pseudoscalar mesons[15]. The two-mixing-angle scheme for the η-η' system is used in these phenomenological discussions, and precise values of the four mixing parameters are extracted from the experimental data. Together with the phenomenological determinations of mixing parameters and the lattice simulation data as inputs, we have then carried out the next-to-next-to-leading order(NNLO) study of the η-η' mixing within the $U(3)$ chiral perturbation theory (χPT). The phenomenological inputs and lattice simulations are successfully reproduced, with reasonable values of low energy constants(LECs)[16]. In this paper, we briefly review the works in Refs. [14-16].

1 Theoretical formalism for the decay processes

1.1 Radiative processes with light-flavor hadrons

To describe the dynamics between the light psuedoscalar mesons and the light-flavor vector resonances, we use the relevant chiral Lagrangian from $R\chi T$ to calculate the decay widths and form factors. We simply elaborate the pertinent chiral Lagrangians in the following. The kinetic terms for the light vector resonances read

$$\mathscr{L}_{\rm kin}(V) = -\frac{1}{2}\left(\nabla^{\lambda}V_{\lambda\mu}\nabla_{\nu}V^{\nu\mu} - \frac{M_V^2}{2}V_{\mu\nu}V^{\mu\nu}\right) \quad (1)$$

with $V^{\nu\mu}$ denoting the vector octet plus singlet described in the anti-symmetric tensor formalism[17]. The transitions between the vectors and the photon are governed by the operator[17].

$$\mathscr{L}_2(V) = -\frac{F_V}{2\sqrt{2}}\left(V_{\mu\nu} - \tilde{f}_+^{\mu\nu}\right) \quad (2)$$

where $\tilde{f}_+^{\mu\nu}$ contain the external source fields. We are only interested in the photon field in this work. The VJP operators with one vector field, one external source and one light pseudoscalar, including the singlet η_0 state, read[14,18].

$$\begin{aligned}\mathscr{L}_{\rm VJP} = {} & \frac{\tilde{c}_1}{M_V}\varepsilon_{\mu\nu\rho\sigma}\langle\{V^{\mu\nu},\tilde{f}_+^{\rho\alpha}\}\nabla_{\alpha}\tilde{u}^{\sigma}\rangle + \\ & \frac{\tilde{c}_2}{M_V}\varepsilon_{\mu\nu\rho\sigma}\langle\{V^{\mu\alpha},\tilde{f}_+^{\rho\sigma}\}\nabla_{\alpha}\tilde{u}^{\nu}\rangle + \\ & \frac{i\tilde{c}_3}{M_V}\varepsilon_{\mu\nu\rho\sigma}\langle\{V^{\mu\nu},\tilde{f}_+^{\rho\sigma}\}\tilde{\chi}_-\rangle + \\ & \frac{i\tilde{c}_4}{M_V}\varepsilon_{\mu\nu\rho\sigma}\langle V^{\mu\nu}[\tilde{f}_-^{\rho\sigma},\tilde{\chi}_+]\rangle + \\ & \frac{\tilde{c}_5}{M_V}\varepsilon_{\mu\nu\rho\sigma}\langle\{\nabla_{\alpha}V^{\mu\nu},\tilde{f}_+^{\rho\alpha}\}\tilde{u}^{\sigma}\rangle + \\ & \frac{\tilde{c}_6}{M_V}\varepsilon_{\mu\nu\rho\sigma}\langle\{\nabla_{\alpha}V^{\mu\alpha},\tilde{f}_+^{\rho\sigma}\}\tilde{u}^{\nu}\rangle + \\ & \frac{\tilde{c}_7}{M_V}\varepsilon_{\mu\nu\rho\sigma}\langle\{\nabla^{\sigma}V^{\mu\nu},\tilde{f}_+^{\rho\alpha}\}\tilde{u}^{\alpha}\rangle - \\ & i\tilde{c}_8 M_V\sqrt{\frac{2}{3}}\varepsilon_{\mu\nu\rho\sigma}\langle V^{\mu\nu}\tilde{f}_+^{\rho\sigma}\rangle\ln(\det\tilde{u}) \end{aligned} \quad (3)$$

where the light pseudoscalar multiplet is incorporated in the $\tilde{u}_{\mu}$, $\tilde{u}$ and $\chi_{\pm}$ fields. The VVP types of effective Lagrangian involving η_0 read[14,18].

$$\begin{aligned}\mathscr{L}_{\rm VVP} = {} & \tilde{d}_1\varepsilon_{\mu\nu\rho\sigma}\langle\{V^{\mu\nu},V^{p\alpha}\}\nabla_{\alpha}\tilde{u}^{\sigma}\rangle + \\ & i\tilde{d}_2\varepsilon_{\mu\nu\rho\sigma}\langle\{V^{\mu\nu},V^{p\alpha}\}\tilde{\chi}_-\rangle + \\ & \tilde{d}_3\varepsilon_{\mu\nu\rho\sigma}\langle\{\nabla_{\alpha}V^{\mu\nu},V^{p\alpha}\}\tilde{u}^{\sigma}\rangle + \\ & \tilde{d}_4\varepsilon_{\mu\nu\rho\sigma}\langle\{\nabla^{\sigma}V^{\mu\nu},V^{p\alpha}\}\tilde{u}^{\alpha}\rangle - \\ & i\tilde{d}_5 M_V^2\sqrt{\frac{2}{3}}\varepsilon_{\mu\nu\rho\sigma}\langle V^{\mu\nu},V^{p\alpha}\rangle\ln(\det\tilde{u}) \end{aligned} \quad (4)$$

In addition, the relevant part of the Wess-Zumino-Witten Lagrangian is

$$\mathscr{L}_{WZW} = \frac{\sqrt{2}N_C}{8\pi^2 F}\varepsilon_{\mu\nu\rho\sigma}(\Phi\partial^\mu v^\nu \partial^\rho v^\sigma) \tag{5}$$

We refer to Refs. [14, 17-18] for further details about the previous Lagrangians. We then calculate the transition amplitudes, depicted by the Feynman diagrams shown in Figs. 1 and 2. With these transition amplitudes, it is straightforward to get the experimentally observed form factors and decay widths[14].

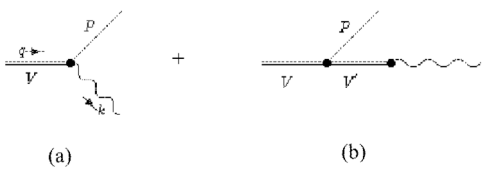

Fig. 1 Feynman diagrams for the $VP\gamma^{(*)}$ types of processes

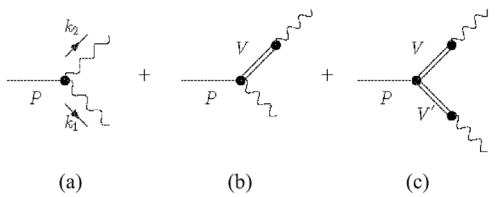

Fig. 2 Feynman diagrams for the $P\gamma\gamma^{(*)}$ types of processes

Before ending this section, we elaborate one more detail about the two-mixing-angle scheme to treat the η and η' mesons. The light pseudoscalar octet plus singlet mesons are incorporated in the $\tilde{u}$ field in the previous Lagrangians and we take the following two-mixing-angle formalism when calculating the amplitudes with η or η' states

$$\begin{pmatrix}\eta\\ \eta'\end{pmatrix} = \frac{1}{F}\begin{pmatrix}F_8\cos\theta_8 & -F_0\sin\theta_0\\ F_8\sin\theta_8 & F_0\cos\theta_0\end{pmatrix}\begin{pmatrix}\eta_s\\ \eta_0\end{pmatrix} \tag{6}$$

where η_0 and η_s stand for the $SU(3)$-flavor singlet and octet states, respectively, and η, η' denote the physical states. The four mixing parameters F_0, F_8, θ_0 and θ_8 will be fitted to experimental data.

1.2 Calculation of the $J/\psi\to VP$, $P\gamma^{(*)}$ amplitudes

In this part, we introduce the effective Lagrangian describing the dynamics of the $J/\psi\to VP$ and $P\gamma^{(*)}$ decays. Both the strong and the electromagnetic (EM) interactions will enter into these decays. We include three terms to describe the strong interactions in the $J/\psi\to VP$ decays

$$\begin{aligned}\mathscr{L}_{\psi VP} &= M_\psi h_1 \varepsilon_{\mu\nu\rho\sigma}\psi^\mu\langle\tilde{u}^\nu V^{\rho\sigma}\rangle +\\ &\frac{1}{M_\psi}h_2\varepsilon_{\mu\nu\rho\sigma}\psi^\mu\langle\{\tilde{u}^\nu, V^{\rho\sigma}\}\tilde{\chi}_+\rangle +\\ &M_\psi h_3\varepsilon_{\mu\nu\rho\sigma}\psi^\mu\langle\tilde{u}^\nu\rangle\langle V^{\rho\sigma}\rangle\end{aligned} \tag{7}$$

Notice that proper M_ψ factors are introduced in the previous equation in order to make the couplings $h_{i=1,2,3}$ dimensionless.

Two effective operators are constructed to describe the $J/\psi P\gamma^{(*)}$ interaction

$$\begin{aligned}\mathscr{L}_{\psi P\gamma} &= g_1\varepsilon_{\mu\nu\rho\sigma}\psi^\mu\langle\tilde{u}^\nu\tilde{f}_+^{\rho\sigma}\rangle +\\ &\frac{1}{M_\psi^2}g_2\varepsilon_{\mu\nu\rho\sigma}\psi^\mu\langle\{\tilde{u}^\nu,\tilde{f}_+^{\rho\sigma}\}\tilde{\chi}_+\rangle\end{aligned} \tag{8}$$

The transition strength between the J/ψ and the photon field reads

$$\mathscr{L}_2^\psi = \frac{-1}{2\sqrt{2}}\frac{f_\psi}{M_\psi}\langle\hat{\psi}_{\mu\nu}\tilde{f}_+^{\mu\nu}\rangle \tag{9}$$

with $\hat{\psi}_{\mu\nu} = \partial_\mu\psi^\nu - \partial_\nu\psi^\mu$.

Together with these effective Lagrangians and also the ones given in Sect. 1.1, we can calculate the $J/\psi\to P\gamma^{(*)}$ and VP amplitudes. The pertinent Feynman diagrams are depicted in Figs. 3 and 4.

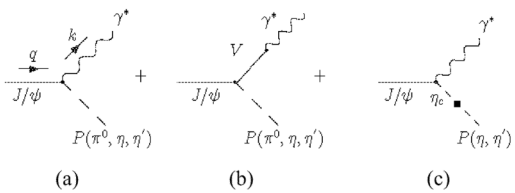

Fig. 3 Relevant Feynman diagrams for the $J/\psi\to P\gamma^*$ decays

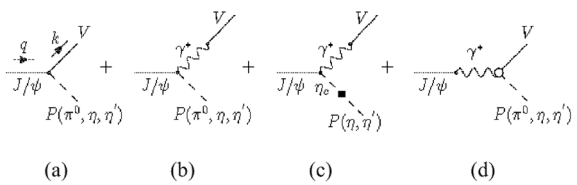

Fig. 4 Relevant Feynman diagrams for the $J/\psi\to VP$ decays

In order to reasonably reproduce the experimental results of the $J/\psi\to\eta'\gamma$ decay widths, it is necessary

to include the mechanism depicted by the Fig. 3(c), i. e. to consider the contribution from the charmonium η_c and also the mixing between η_c and η'[19]. The decay widths and form factors can be easily obtained with the transition amplitudes corresponding to Figs. 3 and 4. We refer to Ref. [15] for further details.

2 Phenomenological discussions

We consider a large amount of experimental data in our work, including the available decay widths of $P\to V\gamma$, $V\to P\gamma$, $P\to\gamma\gamma$, $P\to\gamma l^+ l^-$, $V\to Pl^+ l^-$, $J/\psi\to P\gamma$ and $J/\psi\to VP$[20], with $P=\pi$, K, η, η' and $V=\rho$, K^*, ω, φ. In addition, the form factors of $J/\psi\to\eta'\gamma^*$, $\eta\to\gamma\gamma^*$, $\eta'\to\gamma\gamma^*$, $\varphi\to\eta\gamma^*$ will be also taken into account. We will make a global fit by including all of these data.

Before presenting our fit results, we point out that with the theoretical formalism in Sect. 1 alone it is impossible for us to reasonably reproduce the $J/\psi\to\omega\pi^0$ decay width. We simply include the excited vector ρ' in this channel to perform the fits[15].

A rather good reproduction of the experimental data in our global fit is achieved, with the χ^2/d. o. f close to one. The final results for the form factors of $J/\psi\to\eta'\gamma^*$, $\eta\to\gamma\gamma^*$ and $\eta'\to\gamma\gamma^*$ are given in Figs. 5, 6 and 7, respectively. Due to the large experimental error bars, the $\varphi\to\eta'\gamma^*$ form factor barely plays any important role in the fits and we do not explicitly show the result for this channel[14-15].

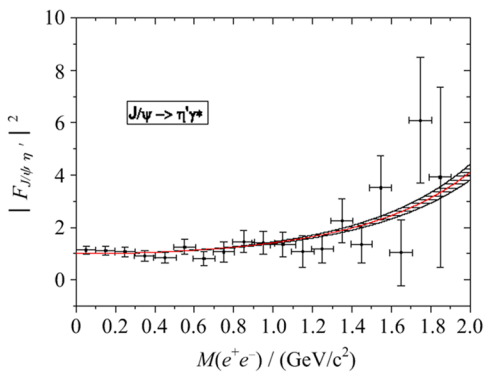

Fig. 5　The $J/\psi\to\eta'\gamma^*$ form factors

The solid (middle) line denotes our central results and the shaded areas represent the error bands at one-sigma level. The data are taken from Ref. [21].

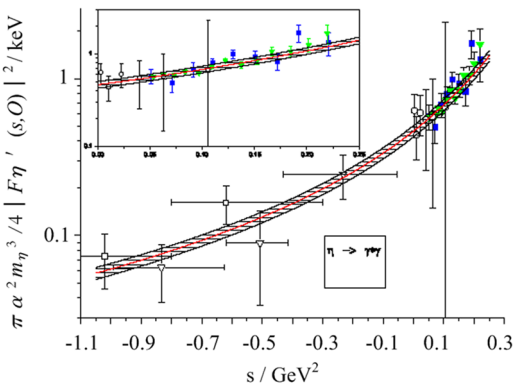

Fig. 6　The $\eta\to\gamma\gamma^*$ form factors

The solid (middle) line denotes our central values and the shaded areas represent the error bands at one-sigma level. The experimental data are taken from Refs. [22-27]. We clearly show the curve in the timelike region of $s>0$ in the framed figure.

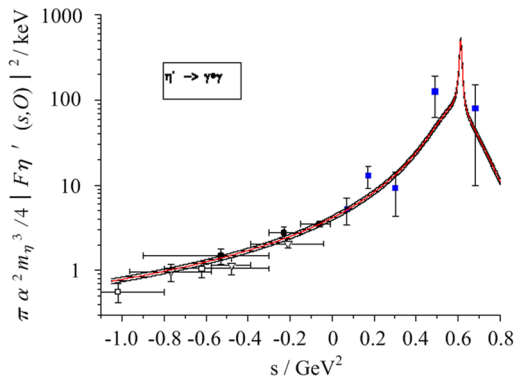

Fig. 7　The $\eta'\to\gamma\gamma^*$ form factors

The solid (middle) line denotes our central results and the shaded areas represent the error bands at one-sigma level. The experimental data are taken from Refs. [24-28].

In Tab. 1, we give the fitted values for the four mixing parameters defined in Eq. 6. In order to highlight the influence of the J/ψ data on the determination of the η-η' mixing, we explicitly show two different fit results. In the global fit, we include all of the previously mentioned experimental data, while in the partial fit situation only the data involving the light-flavor hadrons are taken into account.

Although the values of the mixing parameters from the two fits are compatible, the error bars after including the J/ψ data are clearly smaller than those with only the light-flavor data. Therefore one can conclude that the $J/\psi \to VP$, $P\ \gamma^*$ decays are important for constraining theη-η' mixing. For the remaining fitted parameters, we refer to Ref. [15] for details.

Tab. 1 Mixing parameters from the fits

parameter	global fit	partial fit
F_8/MeV	133.7 ±3.7	126.3 ±6.5
F_0/MeV	118.0 ±5.5	109.7 ±16.6
θ_8	$(-26.7 \pm 1.8)^\circ$	$(-21.1 \pm 6.0)^\circ$
θ_0	$(-11.0 \pm 1.0)^\circ$	$(-2.5 \pm 8.2)^\circ$

Next we analyze the different mechanisms that contribute to the $J/\psi \to Pl^+l^-$ processes. According to the Feynman diagrams in Fig. 3, there are three different kinds of contributions: The contact interacting vertex, the light-vector-resonance exchanges and the η_c-η' mixing. The effects from the intermediate vectors like $J/\psi \to \rho^0 P$, ωP and φP, with ρ^0, ω and φ decaying into the lepton pairs, have been removed when doing experimental analyses for the $J/\psi \to P\ e^+\ e^-$ decays in Ref. [21]. In order to be consistent with the experimental setups, we also drop the Fig. 3 (b) when fitting to the data. Nevertheless, we point out that it is a priori not justified to neglect the contributions from the intermediate light vectors in the $J/\psi \to Pl^+l^-$ decays. We have made a rough estimate that the light vectors can contribute around 30% in the $J/\psi \to \pi^0\ e^+\ e^-$ decay[13], which qualitatively agrees with the findings in Refs. [29-31]. In our case, large destructive interference between the ρ^0 exchange and other mechanisms in the $J/\psi \to \pi^0\gamma$ are observed. As a result, a larger value of the branching ratio of the $J/\psi \to \pi^0\ e^+\ e^-$ is predicted after neglecting the contributions from the intermediate ρ^0 resonance. So it is meaningful and important to make a revised experimental analysis on the $J/\psi \to \pi^0\ e^+\ e^-$ decays by keeping all of the contributions, instead of removing parts of them. In contrast, the contributions from the intermediate light vectors turn out to be negligible in the $J/\psi \to \eta'\gamma$ decay processes. The branching ratios for the $J/\psi \to P\ l^+l^-$ are summarized in Tab. 2.

Tab. 2 Branching ratios ($\times 10^{-5}$) for the $J/\psi \to Pl^+l^-$ decays

type	Exp	our results
$\psi \to \pi^0\ e^+\ e^-$	0.0756 ±0.0141	0.1191 ±0.0138
$\psi \to \eta\ e^+\ e^-$	1.16 ±0.09	1.16 ±0.08
$\psi \to \eta'\ e^+\ e^-$	5.81 ±0.35	5.76 ±0.16
$\psi \to \pi^0\ \mu^+\ \mu^-$	–	0.0280 ±0.0032
$\psi \to \eta\ \mu^+\ \mu^-$	–	0.32 ±0.02
$\psi \to \eta'\ \mu^+\ \mu^-$	–	1.46 ±0.04

Another interesting subject is to analyze the roles of the strong and EM interactions in the $J/\psi \to VP$ decays. In our theoretical formalism, the strong interaction is depicted by the Fig. 4 (a), while the other diagrams correspond to the EM interactions. We confirm that the EM interactions play the dominant roles in the isospin violated decay channels, such as $J/\psi \to \rho^0\eta'$, and $\omega\pi^0$, and the strong interactions dominate in the isospin conserved channels, such as $J/\psi \to \rho\pi$, $\omega\eta'$, $\varphi\eta'$, $K^{*+}K^-$ and $K^{*0}\bar{K}^0$.

3 Chiral extrapolation of the η and η' masses

Previously when addressing the η-η' mixing, we simply adopted the two-mixing-angle scheme in Eq. (6) and do not give any further explanation to derive the formalism. Next we shall use the $U(3)\chi PT$ as an underlying theory to calculate the η-η' mixing pattern. In order to establish a consistent power counting, the simultaneous expansions on the momentum squared, light-quark masses and $1/N_C$, which will be denoted as δ expansion, need to be introduced into $U(3)\chi PT$. Up to NNLO in δ expansion, the pertinent chiral Lagrangians read

$$\mathscr{L}^{(\delta^0)} = \frac{F^2}{4}\langle u_\mu u^\mu\rangle + \frac{F^2}{4}\langle\chi_+\rangle + \frac{F^2}{12}M_0^2X^2 \quad (10)$$

$$\mathscr{L}^{\delta} = L_5\langle u^\mu u_\mu\chi_+\rangle + \frac{L_8}{2}\langle\chi_+\chi_+ + \chi_-\chi_-\rangle + \frac{F^2\Lambda_1}{12}D^\mu X D_\mu X - \frac{F^2\Lambda_2}{12}X\langle\chi_-\rangle \quad (11)$$

$$\mathscr{L}^{(\delta^2)} = \frac{F^2 v_2^{(2)}}{4}X^2\langle\chi_+\rangle + L_4\langle u^\mu u_\mu\rangle\langle\chi_+\rangle + L_6\langle\chi_+\rangle\langle\chi_+\rangle + L_7\langle\chi_-\rangle\langle\chi_-\rangle + L_{18}\langle u_\mu\rangle\langle u^\mu\chi_+\rangle + L_{25}X\langle\chi_+\chi_-\rangle + C_{12}\langle h_{\mu\nu}h^{\mu\nu}\chi_+\rangle + C_{14}\langle u_\mu u^\mu\chi_+\chi_+\rangle + C_{17}\langle u_\mu\chi_+\ u^\mu\chi_+\rangle + C_{19}\langle\chi_+\chi_+\chi_+\rangle + C_{31}\langle\chi_-\chi_-\chi_+\rangle \quad (12)$$

With these chiral Lagrangians, one can then calculate the η-η' mixing pattern and express the mixing parameters in Eq. (6) in terms of the chiral LECs in Eqs. (10), (11) and (12). Due to the lengthy formulas, we refer to Ref. [16] for further details about the relations between the mixing parameters and LECs.

One of the biggest challenges when calculating the η-η' mixing pattern in $U(3)\chi PT$ is to determine the many unknown LECs. The precise lattice simulations of the light pseudoscalar mesons are valuable to constrain the values of the unknown LECs. We shall include in our fits the m_π dependence of the η and η' masses[9-13], the kaon masses[32-33], the π, K decay constants[32-33] and their ratios[34]. The previously determined phenomenological results of the η-η' mixing parameters will be also used to constrain these LECs.

It is interesting to mention that even at leading order the $U(3)\chi PT$, which only has one free parameter, can reasonably reproduce the lattice simulation data, as shown in Fig. 8 (The lattice simulation data are from Refs. [9-13]). While in order to simultaneously describe the lattice simulations on the light pseudoscalar mesons, specially the pion and kaon decay constants, it is essential to include the NNLO contributions. Among the NNLO LECs in Eq. (12), we fix $v_2^{(2)}$, L_{18}, L_{25} to zero, due to their marginal effects in our present discussion. While for the poorly known $\mathcal{O}(p^6)$ LECs C_i, we multiply the values of C_i from Refs. [35-36] by a common factor α in our fits. We find that two different sets of values from Refs. [35-36] lead to more or less similar results. Therefore, we only present the NNLO fit results by taking the values of C_i from Ref. [36] in Tab. 3. The values obtained here are compatible with the recent two-loop determinations of the next-to-leading order LECs[37]. The NNLO reproduction of the lattice simulation data is quite successful[16] and therefore the $U(3)$ chiral perturbation theory can be considered as a useful tool to perform the chiral extrapolation of the lattice data for the light pseudoscalars.

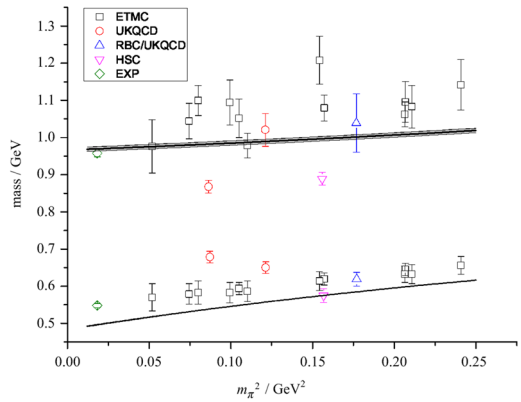

Fig. 8　The LO fit of the η and η' masses

Tab. 3　The values of the parameters from the NNLO fits by taking the $\mathcal{O}(p^6)$ LECs from Ref. [36]

parameter	numerical value
F_8/MeV	$81.7 \pm 1.5 \pm 5.3$
$10^3 \times L_5$	$0.60 \pm 0.11 \pm 0.52$
$10^3 \times L_8$	$0.25 \pm 0.07 \pm 0.31$
Λ_1	$-0.003 \pm 0.060 \pm 0.19$
Λ_2	$0.08 \pm 0.11 \pm 0.20$
$10^3 \times L_4$	$-0.12 \pm 0.06 \pm 0.19$
$10^3 \times L_6$	$-0.05 \pm 0.04 \pm 0.02$
$10^3 \times L_7$	$0.26 \pm 0.05 \pm 0.06$
α	$0.59 \pm 0.09 \pm 0.18$

4　Conclusion

With the effective Lagrangian approach, we have made a comprehensive study of the processes involving η or η' mesons, including the radiative decays with light-flavor hadrons, such as the types of $VP\gamma^*$, $P\gamma\gamma^*$, and also the $J/\psi \to P\gamma^*$ and VP decays, with $P = \pi$, K, η, η' and $V = \rho$, K^*, ω, φ. The modern recipe of the two-mixing-angle scheme was used to describe the η and η' mesons. We made a global fit by considering a large amount of the experimental data. Reliable values of the η-η' mixing parameters, together with the resonance couplings from the effective Lagrangian, have been determined. We pointed out that the contributions from the intermediate light vectors in the $J/\psi \to \pi^0\ \gamma$ and $J/\psi \to \pi^0\ l^+ l^-$ decays, with $l = e$, μ, are important. Therefore a future revised experimental measurement is crucial to the verification of this mechanism.

We further calculate the η-η' mixing pattern from the underlying $U(3)$ chiral perturbation theory. And the four mixing parameters were expressed in terms of the chiral low energy constants. By including the lattice simulation data of the masses of η, η' and kaon, and the pion and kaon decay constants, we carried out a next-to-next-to-leading order study and determine the relevant chiral low energy constants, which are consisten with the recent two-loop results. We conclude that the $U(3)$ chiral perturbation theory can provide a useful tool to perform the chiral extrapolations of the lattice QCD data for the light pseudoscalar mesons.

References

[1] LI H B. η and η' Physics at BES-Ⅲ[J]. Journal of Physics, 2009, 36(8): 85009-85017.

[2] ZHANG Z Y, QIN L Q, FANG S S. Event generators for η/η' rare decays into $\pi^+\pi^- l^+ l^-$ and $e^+e^-\mu^+\mu^-$[J]. Chinese Physics C, 2012, 36(10): 926-931.

[3] FANGS S. η and η' Physics at BES Ⅲ[C]// The 7th International Workshop on Chiral Dynamics. Virginia, 2012: Pos (CD12) 036(1-6).

[4] GAN L P, GASPARIAN A. Search of new physics via eta rare decays[C]// Proceedings of the 6th International Workshop on Chiral Dynamics. Bern, Switzerland. 2009: 048(PoS CD 09).

[5] AMELINO-CAMELIAG, ARCHILLI F, BADONI D, et al. Physics with the KLOE-2 experiment at the upgraded DAφNE[J]. European Physics Journal C, 2010, 68(3-4): 619-681.

[6] BERLOWSKI M, BARGHOLTZ C, BASHKANOV M, et al. Measurement of eta meson decays into lepton-antilepton pairs[J]. Arxiv Cornell University Library, 2007, 77(3): 591-609.

[7] CREDE V, METAG V, SARANTSEV A V, et al. Photoproduction of η and η' mesons off protons[J]. Physical Review C, 2009, 80: 055202.

[8] AKHMETSHIN R R, ANASKIN E V, ARPAGAUS M, et al. Study of conversion decays $\varphi\to\eta e^+e^-$, $\eta\to e^+e^-\gamma$ and $\eta\to\pi^+\pi^- e^+e^-$ at CMD-2[J]. Physics Letter B, 2001, 501(3): 191.

[9] DUDEK J J, EDWARDS R G, JOO B, et al. Isoscalar meson spectroscopy from lattice QCD[J] Physical Review D, 2011, 83(11): 2437-2459.

[10] CHRIST N H, DAWSON C, IZUBUCHI T, et al. The η and η' mesons from lattice QCD[J]. Physical Review Letters, 2010, 105(1): 7-12.

[11] GREGORYE B, IRVING A C, RICHARDS C M, et al. A study of the η and η' mesons with improved staggered fermions[J]. Physical Review D, 2012, 86(1): 014504 (1-9).

[12] OTTNAL K, URBACH C, MICHAEL C. η and η' masses and decay constants from lattice QCD with $N_f = 2+1+1$ quark flavours[C]// Proceedings of 31st International Symposium on Lattice Field Theory. Mainz, Germany, 2013: 253-266.

[13] MICHAEL C, OTTNAL K, URBACH C, et al. η and η' mixing from lattice QCD[J]. Physical Review Letters, 2013, 111(18): 181602.

[14] CHEN Y H, GUO Z H, ZHENG H Q. Study of η-η' mixing from radiative decay processes[J]. Physical Review D, 2012, 85(5): 054018.

[15] CHEN Y H, GUO Z H, ZOU B S. Unified study of $J/\psi\to PV$, $P\gamma^*$ and light hadron radiative processes[J]. Physical Review D, 2015, 91(1): 014010.

[16] GUO X K, GUO Z H, Oller J A, et al. Scrutinizing the η-η' mixing, masses and pseudoscalar decay constants in the framework of $U(3)$ chiral effective field theory[J]. Journal of High Energy Physics, 2015, 6(2): 197-204.

[17] ECKER G, GASSER J, PICH A, et al. The role of resonances in chiral perturbation theory[J]. Nuclear Physics B, 1989, 321(12): 311-342.

[18] RUIZ-FEMENÍA P D, PICH A, PORTOLÉS J. Odd intrinsic parity processes within the resonance effective theory of QCD[J]. Journal of High Energy Physics, 2003, (7): 003(1-18).

[19] CHAO K T. Mixing of η, η' with c overline c, b overline b states and their radiative decays[J]. Nuclear Physics B, 1990, 335(1): 101-114.

[20] KLEIN S R, SARKAR S. Review of particle physics[J]. Chinese Physics C, 2014, 38(1): 594-602.

[21] ABLIKIM M, ACHASOV M N, AI X C, et al. Observation of electromagnetic Dalitz decays $J/\psi\to Pe^+e^-$[J]. Physical Review D, 2014, 89(9): 092008(1-10).

[22] ARNALDI R, BANICZ K, CASTOR J, et al. Study of the electromagnetic transition form-factors in $\eta\to\mu^+\mu^-\gamma$ and $\omega\to\mu^+\mu^-\pi^0$ decays with NA60[J]. Physics Letters B, 2009, 677(5): 260-266.

[23] ACHASOV M N, AULCHENKO V M, BELOBORODOV K I, et al. Study of conversion decays $\varphi\to\eta e^+e^-$ *and* $\eta\to\gamma e^+e^-$ in the experiment with SND detector at the VEPP-2M collider[J]. Physics Letters B, 2001, 504 (4): 275-281.

[24] DZHELYADIN R I, GOLOVKIN S V, KACHANOV V A, et al. Investigation of the electromagnetic structure of

the η meson in the decay $\eta\to\mu^+\mu^-\gamma$[J]. Physics Letters B, 1980, 94(4): 548-550.

[25] DZHELYADIN R I, GOLOVKIN S V, GRITZK M V, et al. Observation of $\eta'\to\mu^+\mu^-\gamma$ decay[J]. Physics Letters B, 1979, 88(3-4): 379-380.

[26] AIHARA H, ALSTONGARNJOST M, AVERY R E, et al. Investigation of the electromagnetic structure of η and η' mesons by two photon interactions [J]. Physical Review Letters, 1990, 64(2): 172-175.

[27] BEHREND H J, CRIEGEE L, FIELD J H, et al. A measurement of the π^0, η and η' electromagnetic form-factors[J]. Zeitschrift Für Physik C, 1991, 49(3): 401-409.

[28] ACCIARRI M, ADRIANI O, AGUILAR-BENITEZ M, et al. Measurement of η' (958) formation in two photon collisions at LEP-1[J]. Physics Letters B, 1998, 418(3-4): 399-410.

[29] KUBIS B, NIECKNIG F. Analysis of the $J/\psi\to\pi^0\gamma^*$ transition form factor[J]. Physical Review D, 2015, 32(2): 5-28.

[30] ROSNER J L. Meson-photon transition form factors in the charmonium energy range[J]. Physical Review D, 2009, 79(9): 27-35.

[31] ZHAO Q. Understanding the radiative decays of vector charmonia to light pseudoscalar mesons [J]. Physics Letters B, 2011, 697(1): 52-57.

[32] AOKI Y, ARTHUR R, BLUM T, et al. Continuum limit physics from 2 + 1 flavor domain wall QCD[J]. Physical Review D, 2011, 83(7): 074508(1-129).

[33] ARTHUR R, BLUM T, BOYLE P A, et al. Domain wall QCD with near-physical pions[J]. Physical Review D, 2012, 87(9): 599-614.

[34] DURRS, FODOR Z, HOELBLING C, et al. The ratio FK/F_π in QCD [J]. Physical Review D, 2010, 81: 054507(1-15).

[35] JIANG S Z, ZHANG Y, LI C, et al. Computation of the p^6 order chiral Lagrangian coefficients [J]. Physical Review D, 2010, 81(1): 252-255.

[36] JIANGS Y, WEI Z L, CHEN Q S, et al. Computation of the $\mathcal{O}(p^6)$ order low-energy constants: An update[J]. Physical Review D, 2015, 92(2): 025014(1-30).

[37] BIJNENS J, ECKER G. Mesonic low-energy constants [J]. Annual Review of Nuclear & Particle Science, 2014, 64: 149-174.

Article ID:0253-2778(2016)06-0502-05

Study of $e^+e^- \to K^+K^-\eta$ process with the CMD-3 detector at VEPP-2000 collider

IVANOV V. L.[1,2], AMIRKHANOV A. N.[1,2], ANISENKOV A. V.[1,2], AULCHENKO V. M.[1,2], BANZAROV V. S.[1], BASHTOVOY N. S.[1], BERKAEV D. E.[1], BONDAR A. E.[1,2], BRAGIN A. V.[1], EIDELMAN S. I.[1,2], EPIFANOV D. A.[1], EPSHTEYN L. B.[1,2,3], EROFEEV A. L.[1,2], FEDOTOVICH G. V.[1,2], GAYAZOV S. E.[1,2], GREBENUK A. A.[1,2], GRIBANOV S. S.[1,2], GRIGORIEV D. N.[1,4], IGNATOV F. V.[1], KARPOV S. V.[1], KAZANIN V. F.[1], KOROBOV A. A.[1,2], KOVALENKO O. A.[1,2], KOZYREV A. N.[1], KOZYREV E. A.[1,2], KROKOVNY P. P.[1,2], KUZMENKO A. E.[1,2], KUZMIN A. S.[1], LOGASHENKO I. B.[1,2], LUKIN P. A.[1,2], MIKHAILOV K. YU.[1,2], OKHAPKIN V. S.[1], PESTOV YU. N.[1], POPOV A. S.[1,2], RAZUVAEV G. P.[1,2], RUBAN A. A.[1], RYSKULOV N. M.[1], RYZHENENKOV A. E.[1,2], SHEBALIN V. E.[1], SHEMYAKIN D. N.[1,2], SHWARTZ B. A.[1,2], SIBIDANOV A. L.[4], SHATUNOV YU. M.[1], SOLODOV E. P.[1,2], TITOV V. M.[1], TALYSHEV A. A.[1,2], VOROBIOV A. I.[1], YUDIN YU. V.[1,2]

(1. *Budker Institute of Nuclear Physics*, *Novosibirsk* 630090, *Russia*; 2. *Novosibirsk State University*, *Novosibirsk* 630090, *Russia*; 3. *Novosibirsk State Technical University*, *Novosibirsk* 630092, *Russia*; 4. *Falkiner High Energy Physics Department*, *University of Sydney*, *Australia*)

Abstract: The results of the study of $e^+e^- \to K^+K^-\eta$ process with the CMD-3 detector are reported. The analysis is based on an integrated luminosity of 22 pb^{-1} collected by the CMD-3 in 2011-2012. It was established that only $\phi(1020)\eta$ intermediate state can be recognized at the current level of CMD-3 statistics. The cross section of $e^+e^- \to \phi(1020)\eta$ process was measured at 30 center-of-mass energy points in the range from 1.59 up to 2.0 GeV. The η meson was treated as a recoil particle and all the modes of η decay were used. A total of 1454 ± 48 events of signal process were selected. The measured cross section was approximated according to vector meson dominance model as a sum of $\phi(1680)$ and nonresonant amplitudes, and the preliminary results for $\phi(1680)$ meson parameters have been obtained.

Key words: hadrons; signal/background separation; cross section

CLC number: O572.3 **Document code**: A doi:10.3969/j.issn.0253-2778.2016.06.009

Citation: IVANOV V L, AMIRKHANOV A N, ANISENKOV A V, et al. Study of $e^+e^- \to K^+K^-\eta$ process with the CMD-3 detector at VEPP-2000 collider[J]. Journal of University of Science and Technology of China, 2016, 46(6): 502-506.

IVANOV V L, AMIRKHANOV A N, ANISENKOV A V, 等. 用 CMD-3 谱仪研究 VEPP-2000 对撞机上的 $e^+e^- \to K^+K^-\eta$ 过程[J]. 中国科学技术大学学报,2016, 46(6): 502-506.

Received: 2015-11-30; **Revised**: 2016-04-20

Foundation item: Supported in Part by the Russian Science Foundation (14-50-00080), Russian Foundation for Basic Research (RFBR 13-02-00215-a, RFBR 13-02-01134-a, RFBR 14-02-00580-a, RFBR 14-02-31275-mol-a, RFBR 14-02-00047-a, RFBR 14-02-31478-mol-a, RFBR 14-02-91332, RFBR 15-02-0567).

Biography: VANOV V. L. (corresponding author), PhD. Research field: electro-positron annihilation into hadrons. E-mail: vyacheslav_lvovich_ivanov@mail.ru

用 CMD-3 谱仪研究 VEPP-2000 对撞机上的 $e^+e^-\to K^+K^-\eta$ 过程

IVANOV V. L.[1,2], AMIRKHANOV A. N.[1,2], ANISENKOV A. V.[1,2], AULCHENKO V. M.[1,2], BANZAROV V. S.[1], BASHTOVOY N. S.[1], BERKAEV D. E.[1], BONDAR A. E.[1,2], BRAGIN A. V.[1], EIDELMAN S. I.[1,2], EPIFANOV D. A.[1], EPSHTEYN L. B.[1,2,3], EROFEEV A. L.[1,2], FEDOTOVICH G. V.[1,2], GAYAZOV S. E.[1,2], GREBENUK A. A.[1,2], GRIBANOV S. S.[1,2], GRIGORIEV D. N.[1,4], IGNATOV F. V.[1], KARPOV S. V.[1], KAZANIN V. F.[1], KOROBOV A. A.[1,2], KOVALENKO O. A.[1,2], KOZYREV A. N.[1], KOZYREV E. A.[1,2], KROKOVNY P. P.[1,2], KUZMENKO A. E.[1,2], KUZMIN A. S.[1], LOGASHENKO I. B.[1,2], LUKIN P. A.[1,2], MIKHAILOV K. YU.[1,2], OKHAPKIN V. S.[1], PESTOV YU. N.[1], POPOV A. S.[1,2], RAZUVAEV G. P.[1,2], RUBAN A. A.[1], RYSKULOV N. M.[1], RYZHENENKOV A. E.[1,2], SHEBALIN V. E.[1], SHEMYAKIN D. N.[1,2], SHWARTZ B. A.[1,2], SIBIDANOV A. L.[4], SHATUNOV YU. M.[1], SOLODOV E. P.[1,2], TITOV V. M.[1], TALYSHEV A. A.[1,2], VOROBIOV A. I.[1], YUDIN YU. V.[1,2]

(1. 俄罗斯布德克尔核物理研究所, 新西伯利亚 630090, 俄罗斯; 2. 国立新西伯利亚大学, 新西伯利亚 630090, 俄罗斯; 3. 国立新西伯利亚理工大学, 新西伯利亚 630090, 俄罗斯; 4. 悉尼大学物理学院高能物理系,悉尼,澳大利亚)

摘要:报道了用 CMD-3 在 2011-2012 年收集的积分亮度为 22 pb^{-1}的研究结果. 在 CMD-3 当前的统计量下,只能被确定 $\phi(1020)\eta$ 中间共振态. 在 1.59-2.0 GeV能区的 30 个能量点测量了 $e^+e^-\to\phi(1020)\eta$. 分析中,将 η 介子当做反冲粒子,穷尽了 η 衰变的所有模式,选出的事例总数为 1454 ± 48. 测量的截面近似为 $\phi(1680)$和非共振振幅按照矢量介子主导模型的叠加,并得到了 $\phi(1680)$介子共振参数的初步结果.

关键词:强子; 信号/本地分离; 截面

0 Introduction

The measurement of the cross section of $e^+e^-\to\phi(1020)\eta\to K^+K^-\eta$ process provides an opportunity to refine the parameters of $\phi(1680)$ meson. Also it is needed for the improvement of the accuracy of the hadronic contribution to the $(g-2)/2$ of muon. The process has been studied earlier by the BaBar Collaboration in the c. m. energy ($E_{\text{c. m.}}$) range from 1.56 to 3.48 GeV in the $\eta\to2\gamma$ decay channel[1], and in the energy range from 1.56 to 2.64 GeV in the $\eta\to\pi^+\pi^-\pi^0$ decay channel[2]. It was found that the main intermediate mechanism is $e^+e^-\to\phi(1680)\to\phi(1020)\eta$, whereas the cross section of so-called non-$\phi(1020)\eta$ part of the process(i. e. with kaons, which have the invariant mass $M_{\text{inv}}(K^+,K^-)>1045$ MeV/c^2) is an order of magnitude lower. The statistics was not enough to study the dynamics of non-$\phi(1020)\eta$ contribution.

We performed the study of $e^+e^-\to K^+K^-\eta$ process with the CMD-3 detector. The structure of the detector and its physical programm are described elsewhere[3-4]. The analysis is based on an integrated luminosity of 22 pb^{-1} collected by the CMD-3 in 2011-2012.

1 Study of $e^+e^-\to K^+K^-\eta$ with CMD-3

1.1 Selection of $K^+K^-\eta$ final state

To select kaons in the $K^+K^-\eta$ final state, we search for a pair of beam-originating tracks, which have zero net charge and ionization losses dE/dx in the drift chamber, typical for kaons with corresponding momenta. For the selected pair we calculate the energy disbalance ΔE:

$$\Delta E\equiv E_{K^+}+E_{K^-}+\sqrt{(-\vec{P}_{K^+}-\vec{P}_{K^-})^2+m_\eta^2}-2E_{\text{beam}}\quad(1)$$

which represents the total energy of the final particles

minus twice beam energy under the assumption that the missing particle is η meson. The ΔE distribution peaks at zero for signal events, so it is used to extract the number of these events at each $E_{\text{c. m.}}$ point.

To search for non-$\phi(1020)\eta$ mechanisms in $\eta\to 2\gamma$ mode, we perform a 4C kinematic fit with all the pairs of photons, and choose the pair having the lowest χ^2. We apply the conditions $M_{\text{inv}}(K^+,K^-)>1045$ MeV/c^2 and $\chi^2<25$. We find 10 events in the experiment (see Fig. 1, (a) invariant mass of the pair of photons, (b) invariant mass of the pair of kaons, (c) energy disbalance ΔE, (d) χ^2 of the 4C kinematic fit), whereas 15.2 events of the $e^+e^-\to\phi(1020)\eta\to K^+K^-2\gamma$ process are expected according to the simulation. Thus, on the basis of the data collected by CMD-3 in 2011-2012 we cannot recognize the contribution of any other intermediate mechanisms, except $e^+e^-\to\phi(1020)\eta$. Moreover, we suspect that the events, which in BaBar study[1] were considered as non-$\phi(1020)\eta$ part of the process, are in fact the events from the tail of $\phi(1020)$.

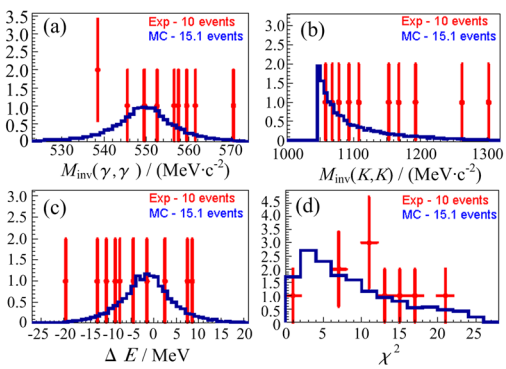

Fig. 1 The experimental (markers with error bars) and simulated (open histograms) distributions

To select kaons from $\phi(1020)$ decay, we apply to the selected pair of kaons the condition $M_{\text{inv}}(K^+,K^-)<1070$ MeV/c^2. Also we search for the other beam-originating tracks with dE/dx, typical for pions. Fig. 2 shows the dE/dx for the selected kaons and pions. It can be seen, that there is no significant particle misidentification (the selected candidates for kaons (dots) and pions (crosses) in the experiment).

1.2 Background processes

If the parameter ΔE belongs to the range from −180 to 150 MeV, the estimations of the expected number of events (according to the cross sections

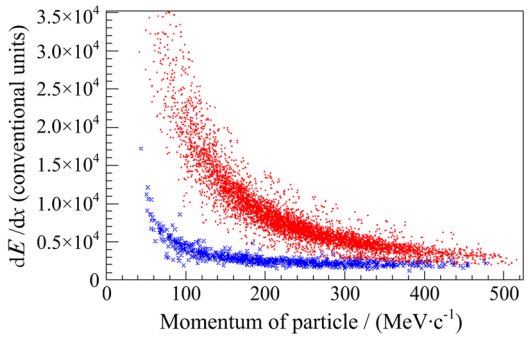

Fig. 2 The distribution of energy losses vs particle momentum

measured by BaBar[1,5]) show that the only significant background processes are: $e^+e^-\to\phi(1020)f_0(500)$, $K^{*\pm}(892)K^{\mp}\pi^0\to K^+K^-\pi^0\pi^0$, $e^+e^-\to K^+K^-\pi^+\pi^-$. As for the latter process, its contribution can be almost completely suppressed. Indeed, if in the event that two charged pions were found, we use a distribution of $M_{\text{missing}2K2\pi}$ parameter (Fig. 3), representing the missing mass for the two kaons and two pions. The events of $e^+e^-\to K^+K^-\pi^+\pi^-$ process are concentrated near the origin of coordinates, and for the suppression of the background we apply the condition $M_{\text{missing}2K2\pi}>100$ MeV/c^2. If in the event that only one charged pion was found, we use a distribution of $M_{\text{missing}2K\pi}$ parameter (Fig. 4), representing the missing mass for the two kaons and one pion. In this case for the background suppression we apply the condition $M_{\text{missing}2K\pi}>300$ MeV/c^2.

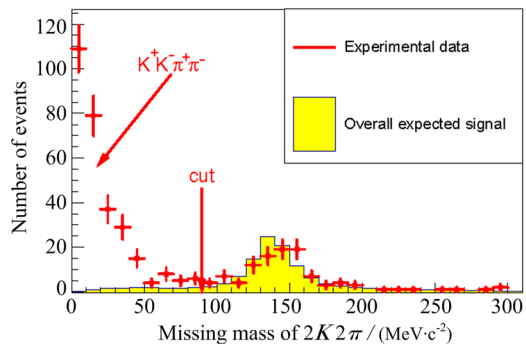

Fig. 3 The distributions of the $M_{\text{missing}2K2\pi}$ parameter

In the experiment (markers with error bars); for the MC of the signal process (filled histogram). The number of events at each bin of the simulated histogram corresponds to the expected number of events in this bin. All the energy points $E_{\text{c. m.}}$ are combined.

The distributions of the missing mass $M_{\text{missing}2K}$ and

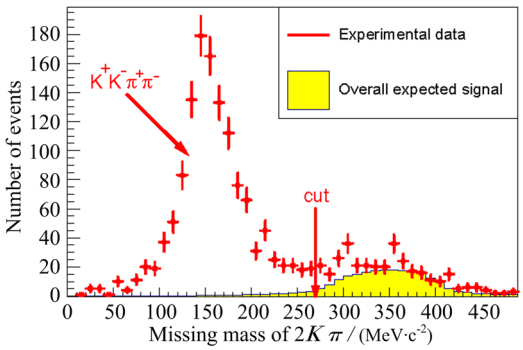

Fig. 4　The distributions of the $M_{\text{missing}2K2\pi}$ parameter

the invariant mass $M_{\text{inv}}(K^+, K^-)$ of two kaons for the experimental and simulated background events are shown in Figs. 5 and 6 correspondingly. In the experiment (markers with error bars); for the MC of $\phi(1020)\pi^0$ (cross-hatched histogram), $K^+K^-\omega$ (hatched histogram), $\phi(1020)f_0(500)\to K^+K^-\pi^0\pi^0$ (dotted line), $K^{*\pm}(892)K^{\mp}\pi^0\to K^+K^-\pi^0\pi^0$ (dotted histogram), $K^+K^-\pi^+\pi^-$ processes (filled histogram), sum of backrounds (solid line). All energy points $E_{\text{c.m.}}$ are combined.

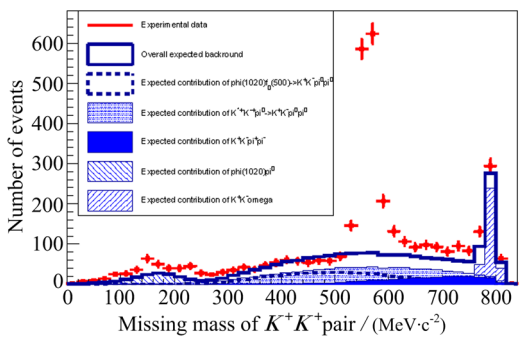

Fig. 5　The distributions of the $M_{\text{missing}2K}$ parameter

1.3　Number of signal events

The distributions of simulated signal and background events in ΔE are fitted at every point of energy. For the signal events the fitting function is the sum of three Gaussian functions with different mean values and widths, the widest of which describes the radiative tail of the distribution. The simulated sum of backgrounds is fitted by a second-degree polynomial. The functions found are used to fit the distribution of experimental events in ΔE with three free parameters: The amplitude and position of the signal function, and

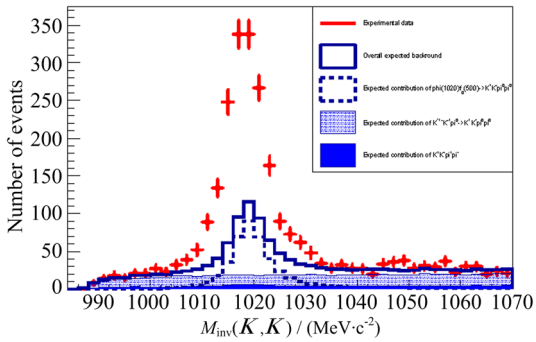

Fig. 6　The distributions of the $M_{\text{inv}}(K^+,K^-)$ parameter

the amplitude of the background function. The integral of the signal function gives the number of signal events at a given energy point ($N_{\text{signal}}(E_{\text{c.m.}})$). So we get the total number of signal $N_{\text{signal,total}} \approx 1454 \pm 48$ events in the experiment. As an example the procedure of signal-background separation at $E_{\text{c.m.}} = 1.96$ GeV is shown in Fig. 7.

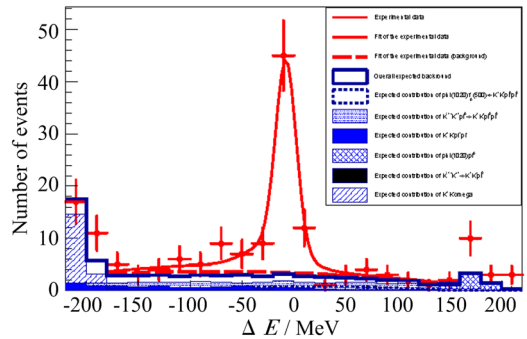

Fig. 7　The distribution of ΔE parameter

In Fig. 7, the distribution of ΔE parameter at $E_{\text{c.m.}} = 1.96$ GeV: in the experiment (markers with error bars); for the MC of $\phi(1020)\pi^0$ process (cross-hatched histogram); for the MC of $K^+K^-\omega$ process (hatched histogram); for the MC of $\phi(1020)f_0(500)\to K^+K^-\pi^0\pi^0$ process (dotted line); for the MC of $K^{*\pm}(892)K^{\mp}\pi^0\to K^+K^-\pi^0\pi^0$ process (dotted histogram); for the MC of $K^+K^-\pi^+\pi^-$ process (filled histogram). Also the fit of the experimental distribution (solid line) and the fit of background (dashed line) are shown.

1.4　Cross section of $e^+e^-\to\phi(1020)\eta$ process

The cross section of the $e^+e^-\to\phi(1020)\eta$ process was calculated at each $E_{\text{c.m.}}$ according to the

expression:

$$\sigma_{\phi(1020)\eta} = \frac{N_{\text{signal}} \cdot (1+\delta_{\text{eff}})}{L \cdot \varepsilon_{\text{MC}} \cdot \varepsilon_{\text{trig}} \cdot (1+\delta_{\text{rad}}) \cdot B(\phi(1020)\to K^+K^-)} \quad (2)$$

where L is the collected luminosity at the fixed energy point, ε_{MC} is the efficiency of registration of the events of the signal process, determined from simulation, $1+\delta_{\text{eff}}$ is the correction to the efficiency of registration, $\varepsilon_{\text{trig}}$ is the efficiency of trigger, and $(1+\delta_{\text{rad}})$ is the radiative correction. The results of calculation are presented in Fig. 8 along with the BaBar data.

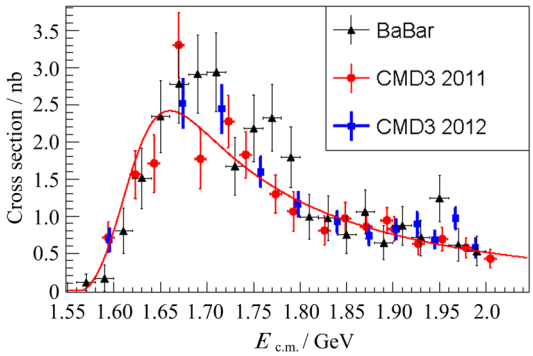

Fig. 8 The cross section of $e^+e^-\to\phi(1020)\eta$ process

CMD-3 results, based on the data collected in 2011 (circular markers) and in 2012 (squared markers) years; BaBar results, measured in $\eta\to 2\gamma$ mode (triangle markers).

1.5 Approximation of the cross section

We fit the cross section using the same parametrization, as that was used in BaBar study [1]:

$$\sigma_{\phi(1020)\eta} = 12\pi P_{\phi(1020)\eta}(s)\left|\frac{A^{\text{n.r.}}_{\phi(1020)\eta}}{s} + \sqrt{B^{\phi(1680)}_{\phi(1020)\eta}\Gamma^{\phi(1680)}_{ee}}\frac{\sqrt{\dfrac{\Gamma_{\phi(1680)}}{P_{\phi(1020)\eta}(M^2_{\phi(1680)})}}e^{i\Psi_{\phi(1680)}}}{s-M^2_{\phi(1680)}+i\sqrt{s}\Gamma_{\phi(1680)}(s)}\right|^2 \quad (3)$$

Here $P_{\phi(1020)\eta}$ is the $\phi(1020)\eta$ phase space, $A^{\text{n.r.}}_{\phi(1020)\eta}$ describes the possible contribution of some resonance below the reaction threshold (presumably, it might be $\phi(1020)$), and the second term under the module sign describes $\phi(1680)\to\phi(1020)\eta$ contribution in accordance with the vector meson dominance model. We perform a fit of CMD-3 data together with the BaBar data for c. m. energies from 2.3 to 3.46 GeV, taken from Ref. [1] (which allows to fix the $A^{\text{n.r.}}_{\phi(1020)\eta}$ term), and a fit of BaBar data. The preliminary results for the $\phi(1680)$ parameters, derived from the fit of CMD-3 and BaBar data, are listed in Tab. 1.

Tab. 1 Results of the cross section approximation

Parameter	BaBar	CMD-3
χ^2/n. d. f	40.0/44	56.9/54
$\Gamma^{\phi(1680)\eta}_{ee}B^{\phi(1680)}_{\phi(1020)\eta}$/eV	111.2±17.0	115.4±17.4
$M_{\phi(1680)}$/MeV	1682.3±10.0	1666.6±7.3
$\Gamma_{\phi(1680)}$/MeV	175.8±38.0	222.7±42.6
σ^{peak}/nb	2.92±0.7	2.50±0.67
$\Psi_{\phi(1680)}$	−1.33±0.12	−1.1±0.12
$A^{\text{n.r.}}_f$/(nb·GeV^1)	0.11±0.02	0.095±0.016

2 Conclusion

We established that in the $e^+e^-\to K^+K^-\eta$ process only $\phi(1020)\eta$ intermediate state can be recognized at the current level of CMD-3 statistics. The cross section of $e^+e^-\to\phi(1020)\eta$ process was measured at 30 center-of-mass energy points in the range from 1.59 up to 2.0 GeV. The total of 1454±48 events of signal process were selected. The measured cross section was approximated according to vector meson dominance model as a sum of $\phi(1680)$ and nonresonant amplitudes, and preliminary results for $\phi(1680)$ meson parameters have been obtained.

References

[1] AUBERT B, BONA M, BOUTIGNY D, et al. Measurements of $e^+e^-\to K^+K^-\eta$, $K^+K^-\pi^0$ and $K^0_SK^\pm\pi^\mp$ cross sections using initial state radiation events [J]. Physical Review D, 2008, 77: 092002.

[2] AUBERT B, BARATE R, BOUTIGNY D, et al. Study of $e^+e^-\to\pi^+\pi^-\pi^0$ process using initial state radiation with BABAR[J]. Physical Review D, 2007, 76: 092005.

[3] DANILOV V V, IVANOV P M, KOOP I A, et al. The concept of round colliding beams[C]// Proceedings of the 5th European Particle Accelerator Conference. 1996: 1149-1151.

[4] EIDELMAN S. Physics at VEPP-2000[J]. Nuclear Physics B-Proceedings Supplements, 2006, 162(1):323-326.

[5] AUBERT B, BONA M, BOUTIGNY D, et al. Erratum: The $e^+e^-\to 2(\pi^+\pi^-)\pi^0$, $2(\pi^+\pi^-)\eta$, $K^+K^-\pi^+\pi^-\pi^0$ and $K^+K^-\pi^+\pi^-\eta$ cross sections measured with initial-state radiation[J]. Physical Review D, 2007, 76: 092005.

Article ID:0253-2778(2016)06-0507-07

Study of the process $e^+e^- \to K\bar{K}$ in the center-of-mass energy range 1004-1060 MeV with the CMD-3 detector at e^+e^- VEPP-2000 collider

KOZYREV E. A.[1,2], AMIRKHANOV A. N.[1,2], ANISENKOV A. V.[1,2], M. AULCHENKO V.[1,2], BANZAROV V. S.[1], BASHTOVOY N. S.[1], BERKAEV D. E.[1], BONDAR A. E.[1,2], BRAGIN A. V.[1], EIDELMAN S. I.[1,2], A. EPIFANOV D.[1], EPSHTEYN L. B.[1,2,3], EROFEEV A. L.[1,2], FEDOTOVICH G. V.[1,2], GAYAZOV S. E.[1,2], GREBENUK A. A.[1,2], GRIBANOV S. S.[1,2], GRIGORIEV D. N.[1,4], IGNATOV F. V.[1], IVANOV V. L.[1,2], KARPOV S. V.[1], KASAEV A. S.[1], KAZANIN V. F.[1,2], IRPOTIN A. N.[1], KOROBOV A. A.[1,2], KOVALENKO O. A.[1,2], KOZYREV A. N.[1,2], KOOP I. A.[1], KROKOVNY P. P.[1,2], KUZMENKO A. E.[1,2], KUZMIN A. S.[1,2], LOGASHENKO I. B.[1,2], LUKIN P. A.[1,2], MIKHAILOV K. YU.[1,2], OKHAPKIN V. S.[1], OTBOEV A. V.[1], PESTOV YU. N[1], POPOV A. S.[1,2], RAZUVAEV G. P.[1,2], RUBAN A. A.[1], RYSKULOV N. M.[1], RYZHENENKOV A. E.[1,2], SENCHENKO A. I.[1], SHEBALIN V. E.[1], SHEMYAKIN V. E.[1,2], SHWARTZ A. S.[1,2], SHWARTZ D. B.[1,2], SIBIDANOV A. L.[4], SHATUNOV P. YU.[1], SHATUNOV YU. M.[1], SOLODOV E. P.[1,2], TITOV V. M.[1], TALYSHEV A. A.[1,2], VOROBIOV A. I.[1], YUDIN YU. V.[1,2]

(1. *Budker Institute of Nuclear Physics*, *Novosibirsk* 630090, *Russia*;
2. *Novosibirsk State University*, *Novosibirsk* 630090, *Russia*;
3. *Novosibirsk State Technical University*, *Novosibirsk* 630092, *Russia*;
4. *Falkiner High Energy Physics Department*, *School of Physics*, *University of Sydney*, *Australia*)

Abstract: The $e^+e^- \to K_S^0 K_L^0$ and $e^+e^- \to K^-K^+$ cross sections have been measured in the center-of-mass energy range 1004-1060 MeV for 25 energy points with about 2%-3% systematic uncertainties. The analysis is based on 5.5 pb^{-1} of integrated luminosity collected with the CMD-3 detector at the VEPP-2000 e^+e^- collider. The measured cross section is approximated according to vector meson dominance model as a sum of ϕ, ω, ρ-like amplitudes and their excitations, and $\phi(1020)$ meson parameters have been obtained.

Key words: hadrons; electron positron collider; kaon form factor

CLC number: O572.3 **Document code**: A doi:10.3969/j.issn.0253-2778.2016.06.010

Citation: KOZYREV E A, AMIRKHANOV A N, ANISENKOV A V, et al. Study of the process $e^+e^- \to K\bar{K}$ in the center-of-mass energy range 1004-1060 MeV with the CMD-3 detector at e^+e^- VEPP-2000 collider[J]. Journal of University of Science and Technology of China, 2016,46(6): 507-513.
KOZYREV E A, AMIRKHANOV A N, ANISENKOV A V, 等. VEPP-2000 e^+e^- 对撞机上用 CMD-3 谱仪研究 1004-1060 MeV 能区的 $e^+e^- \to K\bar{K}$ 过程[J]. 中国科学技术大学学报,2016,46(6): 507-513.

Received:2015-11-30; **Revised**:2016-04-20

Foundation item:Supported in Part by the Russian Education and Science Ministry (RFMEFI61014X0002), Russian Foundation for Basic Research (RFBR 13-02-00991-a, RFBR 13-02-00215-a, RFBR12-02-01032-a, RFBR 13-02-01134-a, RFBR 14-02-00580-a, RFBR 14-02-31275-mol-a, RFBR 14-02-00047-a, RFBR 14-02-31478-mol-a, RFBR 14-02-91332 and the DFG grant HA 1457/9-1).

Biography:KOZYREV E. A. (corresponding author), born in 1991, PhD. Research field: electro-positron annihilation into hadrons. E-mail: e.a.kozyrev@inp.nsk.su

VEPP-2000 e^+e^- 对撞机上用 CMD-3 谱仪研究 1004-1060 MeV 能区的 $e^+e^- \to K\bar{K}$ 过程

KOZYREV E. A.[1,2], AMIRKHANOV A. N.[1,2], ANISENKOV A. V.[1,2], M. AULCHENKO V.[1,2], BANZAROV V. S.[1], BASHTOVOY N. S.[1], BERKAEV D. E.[1], BONDAR A. E.[1,2], BRAGIN A. V.[1], EIDELMAN S. I.[1,2], A. EPIFANOV D.[1], EPSHTEYN L. B.[1,2,3], EROFEEV A. L.[1,2], FEDOTOVICH G. V.[1,2], GAYAZOV S. E.[1,2], GREBENUK A. A.[1,2], GRIBANOV S. S.[1,2], GRIGORIEV D. N.[1,4], IGNATOV F. V.[1], IVANOV V. L.[1,2], KARPOV S. V.[1], KASAEV A. S.[1], KAZANIN V. F.[1,2], IRPOTIN A. N.[1], KOROBOV A. A.[1,2], KOVALENKO O. A.[1,2], KOZYREV A. N.[1,2], KOOP I. A.[1], KROKOVNY P. P.[1,2], KUZMENKO A. E.[1,2], KUZMIN A. S.[1,2], LOGASHENKO I. B.[1,2], LUKIN P. A.[1,2], MIKHAILOV K. YU.[1,2], OKHAPKIN V. S.[1], OTBOEV A. V.[1], PESTOV YU. N[1], POPOV A. S.[1,2], RAZUVAEV G. P.[1,2], RUBAN A. A.[1], RYSKULOV N. M.[1], RYZHENENKOV A. E.[1,2], SENCHENKO A. I.[1], SHEBALIN V. E.[1], SHEMYAKIN V. E.[1,2], SHWARTZ A. S.[1,2], SHWARTZ D. B.[1,2], SIBIDANOV A. L.[4], SHATUNOV P. YU.[1], SHATUNOV YU. M.[1], SOLODOV E. P.[1,2], TITOV V. M.[1], TALYSHEV A. A.[1,2], VOROBIOV A. I.[1], YUDIN YU. V.[1,2]

(1. 俄罗斯布德克尔核物理研究所, 新西伯利亚 630090, 俄罗斯;
2. 国立新西伯利亚大学, 新西伯利亚 630090, 俄罗斯;
3. 国立新西伯利亚理工大学, 新西伯利亚 630090, 俄罗斯;
4. 悉尼大学物理学院高能物理系,悉尼,澳大利亚)

摘要:在质心能量 1004-1060MeV 之间的 25 个能量点测量了 $e^+e^- \to K_S^0K_L^0$ 和 $e^+e^- \to K^-K^+$ 截面,系统误差大约为 2%-3%. 分析是基于 VEPP-2000 e^+e^- 对撞机上 CMD-3 收集的积分亮度为 5.5 pb^{-1} 的实验数据. 测量的截面可近似看作 ϕ, ω, ρ 类似的振幅及其激发态按照矢量介子主导模型的叠加,得到了 $\phi(1020)$ 介子的共振参数.

关键词:强子; 正负电子对撞机; 介子形状因子

0 Introduction

Investigation of e^+e^- annihilation into hadrons at low energies provides unique information about interaction of light quarks. Precise measurement of the $e^+e^- \to K\bar{K}$ cross section allows to study properties of the light vector mesons with $J^{PC} = 1^{--}$, and is required for the precise calculation of strong interaction contributions to $(g-2)_\mu$ and $\alpha(M_Z)$ values[1]. A significant deviation of coupling constants ratio $\frac{g_\phi \to K^+K^-}{g_\phi \to K_SK_L}$ from a theoretical prediction requires new comprehensive measurement of the cross sections[2].

The most precise previous study of the process has been performed by the CMD-2[3-4], SND[5] and BaBar[6-7] detectors. In this paper we present new measurement of the $e^+e^- \to K_S^0K_L^0$ and $e^+e^- \to K^-K^+$ cross section, characterized by statistical advantage and performed in the center-of-mass energy $E_{c.m.}$ range 1004-1060 MeV at 25 energy points. Also the paper contains the results of the cross section interpretation according to the vector meson dominance (VMD) model.

1 CMD-3 detector and data set

The Cryogenic Magnetic Detector (CMD-3) is installed in one of two interaction regions of VEPP-2000 collider[8], and is described elsewhere[9]. The detector tracking system consists of the cylindrical drift chamber(DC) and double-layer cylindrical multi-wire

proportional Z-chamber, both used for a trigger, and both are installed inside thin ($0.2\ X_0$) superconducting solenoid with 1.3 T field. DC contains 1 218 hexagonal cells and allows to measure charged particle momentum with 1.5%-4.5% accuracy in the 100-1000 MeV/c range, and provides the measurement of the polar (θ) and azimuth (ϕ) angles with 20 mrad and 3.5-8.0 mrad accuracy, respectively. An amplitude information from the DC wires is used to measure the ionization losses dE/dx of charged particles with $\sigma_{dE/dx} \approx 11\%$-$14\%$ accuracy for minimum ionization particles (m. i. p.). A barrel liquid xenon (LXe) with 5.4 X_0 and CsI crystal with 8.1 X_0 electromagnetic calorimeters are placed outside the solenoid. The BGO crystals with 13.4 X_0 are used as the end-cap calorimeters. Return yoke of the detector is surrounded by the scintillation counters, which are required for cosmic events veto.

To study a detector response to investigated processes and obtain a detection efficiency, we have developed a Monte Carlo (MC) simulation of our detector based on GEANT4[10] package, and all simulated events pass all our reconstruction and selection procedures. The MC simulation includes photon jet radiation by the initial electron or positron, calculated according to Ref. [11].

The analysis is based on 5.5 pb^{-1} of integrated luminosity, collected in two scans of ϕ(1020) resonance region at 25 energy points in the $E_{c.m.}$ = 1004-1060 MeV range.

The beam energy E_{beam} has been monitored by using the back-scattering-laser-light system[12] which determines $E_{c.m.}$ at each energy point with about 0.06 MeV accuracy.

2　$e^+e^- \to K\bar{K}$ event selection

At energies under studied K_S^0-meson can be produced only simultaneously with K_L^0-meson. So, signal identification of the process $e^+e^- \to K_S^0K_L^0$ is based on the detection of two pions from the $K_S^0 \to \pi^+\pi^-$ decay. For each pair of oppositely charged tracks in the event we perform a kinematic fit with the requirement to have a common vertex, and retain track parameters associated with this vertex. Assuming tracks to be pions, the pair with the best χ^2 from the vertex fit and with the invariant mass in the range 420-580 MeV/c^2 is considered as a K_S^0 candidate. The following requirements are applied to the events with found K_S^0 candidate.

(Ⅰ) The longitudinal and transverse distances of the vertex position are required to have $|Z_{K_S^0}| < 10$ cm and $|\rho_{K_S^0}| < 6$ cm, respectively;

(Ⅱ) Each track has momentum $130 < P_{\pi^\pm} < 320$ MeV/c corresponding to the kinematically allowed region for pions from the K_S^0 decay;

(Ⅲ) Each track has the ionization losses $dE/dx_{\pi^\pm} < dE/dx_{m.i.p} + 3 \times \sigma_{dE/dx_{m.i.p}}$ to reject charged kaons and background protons. The last two requirements are illustrated in Fig. 1 by lines for all detected tracks at the energy point E_{beam} = 505 MeV;

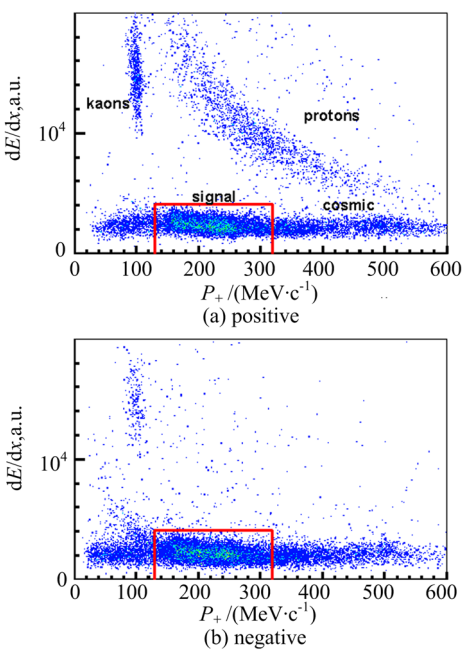

Fig. 1　The ionization losses vs momentum

(Ⅳ) The total reconstructed momentum of the K_S^0 candidate, $P_{K_S^0}$, is required to be within five standard deviations from the nominal momentum at each energy point.

We determine the number of signal events for data and simulation by approximation of two pion invariant

mass, shown in the Fig. 2 (at the beam energy 505 MeV for simulation(a) and data (b). The short dotted line corresponds to a signal profile, and the long dotted line is for the background), by a sum of signal and background profiles. The signal shape is described by the sum of three Gaussian functions with parameters fixed from the simulation, but with additional Gaussian smearing to account for the detector response. A background, predominantly caused by collider processes $e^+e^- \to \pi^+\pi^- 2\pi^0$, $4\pi^\pm$, 3π, K^+K^- and cosmic muons, is described by second order polynomial function and is presented in both data and MC-simulation. The background in simulation corresponds to tails of signal with wrong reconstructed parameters of pions. By varying shapes of the functions used, we estimate uncertainty in number of extracted signal events not more than 1.1%.

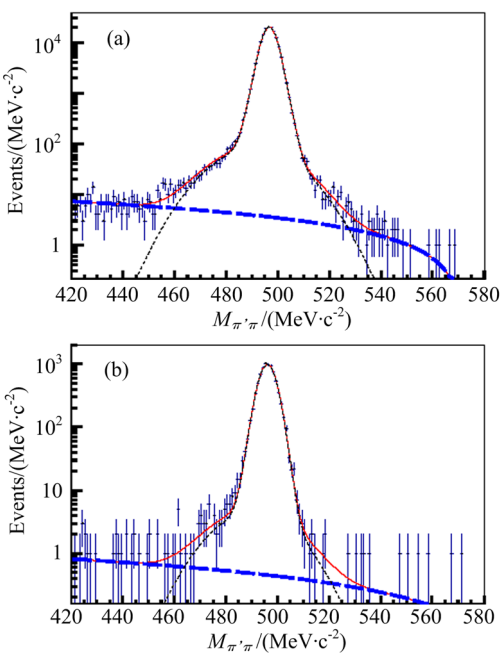

Fig. 2 The approximation of the invariant mass of two pions

The detection efficiency $\epsilon(K_S^0K_L^0)$ is obtained by dividing the number of MC simulated events after reconstruction and selections described above, by the total number of generated $K_S^0K_L^0$ pairs. Fig. 3 shows the obtained detection efficiency (squares) vs c. m. energy. The energy behavior as well as the absolute value ($\approx 35\%$) is predominantly due to pions polar angle selection criterion. The efficiencies of single tracks of charged kaons ($\varepsilon(K^+)$, $\varepsilon(K^-)$); The efficiency of both kaons detection ($\varepsilon(K^+K^-)$)-circles; The efficiency of K_S-meson ($\varepsilon(K_S^0)$)-squares.

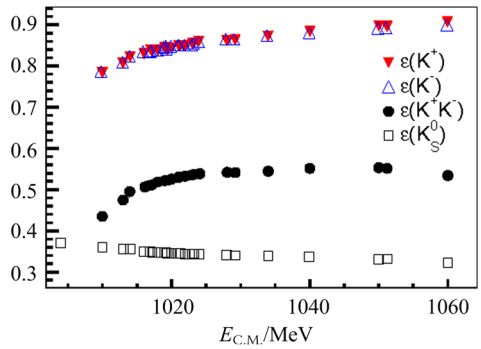

Fig. 3 The detection efficiency vs energy from simulation

The detection of the charged mode ($e^+e^- \to K^-K^+$) is based on the search of two central collinear tracks of kaons in DC with defined momentums approximately equal to $\sqrt{E^2_{c.m.}/4 - m^2_{K^+}}$ with accuracy of detector resolution. Additional selection reveals that kaon track has ionization losses significantly larger than the ones of m. i. p. due to relatively small velocity of kaons under study $\beta = 0.2$-0.4 (as shown in Fig. 1). The level of remaining background is less than 0.5%.

The collinear configuration of the process allows to test MC simulation by the determination of the efficiencies of each kaon in data as well as in MC. The experimental efficiencies of single positive and negative tracks($\varepsilon(K^+)$, $\varepsilon(K^-)$) are shown by triangles in Fig. 3 and increases from 78% to 90% across the energy region under study. The deviation of efficiencies of single tracks in data from MC is less then 1%. Circles in the figure correspond to total simulated detection efficiency ($\varepsilon(K^+K^-)$) of K^+K^- final state, constituted by geometrical efficiency due to polar angle selection ($\approx 73\%$) as well as by the values of $\varepsilon(K^+)$, $\varepsilon(K^-)$.

3 Cross section of $e^+e^- \to K\bar{K}$ and systematic uncertainties

The experimental Born cross section of the $e^+e^- \to K\bar{K}$ process has been calculated for each energy point according to the expression:

$$\sigma^{\text{born}} = \frac{N^{\text{exp}}}{\epsilon_{\text{reg}}\epsilon_{\text{trig}}L(1+\delta_{\text{rad}})}\delta^{\text{en. disper}} \quad (1)$$

where ϵ_{reg} is a detection efficiency, ϵ_{trig} is a trigger efficiency, L is the integrated luminosity, $1+\delta_{\text{rad}}$ is a radiative correction, and $\delta^{en.\ disper.}$ represents a correction due to the energy dispersion of the electron-positron beams.

The trigger efficiency is studied using responses of two independent triggers, charged and neutral, for selected signal events, and is found to be close to unity $\epsilon_{\text{trigg}} = 0.998 \pm 0.001$. The integrated luminosity L is determined by the processes $e^+e^-\to e^+e^-$ and $e^+e^-\to\gamma\gamma$ with about 1%[13] accuracy. The initial state radiative correction $1+\delta_{\text{rad}}$ is calculated using structure function method with an accuracy better than 0.3%[14]. The dispersion of the electron-positron c.m. energy is about 300 keV, significant in comparison with the width of ϕ meson, and we introduce the correction of the cross section, which has a maximum value of 1.028 ± 0.007 for both channel in the peak of ϕ resonance. The resulting cross sections are shown in Fig. 4.

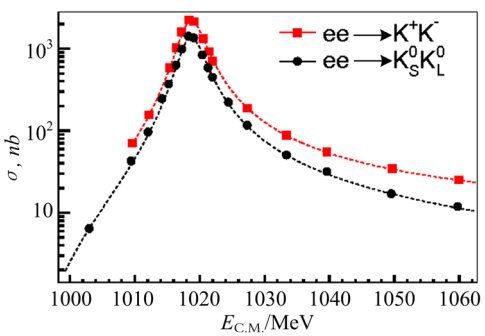

Fig. 4　Preliminary results of measurement

The uncertainty in $e^+e^-\to K_S^0K_L^0$ cross section is dominated by the signal extraction procedure used two pion mass approximation (Fig. 2). Moreover, MC simulation doesn't exactly reproduce all detector responses, and we perform some additional study to obtain corrections for data-MC difference in the detection efficiency. We observe good data-MC agreement for the charged pion detection inefficiency ($\approx 1\%$), introduce no efficiency correction, and estimate uncertainty in the detection as 0.5%. By variation of corresponding selection criteria we estimate uncertainty due to the data-MC difference in the angular and momentum resolutions as 0.4%, and other selection criteria contribute 0.5%.

The uncertainty in $e^+e^-\to K^+K^-$ cross section is dominated by inexact knowledge of angular acceptance of kaons. This systematic uncertainty (3%) is examined using Z-chamber which surrounds DC. Unlike pions in neutral channel the charged pair of kaons have much more ionization losses and collinear configuration that leads to strong correlation in detector response to charged kaons tracks.

The systematic errors of the $e^+e^-\to K_S^0K_L^0$ and $e^+e^-\to K^+K^-$ cross sections measurement, discussed above, are summarized in Tab. 1, and in total estimated as 1.8% and 3.2%, respectively.

Tab. 1　Summary of systematic errors in the $e^+e^-\to K\bar{K}$ cross section measurement

source systematic error	$e^+e^-\to K_S^0K_L^0$	$e^+e^-\to K^+K^-$
signal extraction	1.1	0.3
detection efficiency	1.0	3
radiative correction	0.3	0.3
energy dispersion correction	0.3	0.3
trigger efficiency	0.1	0.1
luminosity	1.0	1.0
total	1.8	3.2

4　Cross section interpretation

Our data in the studied energy range allows to obtain $\phi(1020)$ parameters with good accuracy. We approximate the energy dependence of the cross section according to a vector meson dominance (VMD) model as a sum of ϕ, ω, ρ-like amplitudes[15]:

$$\sigma_{e^+e^-\to K\bar{K}}(s) = \frac{8\pi\alpha}{3s^{5/2}}p_K^3\frac{Z(s)}{Z(m_{\phi^2})}\cdot \left|\frac{g_{\phi\gamma}g_{\phi KK}}{D_\phi(s)} \pm \frac{g_{\rho\gamma}g_{\rho KK}}{D_\rho(s)} + \frac{g_{\omega\gamma}g_{\omega KK}}{D_\omega(s)} + A_{\phi',\rho',\omega'}\right| \quad (2)$$

where $s = E_{\text{c.m.}}^2$, p_K is a kaon momentum, $Z(s) = 1 + \frac{\pi\alpha}{2\beta}$ is the Sommerfeld-Gamov-Sakharov factor for charged kaons with velocity $\beta = \sqrt{1-4m_K^2/s}$, $D_V(s) = m_V^2 - s - i\sqrt{s}\Gamma_V(s)$, m_V, and Γ_V are mass and width of major intermediate resonances: $V =$

$\rho(770)$, $\omega(782)$, $\phi(1020)$. The sign before ρ-amplitude is plus for charged channel and minus for neutral one due to quark structure of kaons and ρ-meson. The energy dependence of the decay width is expressed via sum of branching fractions and phase space energy dependence $P_{V\to f}(s)$ of all decay modes as (see Refs. [5-15]):

$$\Gamma_V(s) = \Gamma_V \sum_{V\to f} B_{V\to f} \frac{P_{V\to f}(s)}{P_{V\to f}(m_V^2)}.$$

The coupling constants of the intermediate vector meson V with initial and final states can be presented as:

$$g_{V\gamma} = \sqrt{\frac{3m_V^3\Gamma_{Vee}}{4\pi\alpha}},\ g_{VK\bar{K}} = \sqrt{\frac{6\pi m_V^2\Gamma_V B_{VK\bar{K}}}{p_V^3(m_V)}},$$

where Γ_{Vee} and $B_{VK\bar{K}}$ are electronic width and decay branching fraction to pair of kaons.

In our approximation we use values of mass (Tab. 1), total width, and electronic width of $\rho(770)$ and $\omega(782)$: $\Gamma_{\rho\to ee} = 7.04 \pm 0.06$ keV, $\Gamma_{\omega\to ee} = 0.60 \pm 0.02$ keV[16]. The branching fractions of $\rho(770)$ and $\omega(782)$ to a pair of kaons are unknown, and we use the relation $g_{\omega K_S^0 K_L^0} = -g_{\rho K_S^0 K_L^0} = g_{\phi K_S^0 K_L^0}/\sqrt{2}$, based on the quark model with "ideal" mixing and exact SU(3) symmetry of u-, d-, s-quarks[15]. In order to take into account possible breaking of the assumption both $g_{\rho K_S^0 K_L^0}$ and $g_{\phi K_S^0 K_L^0}$ are multiplied by the union constant $r_{\rho/\omega}$.

The amplitude $A_{\phi',\rho',\omega'}$ denotes a contribution of excited $\omega(1420)$, $\rho(1450)$ and $\phi(1680)$ vector meson states to the $\phi(1020)$ mass region. Using BaBar[6-7] data above 1.06 GeV for the $e^+e^-\to K_S^0K_L^0$ and $e^+e^-\to K^+K^-$ reactions we fix the contribution of higher energy states.

We fit the cross sections of $e^+e^-\to K_S^0K_L^0$ and $e^+e^-\to K^+K^-$ with float m_ϕ, Γ_ϕ, $\Gamma_{\phi\to e^+e^-}\times B_{\phi\to K_S^0K_L^0}$, $\Gamma_{\phi\to e^+e^-}\times B_{\phi\to K^+K^-}$ and $g_{\rho/\omega}$ parameters. The obtained fit is shown in the Fig. 4 with the following parameters, which contain statistical errors as well as systematic and model-dependent uncertainties:

$$\left.\begin{aligned} m_\phi &= 1019.464 \pm 0.060\ \text{MeV/c}^2 \\ \Gamma_\phi &= 4.247 \pm 0.015\ \text{MeV} \\ \Gamma_{\phi\to ee}B_{\phi\to K_S^0K_L^0} &= 0.429 \pm 0.009\ \text{keV} \\ \Gamma_{\phi\to ee}B_{\phi\to K^+K^-} &= 0.679 \pm 0.022\ \text{keV} \\ r_{\rho/\omega} &= 0.76 \pm 0.11 \\ g_{V\to K^+K^-}/g_{V\to K_S^0K_L^0} &= 0.995 \pm 0.035 \end{aligned}\right\} \quad (3)$$

The difference of charged and neutral cross-sections for 24 energy points defined as $R_{c/n} = \sigma_{e^+e^-\to K^+K^-}\times\frac{p_{K^0}^3(s)}{p_{K^\pm}^3(s)}\times\frac{1}{Z(s)} - \sigma_{e^+e^-\to K_S^0K_L^0}$ is shown in Fig. 5. The difference $R_{c/n}$ is predominantly caused by interference term of resonance amplitudes of ϕ-meson and isovector ρ-meson. The shaded area corresponds to 1.8% and 3.2% systematic uncertainties in data for neutral and charged channel respectively. The result of the fit discussed above is shown by solid line that leads to agreement $\chi^2 = 37$. It should be mentioned that the case with $A_{\phi',\rho',\omega'} = 0$ and naive theoretical prediction $g_{V\to K^+K^-} = g_{V\to K_S^0K_L^0}$, $r_{\rho/\omega} = 1$ also gives an adequate description of experimental $R_{c/n}$. This case is characterized by $\chi^2 = 51$ and shown by the short dotted line, while long dotted lines correspond to the same theoretical prediction with $r_{\rho/\omega} = 0.5$ or 1.5 and differ strongly from data.

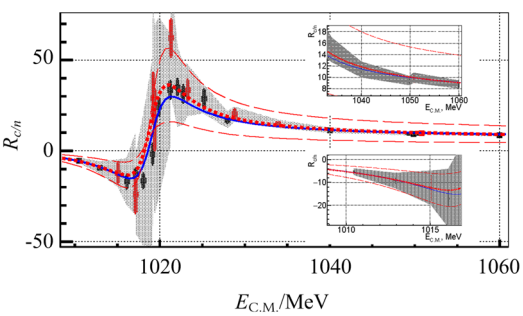

Fig. 5 The difference of charged and neutral cross-sections

5 Conclusion

Using pions from the $K_S^0\to\pi^+\pi^-$ decay and collinear charge kaons in DC we observed 6.5×10^5 and 1.6×10^6 events of the $e^+e^-\to K_S^0K_L^0$ and $e^+e^-\to K^+K^-$ processes respectively in the 1004-1060 MeV c.m. energy range, and measured its cross section with 1.8%-3.2% systematic error. Using VMD model the parameters of ϕ-meson are preliminary measured (Eq. (3)). The obtained deviation of ρ, ω amplitudes from naive theoretical prediction $r_{\rho/\omega} = 0.76 \pm 0.11$ allows to estimate the precision of used VMD-based phenomenological model as 25%. Moreover, obtained ratio $g_{V\to K^+K^-}/g_{V\to K_S^0K_L^0} = 0.995 \pm 0.035$ demonstrates the precision of SU(2)-symmetry better than 3.5%.

References

[1] DAVIER M, HOECKER A, MALAESCU B, et al. Reevaluation of the hadronic contributions to the muon $g-2$ and to $\alpha(M_Z^2)$ [J]. European Physics Journal C, 2011, 71(1): 1-13.

[2] BRAMON A, ESCRIBANO R, LUCIO J L, et al. The ratio $\Phi \to K^+K^-/K^0\bar{K}^0$ [J]. Physics Letters B, 2000, 486 (3-4): 406-413.

[3] AKHMETSHIN R R, AULCHENKI V M, BANZAROV V S, et al. Measurement of $\phi(1020)$ meson leptonic width with CMD-2 detector at VEPP-2M collider [J]. Physics Letters B, 2011, 695(5): 412-418.

[4] AKHMETSHIN R R, AULCHENKI V M, BANZAROV V S, et al. Measurement of $e^+e^- \to \phi \to K^+K^-$ $e^+e^- \to \phi \to K^+K^-$ cross section with the CMD-2 detector at VEPP-2M collider [J]. Physics Letters B, 2008, 669 (3-4): 217-222.

[5] ACHASOV M N, BELOBORODOV K I, BERDYUGIN A V, et al. Measurements of the parameters of the $\varphi(1020)$ resonance through studies of the processes $e^+e^- \to K^+K^-$, K_SK_L and $\pi^+\pi^-\pi^0$ [J]. Physical Review D, 2001, 63(7): 072002.

[6] LEES J P, POIREAU V, TISSERAND V, et al. Cross sections for the reactions $e^+e^- \to K_S^0K_L^0$, $K_S^0K_L^0\pi^+\pi^-$, $K_S^0K_S^0\pi^+\pi^-$, and $K_S^0K_S^0\pi^+\pi^-$ from events with initial-state radiation [J]. Physical Review D, 2014, 89 (9): 092002.

[7] LEES J P, POIREAU V, TISSERAND V, et al. Precision measurement of the $e^+e^- \to K^+K^-(\gamma)$ cross section with the initial-state radiation method at BABAR [J]. Physical Review D, 2013, 88(3): 032013.

[8] SHATUNOV YU M, EVSTINGEEV A V, GANYUSHIN D I, et al. Project of a new electron-positron collider VEPP-2000 [C]// Proceedings of the 7th European Particle Accelerator Conference. Vienna, Austria, 2000: 439-441.

[9] KHAZIN B I. Physics and detectors for VEPP-2000 [J]. Nuclear Physics B-Proceedings Supplements, 2008, 181: 376-380.

[10] AGOSTINELLI S, ALLISON J, AMAKO K, et al. GEANT4-a simulation toolkit [J]. Nuclear Instruments and Methods in Physics Research Section A, 2003, 506: 250-303.

[11] ARBUZOVA B, FEDOTOCICH G V, IGNATOV F V, et al. Monte-Carlo generator for e^+e^- annihilation into lepton and hadron pairs with precise radiative corrections [J]. European Physical Journal C, 2006, 46 (3): 689-703.

[12] ABAKUMOVA E V, ACHASOV M N, BERKAEV D E, et al. Backscattering of laser radiation on ultra-relativistic electrons in transverse magnetic field: Evidence of photon interference in a MeV scale [J]. Physical Review Letters, 2013, 110(14): 140402.

[13] AKHMETSHIN R R, ANISYONKOV A V, AHOKHIN S A, et al. First results from the CMD-3 detector at the VEPP-2000 collider [J]. Nuclear Physics B Proceedings Supplements, 2012, 225-227: 69-71.

[14] KURAEV E A, FADIN V S. Radiative corrections to the cross section for single-photon annihilation of an e^+e^- pair at high energy [J]. Soviet Journal of Nuclear Physics, 1985, 41(733): 466-469.

[15] BRUCH C, KHODJAMIRIAN A, KUHN J. Modeling the pion and kaon form factors in the time-like region [J]. European Physics Journal C, 2005, 39(1): 41-54.

[16] OLIVE K A, AGASHE K, AMSLER C, et al. The review of particle physics [J]. Chinese Physics C, 2014, 38: 090001.

Article ID:0253-2778(2016)06-0514-09

Measurement of $e^+e^- \to \eta\pi^+\pi^-$ and $e^+e^- \to \omega\pi^+\pi^-$ cross sections with the CMD-3 detector at the VEPP-2000 collider

POPOV A. S.[1,2], AKHMETSHIN R. R.[1,2], AMIRKHANOV A. N.[1,2], ANISENKOV A. V.[1,2], AULCHENKO V. M.[1,2], BANZAROV V. S.[1], BASHTOVOY N. S.[1], BERKAEV D. E.[1,2], BONDAR A. E.[1,2], BRAGIN A. V.[1], EIDELMAN D. E.[1,2], EPIFANOV D. A.[1,5], EPSHTEYN L. B.[1,3], EROFEEV A. L.[1,2], FEDOTOVICH G. V.[1,2], GAYAZOV S. E.[1,2], GREBENUK A. A.[1,2], GRIBANOV S. S.[1,2], GRIGORIEV D. N.[1,2,3], GROMOV E. M.[1,2], IGNATIN F. V.[1], IVANOV V. L.[1,2], KARPOV S. V.[1], KASAEV A. S.[1], KORPOTIN A. N.[1], KOOP I. A.[1,2], KOVALENKO O. A.[1,2], KAZANIN V. F.[1,2], KOZYREV A. N.[1], KOZYREV E. A.[1,2], KROKOVNY P. P.[1,2], KUZMENKO A. E.[1,3], KUZMIN A. S.[1,2], LOGASHENKO I. B.[1,2], LIKIN P. A.[1,2], MIKHAILOV K. YU.[1], OKHAPKIN V. S.[1], OTBOEV A. V.[1], PESTOV YU. N.[1], PIVOVAROV S. G.[1], RAZUVAEV G. P.[1,2], ROMANOV A. L.[1], RUBAN A. A.[1,2], RYSKULOV N. M.[1], RYZHENENKOV A. E.[1,2], SHEBALIN V. E.[1,2], SHEMYAKIN D. N.[1,2], SHWARTZ B. A.[1,2], SHWARTZ D. B.[1,2], SIBIDANLOV A. L.[1,4], SHATUNOV P. YU.[1], SHATUNOV YU. M.[1], SOLODOV E. P.[1,2], TITOV V. M.[1], TALYSHEV A. A.[1,2], VOROBIOV A. I..[1], YUDIN YU. V.[1], ZHARINOV YU. M.[1]

(1. *Budker Institute of Nuclear Physics*, *Novosibirsk* 630090, *Russia*;
2. *Novosibirsk State University*, *Novosibirsk* 630090, *Russia*;
3. *Novosibirsk State Technical University*, *Novosibirsk* 630092, *Russia*;
4. *Falkiner High Energy Physics Department*, *School of Physics*, *University of Sydney*, *Australia*
5. *Department of Physics*, *University of Tokyo*, 7-3-1 *Hongo Bunkyo-ku Tokyo* 113-0033, *Japan*)

Abstract: The processes $e^+e^- \to \eta\pi^+\pi^- \to \gamma\gamma\pi^+\pi^-$, $e^+e^- \to \eta\pi^+\pi^- \to \pi^0\pi^+\pi^-\pi^+\pi^-$ and $e^+e^- \to \omega\pi^+\pi^- \to \pi^0\pi^+\pi^-\pi^+\pi^-$ have been studied with the CMD-3 detector at the VEPP-2000 collider. For analysis data collected in the center-of-mass energy range from 1.2 to 2.0 GeV is used. Studied data corresponding to an integrated luminosity of 3×10^4 nb^{-1} were recorded in 2011 and 2012. The Born cross section of $e^+e^- \to \eta\pi^+\pi^-$ has been measured in the $\eta \to \gamma\gamma$ channel and is in good agreement with results obtained in other experiments. There are also preliminary results for the $e^+e^- \to \eta\pi^+\pi^-$ and $e^+e^- \to \omega\pi^+\pi^-$ Born cross sections in the $\eta \to \pi^+\pi^-\pi^0$ and $\omega \to \pi^+\pi^-\pi^0$ final states, respectively. The $e^+e^- \to \eta\pi^+\pi^-$ Born cross section data have been used to determine the $\tau^- \to \eta\pi^-\pi^0\nu^\tau$ decay branching fraction.

Key words: cross section; $\eta\pi^+\pi^-$; $\omega\pi^+\pi^-$; hadrons; branching; τ

CLC number: O572.3 **Document code**: A doi:10.3969/j.issn.0253-2778.2016.06.011

Received: 2015-11-30; **Revised**: 2016-04-20

Foundation item: Supported by Russian Foundation for Basic Research (15-02-05674).

Biography: POPOV A S (corresponding author), Professor/PhD. Research field: high energy physics. E-mail: aspopov1@inp.nsk.su

Citation: POPOV A S, AKHMETSHIN R R, AMIRKHANOV A N, et al. Measurement of $e^+e^-\to\eta\pi^+\pi^-$ and $e^+e^-\to\omega\pi^+\pi^-$ cross sections with the CMD-3 detector at the VEPP-2000 collider[J]. Journal of University of Science and Technology of China, 2016,46(6): 514-522.
POPOV A S, AKHMETSHIN R R, AMIRKHANOV A N, 等. VEPP-2000 e^+e^- 对撞机上用 CMD-3 探测器测量 $e^+e^-\to\eta\pi^+\pi^-$ 和 $e^+e^-\to\omega\pi^+\pi^-$ 的截面[J]. 中国科学技术大学学报,2016,46(6): 514-522.

VEPP-2000 e^+e^- 对撞机上用 CMD-3 探测器测量 $e^+e^-\to\eta\pi^+\pi^-$ 和 $e^+e^-\to\omega\pi^+\pi^-$ 的截面

POPOV A. S.[1,2], AKHMETSHIN R. R.[1,2], AMIRKHANOV A. N.[1,2], ANISENKOV A. V.[1,2], AULCHENKO V. M.[1,2], BANZAROV V. S.[1], BASHTOVOY N. S.[1], BERKAEV D. E.[1,2], BONDAR A. E.[1,2], BRAGIN A. V.[1], EIDELMAN D. E.[1,2], EPIFANOV D. A.[1,5], EPSHTEYN L. B.[1,3], EROFEEV A. L.[1,2], FEDOTOVICH G. V.[1,2], GAYAZOV S. E.[1,2], GREBENUK A. A.[1,2], GRIBANOV S. S.[1,2], GRIGORIEV D. N.[1,2,3], GROMOV E. M.[1,2], IGNATIN F. V.[1], IVANOV V. L.[1,2], KARPOV S. V.[1], KASAEV A. S.[1], KORPOTIN A. N.[1], KOOP I. A.[1,2], KOVALENKO O. A.[1,2], KAZANIN V. F.[1,2], KOZYREV A. N.[1], KOZYREV E. A.[1,2], KROKOVNY P. P.[1,2], KUZMENKO A. E.[1,3], KUZMIN A. S.[1,2], LOGASHENKO I. B.[1,2], LIKIN P. A.[1,2], MIKHAILOV K. YU.[1], OKHAPKIN V. S.[1], OTBOEV A. V.[1], PESTOV YU. N.[1], PIVOVAROV S. G.[1], RAZUVAEV G. P.[1,2], ROMANOV A. L.[1], RUBAN A. A.[1,2], RYSKULOV N. M.[1], RYZHENENKOV A. E.[1,2], SHEBALIN V. E.[1,2], SHEMYAKIN D. N.[1,2], SHWARTZ B. A.[1,2], SHWARTZ D. B.[1,2], SIBIDANLOV A. L.[1,4], SHATUNOV P. YU.[1], SHATUNOV YU. M.[1], SOLODOV E. P.[1,2], TITOV V. M.[1], TALYSHEV A. A.[1,2], VOROBIOV A. I..[1], YUDIN YU. V.[1], ZHARINOV YU. M.[1]

(1. 俄罗斯布德克尔核物理研究所, 新西伯利亚 630090, 俄罗斯;
2. 国立新西伯利亚大学, 新西伯利亚 630090, 俄罗斯;
3. 国立新西伯利亚理工大学, 新西伯利亚 630090, 俄罗斯;
4. 悉尼大学物理学院高能物理系,悉尼,澳大利亚;
5. 东京大学物理系, 东京 113-0033, 日本)

摘要:在 VEPP-2000e^+e^- 对撞机上,CMD-3 探测器研究了 $e^+e^-\to\eta\pi^+\pi^-\to\gamma\gamma\pi^+\pi^-$, $e^+e^-\to\eta\pi^+\pi^-\to\pi^0\pi^+\pi^-\pi^+\pi^-$ 以及 $e^+e^-\to\omega\pi^+\pi^-\to\pi^0\pi^+\pi^-\pi^+\pi^-$ 等过程. 分析使用的是 2011 和 2012 年在 1.2-2.0GeV 能区收集的相应积分亮度为 $3\times10^4\,\mathrm{nb}^{-1}$ 的数据. 用 $\eta\to\gamma\gamma$ 道测量了 $e^+e^-\to\eta\pi^+\pi^-$ 的波恩截面,结果与相关的实验结论相吻合;还用末态 $\eta\to\pi^+\pi^-\pi^0$ 和 $\omega\to\pi^+\pi^-\pi^0$ 分别得到了 $e^+e^-\to\eta\pi^+\pi^-$ 和 $e^+e^-\to\omega\pi^+\pi^-$ 波恩截面的初步结果;$e^+e^-\to\eta\pi^+\pi^-$ 波恩截面的数值还被用于确定 $\tau^-\to\eta\pi^-\pi^0\nu^\tau$ 的衰变分支比.

关键词:截面; $\eta\pi^+\pi^-$; $\omega\pi^+\pi^-$; 强子; τ

0 Introduction

The total cross section of e^+e^- pair annihilation into hadrons can be used for the calculation of the muon anomalous magnetic moment. For this reason, we need to know all significant exclusive contributions to the $e^+e^-\to$hadrons cross section. The Born cross sections of $e^+e^-\to\eta\pi^+\pi^-$ and $e^+e^-\to\omega\pi^+\pi^-$ are two examples of such exclusive channels.

Dynamics of studied processes are particularly useful for testing various phenomenological models, among them models, which allow to describe different

contributions to the $\eta\pi^+\pi^-$ internal structure besides $\rho(770)\eta$. The test can be performed by studying the $\pi^+\pi^-$ invariant mass and angular distributions of final particles.

The $e^+e^-\to\eta\pi^+\pi^-$ Feynman diagram for the model of vector dominance (VDM) is shown in Fig. 1. Two of possible Feynman VDM diagrams that provide a main contribution to the process $e^+e^-\to\pi^+\pi^-\pi^+\pi^-\pi^0$ are shown in Fig. 2.

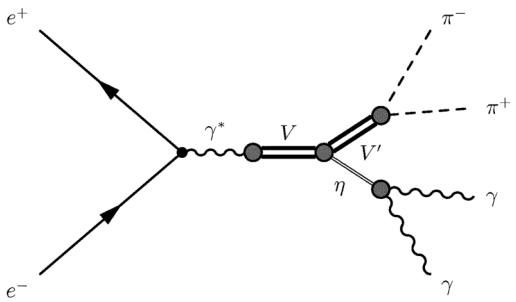

Fig. 1 Feynman diagram describing

In Fig. 1, Feynman diagram describing the $e^+e^-\to\eta\pi^+\pi^-$, $\eta\to\gamma\gamma$ in the vector-meson dominance model (VDM), where $V=\rho(770)$, $\rho(1450)$, $\rho(1700)$, $V'=\rho(770)$.

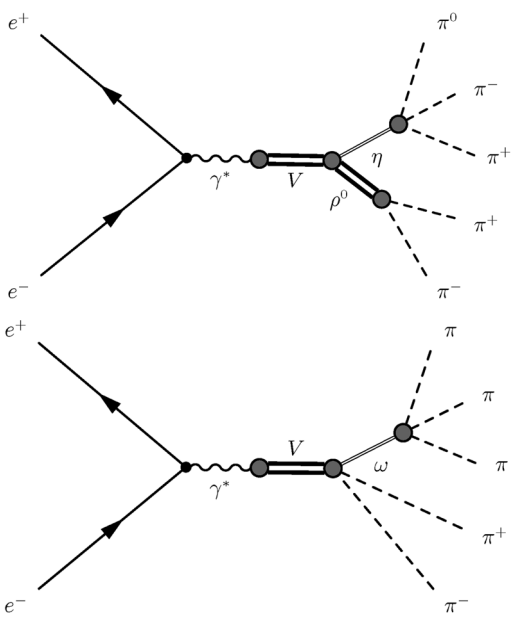

Fig. 2 Feynman diagrams of two main contributions to internal structure of the $e^+e^-\to\pi^+\pi^-\pi^+\pi^-\pi^0$ process

The result of the measurement of the $e^+e^-\to\eta\pi^+\pi^-$ can be used to find the $\eta\to\gamma^*\gamma^*$ transition form factor[1] and to test the conservation of vector current (CVC), which relates the $\tau^-\to\eta\pi^-\pi^0\nu_\tau$ decay rate with the $e^+e^-\to\eta\pi^+\pi^-$ cross section[2].

Measurements of the $e^+e^-\to\eta\pi^+\pi^-$ cross section have been also performed in the SND, BaBar and CMD-2 experiments[3-11]. The $e^+e^-\to\omega\pi^+\pi^-$ Born cross section measurement has been performed in the BaBar experiment[8].

1 Experiment

CMD-3 (Fig. 3) is the general-purpose cryogenic magnetic detector installed at the electron-positron collider VEPP-2000, which is situated in Budker Institute of Nuclear Physics(BINP). In order to reach the design luminosity in the single-bunch mode the round beam technique is used. This collider operates in the center-of-mass energy range from 0.32 GeV to 2.00 GeV.

The tracking system of the CMD-3 detector consists of a double-layer multiwire proportional Z-chamber and a cylindrical drift chamber with hexagonal cells, whose volume is filled with the argon-isobutane gas mixture. The magnetic field in the track system is provided by the superconducting solenoid, which surrounds the drift and Z- chambers. In 2011 the magnetic field was equal to 1.0 T and in 2012 to 1.3 T. The barrel electromagnetic calorimeter is outside of the superconducting solenoid and consists of two parts. The first part of the barrel electromagnetic calorimeter is the Liquid Xenon calorimeter ($5.4X_0$), which allows to measure the coordinates of photons with the accuracy of 1-2 mm. The second part is the CsI crystal calorimeter ($8.1X_0$). There is also the endcap BGO crystal calorimeter ($13.4X_0$), the time-of-flight and the muon system.

2 $e^+e^-\to\eta\pi^+\pi^-$, $\eta\to\gamma\gamma$

2.1 Event selection

(Ⅰ) Each event must have at least two tracks. Furthermore, two and only two tracks must be central and have zero total charge.

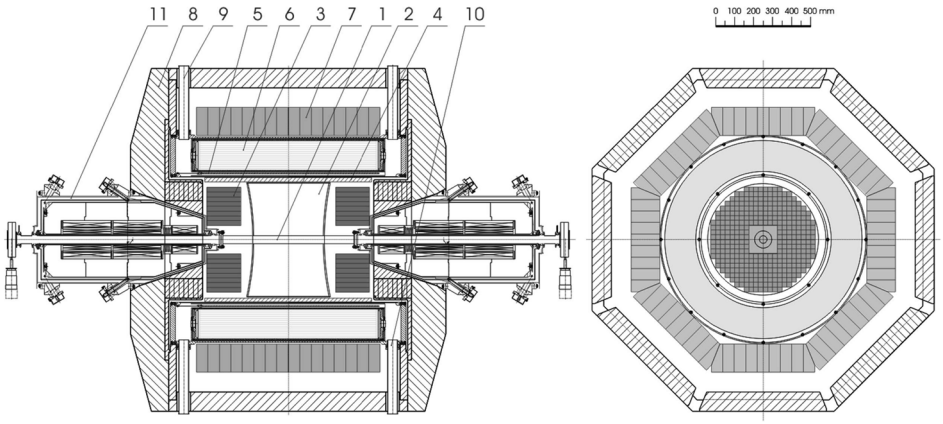

1 – vacuum chamber, 2 – drift chamber, 3 – BGO endcap calorimeter, 4 – Z-chamber, 5 – superconducting solenoid, 6 – LXe calorimetersuperconducting solenoid, 7 – CsI barrel calorimeter, 8 – iron yoke, 9 – iron yoke, 10 – vacuum pumpdown, 11 – VEPP2000 superconducting magnetic lenses

Fig. 3　CMD-3 detector

(Ⅱ) Presence of at least two photons is required.

(Ⅲ) Bhabha background suppression. The selection criterion for track momentum noncollinearity, restriction on the energy release of two good tracks in calorimeters.

(Ⅳ) Kinematic fit for each pair of photons. Searching the pair of photons, which gives the minimal χ^2 after a kinematic fit.

(Ⅴ) Restriction on the χ^2 after the kinematic fit: $\chi^2<60$.

2.2　Simulation of the $e^+e^-\to\eta\pi^+\pi^-$ process and detection efficiency

Simulation of the $e^+e^-\to\eta\pi^+\pi^-$ process has been performed using the Monte Carlo method. For this goal we need to know the dependence of the $e^+e^-\to\eta\pi^+\pi^-$ invariant amplitude on momenta of the final particles. This dependence has the form:

$$M_{e^+e^-\to\eta\pi^+\pi^-}\sim\frac{\epsilon_{\alpha\beta\lambda\delta}J_l^\alpha P_\eta^\beta P_{\pi^+}^\gamma P_{\pi^-}^\delta}{D_\rho(P_\rho=P_{\pi^+}+P_{\pi^-})}\qquad(1)$$

where P_{η,π^+,π^-} are momenta of final particles, J_l is the lepton current and $D(P_\rho)$ is the inverse propagator of the ρ-meson.

The detection efficiency has been found using Monte Carlo simulation of $e^+e^-\to\eta\pi^+\pi^-$. Taking into account track loss and differences between the simulated and experimental distributions the detection efficiency correction has been performed. The corrected detection efficiency is shown in Fig. 4.

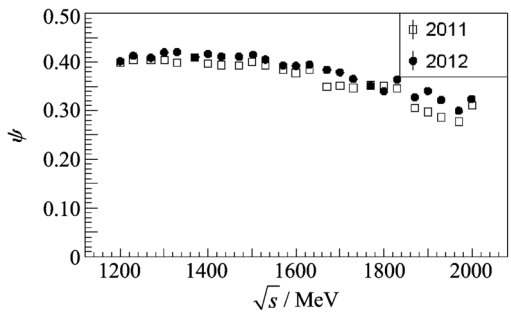

Fig. 4　Detection efficiency for the process $e^+e^-\to\eta\pi^+\pi^-$, $\eta\to\gamma\gamma$

2.3　Internal structure of the $\eta\pi^+\pi^-$ final state

The two-pion invariant mass distribution shown in Fig. 5 has a peak of the $\rho(770)$ resonance. The $\pi^+\pi^-$ invariant mass spectrum from simulation is in good agreement with the same spectrum from experiment. Simulation takes into account just the $\eta\rho(770)$ internal state. Good agreement between the $\pi^+\pi^-$ invariant mass spectra from simulation and experiment means that the $\eta\rho(770)$ internal state dominates in the $e^+e^-\to\eta\pi^+\pi^-$ process.

In Fig. 5, the $\pi^+\pi^-$ invariant mass spectrum in the center-of-mass energy range 1475-1725 MeV with hard selection criteria: $N_\gamma=2$, $\chi^2<30$. N_γ is the number of photons in an event. All other selection

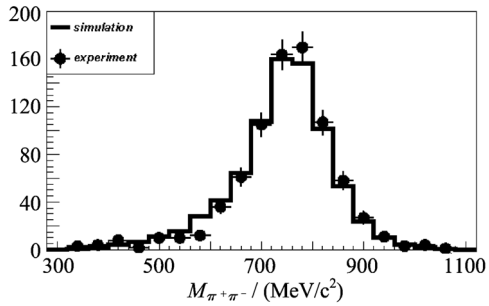

Fig. 5 The $\pi^+\pi^-$ invariant mass spectrum

criteria are standard. The two π-meson invariant mass spectrum from the simulation is normalized to the number of events in the experimental spectrum.

Fig. 6 shows the distribution of the η-meson polar angle. The distribution from simulation of the $e^+e^- \to \eta\pi^+\pi^-$ process is in good agreement with the same distribution from experiment. The shape of the η-meson polar angle distributions seems to be very close to $1+\cos\theta_\eta^2$.

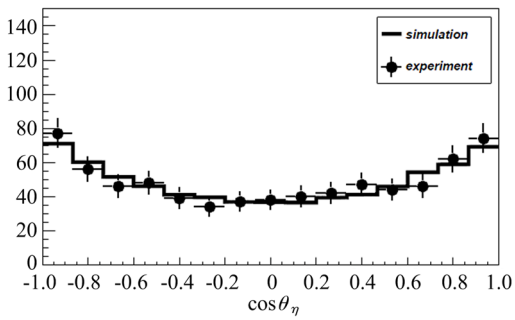

Fig. 6 Cosine of the polar angle of the η-meson

In Fig. 6, cosine of the polar angle of the η-meson in the center-of-mass energy range 1475-1725 MeV with hard selection criteria: $N_\gamma = 2$, $\chi^2 < 30$. N_γ is the number of photons in an event. All other selection criteria are standard. The distribution from simulation is normalized to the number of events in the experimental distribution.

2.4 Measurement of the $\eta\pi^+\pi^-$ event yield

Spectra of the two-photon invariant mass from simulation of $e^+e^- \to \eta\pi^+\pi^-$ have been fitted by a linear combination of normal distributions normalized to the free parameter, which gives the number of events in each simulation spectrum. The example of the fitted two-photon invariant mass spectrum for the point with the center-of-mass energy of 1500 MeV in simulation is shown in Fig. 7 (at the center-of-mass energy of 1500 MeV of in simulation).

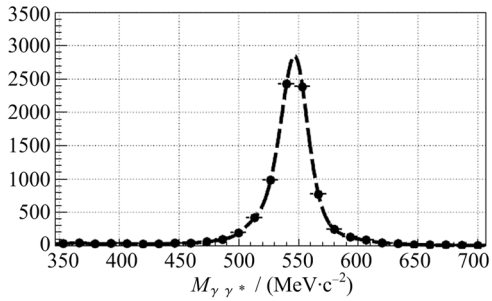

Fig. 7 Fit of the two-photon invariant mass spectrum

The experimental two-photon invariant mass spectra have been fitted by a sum of the second-order polynomial and shifted fit function from simulation with a resolution correction. All parameters in the fit function from simulation besides the number of events are fixed. The shift of the fit function from simulation along the two-photon invariant mass axis is a free fit parameter. The resolution correction dispersion and parameters of the second-order polynomial are also free. An example of the fitted two-photon invariant mass in experiment at 1500 MeV is shown in Fig. 8 (at 1500 MeV in experiment).

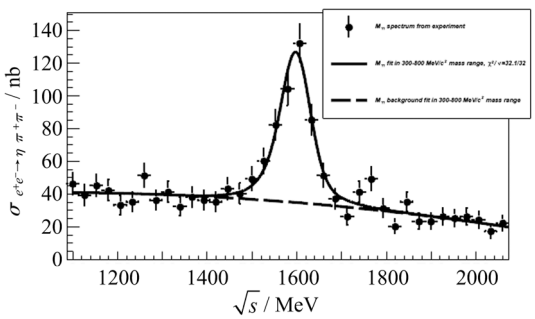

Fig. 8 Fit of the two-photon invariant mass spectrum

2.5 Results and discussion

The visible cross section at the ith center-of-mass energy point is determined as

$$\sigma_{\rm vis}(E_i) = \frac{N(E_i)}{\epsilon(E_i)B(\eta\to\gamma\gamma)L(E_i)} \quad (2)$$

where E_i is the ith center-of-mass energy, N is event yield, ϵ is detection efficiency, $B(\eta\to\gamma\gamma)$ is branching fraction at the $\eta\to\gamma\gamma$ decay and L is luminosity. Luminosity is measured using Bhabha scattering[12].

The relation between the visible and Born cross sections is given by the following formula[13].

$$\sigma_{\rm vis}(s) = \int_0^{1-\frac{(2m_\pi+m_\eta)^2}{s}} {\rm d}x\sigma_B(s(1-x))F(x,s) \quad (3)$$

where $\sigma_{\rm vis}$ and σ_B are the visible and the Born cross sections, respectively, $F(x,s)$ is the ISR radiator function, m_π and m_η are masses of π-meson and η-meson, respectively. This relation is used to fit the visible cross section and get VDM parameterization parameters of the Born cross section. Then the Born cross section experimental data can be represented as

$$\left.\begin{aligned}\sigma_B(E_i) &= \frac{\sigma_{\rm vis}(E_i)}{1+\delta(E_i)}\\ 1+\delta(E_i) &= \frac{\sigma_{\rm vis}^{\rm fit}(E_i)}{\sigma_B^{\rm fit}(E_i)}\end{aligned}\right\} \quad (4)$$

where $\sigma_{\rm vis}$ is the experimental visible cross section, E_i is the ith center-of-mass energy, δ is a radiative correction, $\sigma_{\rm vis}^{\rm fit}$ and $\sigma_B^{\rm fit}$ are visible and Born cross section fit functions, respectively. Energy dependence of the $e^+e^-\to\eta\pi^+\pi^-$ Born cross section is shown in Fig. 9. The systematic uncertainty in the measured Born cross section is 4.3.

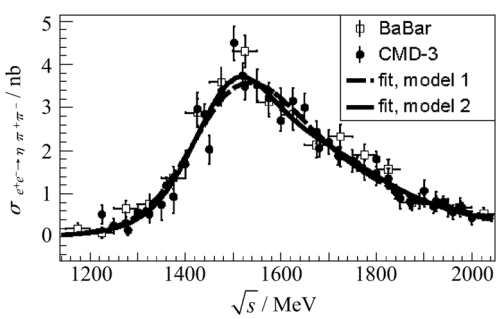

Fig. 9　The Born cross section of the $e^+e^-\to\eta\pi^+\pi^-$ process measured in the $\eta\to\gamma\gamma$ channel

The function used for the parameterization of the $e^+e^-\to\eta\pi^+\pi^-$ Born cross section is based on the VDM model with several isovectors (the isoscalar part is suppressed by G-parity conservation) contributions of the states $\rho(770)$, $\rho(1450)$ and $\rho(1700)$ decaying to $\eta\rho(770)$[3,14]:

$$\left.\begin{aligned}\sigma_B(s) &= \int_{4m_\pi^2}^{(\sqrt{s}-m_\eta)^2}\frac{{\rm d}\sigma}{{\rm d}q^2}(s,q^2)\,{\rm d}q^2\\ \frac{{\rm d}\sigma}{{\rm d}q^2}(s,q^2) &= \frac{4\alpha^2}{3s\sqrt{s}}\frac{\sqrt{q^2}\Gamma_\rho(q^2)p_\eta^3(s,q^2)}{(q^2-m_\rho^2)^2+(\sqrt{q^2}\Gamma_\rho(q^2))^2}|F_s|^2\\ p_\eta^2 &= \frac{(s-m_\eta^2-q^2)^2-4m_\eta^2q^2}{4s}\\ \Gamma_\rho(q^2) &= \Gamma_\rho(m_\rho^2)\frac{m_\rho^2}{q^2}\left(\frac{p_\pi^2(q^2)}{p_\pi^2(m_\rho^2)}\right)^{\frac{3}{2}}\\ p_\pi^2(q^2) &= q^2/4-m_\pi^2\end{aligned}\right\} \quad (5)$$

where q is the momentum of the 2π system, and form factor $F(s)$ corresponds to transition $\gamma^*\to\eta\rho$:

$$\left.\begin{aligned}F(s) &= \sum_V\frac{m_V^2}{g_{V\gamma}}\frac{g_{V\rho\eta}}{s-m_V^2+i\sqrt{s}\Gamma_V(s)}\\ V &= \rho(770),\rho(1450),\rho(1700)\end{aligned}\right\} \quad (6)$$

The parameters $g_{V\rho\eta}$ and $g_{V\gamma}$ are the coupling constants for the transitions $V\to\rho\ \eta$ and $V\to\gamma^*$ and should be redefined as $g_{V\rho\eta}/g_{V\gamma}=g_Ve^{i\phi_V}$. The coupling constants related to $\rho(770)\to\rho(770)\eta$ are calculated using data on the partial widths for the decays $\rho(770)\to e^+e^-$ and $\rho(770)\to\eta\gamma$[3,15]:

$$\left.\begin{aligned}g_{\rho\gamma}^2 &= \frac{4\pi}{3}\alpha^2\frac{m_\rho}{\Gamma(\rho\to e^+e^-)},\ g_{\rho\gamma}\approx 4.96\\ g_{\rho\eta\gamma}^2 &= \frac{24}{\alpha}m_\rho^3\frac{\Gamma(\rho\to\eta\gamma)}{(m_V^2+m_\eta^2)^3},\ g_{\rho\eta\gamma}\approx 1.59\ {\rm GeV}^{-1}\\ g_{\rho\rho\eta} &= g_{\rho\gamma}g_{\rho\eta\gamma}\approx 7.86\ {\rm GeV}^{-1}\end{aligned}\right\} \quad (7)$$

The best phase combination $\phi_{\rho(770)}=0$ and $\phi_{\rho(1450)}=\phi_{\rho(1700)}=\pi$ was obtained and fixed in the following approximation. The parameters of the $\rho(770)$ resonane are fixed at the nominal values. The " model 1 " contains free parameters $g_{\rho(1450)}$, $M_{\rho(1450)}$, $\Gamma_{\rho(1450)}$, but parameters $g_{\rho(1700)}$, $M_{\rho(1700)}$, $\Gamma_{\rho(1700)}$ are fixed ($g_{\rho(1700)}=0$). The " model 2 " contains free parameters $g_{\rho(1450)}$, $M_{\rho(1450)}$, $\Gamma_{\rho(1450)}$ and the parameters of the $\rho(1700)$ resonance are also free.

The contribution of the $\rho(1700)$ obtained in the fit in "model 2" is not statisticaly significant. The value of χ^2/ν for the fit in "model 1" is 53.27/46, where ν is the number of degrees of freedom. This value corresponds to the probability $P(\chi^2,\nu)\approx 21\%$. The value of χ^2/ν for the fit in "model 2" is 50.26/43, which corresponds to the probability $P(\chi^2,\nu)\approx 21\%$.

The $e^+e^-\to\eta\pi^+\pi^-$ Born cross section can be used to calculate the $\tau^-\to\eta\pi^-\pi^0\nu_\tau$ branching fraction. To reach this goal we need to use the following formula, which has been obtained under the CVC hypothesis[3,16].

$$\frac{B(\tau^-\to\eta\pi^-\pi^0\nu^\tau)}{B(\tau^-\to\nu_\tau e^-\bar{\nu}_e)}=\frac{3m_\tau^2\cos^2\theta_C}{2\pi\alpha^2}\times \int_0^1 dx x(1-x)^2(1+2x)\sigma_{e^+e^-\to\eta\pi^+\pi^-}(m_\tau^2x) \quad (8)$$

Calculations performed for our $e^+e^-\to\eta\pi^+\pi^-$ Born cross section data using this formula give us the following result for the $\tau^-\to\eta\pi^-\pi^0\nu_\tau$ branching fraction

$$B(\tau^-\to\eta\pi^-\pi^0\nu^\tau)=(0.147\pm0.003\pm0.006)\% \quad (9)$$

which is in agreement with the world average experimental value $(0.139\pm0.01)\%$[15], the SND CVC result $(0.156\pm0.004\pm0.010)\%$[3] and with the CVC result $(0.153\pm0.018)\%$ for the earlier $e^+e^-\to\eta\pi^+\pi^-$ data[2]. The first uncertainty in the $B(\tau^-\to\eta\pi^-\pi^0\nu^\tau)$ branching fraction (Eq. (9) is statistical, the second is systematic). The statistical uncertainty has been calculated in the following way. All parameters in the VDM fit function of the $e^+e^-\to\eta\pi^+\pi^-$ Born cross section have been fixed. This function has been multiplied by a free parameter, which plays the role of a relative amplitude. The cross section has been fitted by this function. The uncertainty in the value of the free parameter in the fit function is the same as a relative statistical uncertainty in the $B(\tau^-\to\eta\pi^-\pi^0\nu^\tau)$ branching fraction. For the calculation of a systematic uncertainty in the $B(\tau^-\to\eta\pi^-\pi^0\nu^\tau)$ branching fraction the systematic uncertainty in the $e^+e^-\to\eta\pi^+\pi^-$ Born cross section (4.3%) has been used.

3 $e^+e^-\to\eta\pi^+\pi^-\to\pi^+\pi^-\pi^+\pi^-\pi^0$ and $e^+e^-\to\omega\pi^+\pi^-\to\pi^+\pi^-\pi^+\pi^-\pi^0$

3.1 Event selection

(Ⅰ) Each event must have at least four tracks. Furthermore, four and only four tracks must be central with zero total charge.

(Ⅱ) Presence of at least two photons is required.

(Ⅲ) Kinematic fit for each possible photon pair combinations in $e^+e^-\to\pi^+\pi^-\pi^+\pi^-\pi^0$ hypothesis, which requires energy-momentum conservation and origination of all particles from one vertex. Searching for a pair of photons, which gives the minimal chi square $\chi^2_{5\pi}$ after a kinematic fit. Selection criterion: $\chi^2_{5\pi}<50$.

(Ⅳ) Restriction on the two-photon invariant mass: $90<M_{\gamma\gamma}<200$.

(Ⅴ) Kinematic fit in $e^+e^-\to\pi^+\pi^-\pi^+\pi^-$ hypothesis. Selection criterion $\chi^2_{4\pi}>300$ to suppress background from $e^+e^-\to\pi^+\pi^-\pi^+\pi^-$ process.

(Ⅵ) Kinematic fit with $M_{\gamma\gamma}=M_{\pi^0}$ requirement, which is needed to improve resolution in the $\pi^+\pi^-\pi^0$ invariant mass spectra.

3.2 Simulation of the $e^+e^-\to\eta\pi^+\pi^-$ and $e^+e^-\to\omega\pi^+\pi^-$

The simulation of the $e^+e^-\to\pi^+\pi^-\pi^+\pi^-\pi^0$ process has been performed in assumption that the intermediate states corresponding to the first and the second feynman diagrams from Fig. 2 gives the dominant contribution to the $e^+e^-\to\pi^+\pi^-\pi^+\pi^-\pi^0$ process.

The detection efficiencies of the $e^+e^-\to\eta\pi^+\pi^-$ and $e^+e^-\to\omega\pi^+\pi^-$ have been determined from simulation. These detection efficiencies are shown in Fig. 10 (Detection efficiencies for the $e^+e^-\to\eta\pi^+\pi^-$ and $e^+e^-\to\omega\pi^+\pi^-$ in $\eta\to\pi^+\pi^-\pi^0$ and $\omega\to\pi^+\pi^-\pi^0$ channels).

3.3 $\eta\pi^+\pi^-$ and $\omega\pi^+\pi^-$ event yield

The $\pi^+\pi^-\pi^0$ invariant mass spectra from simulation have been fitted using linear combination of

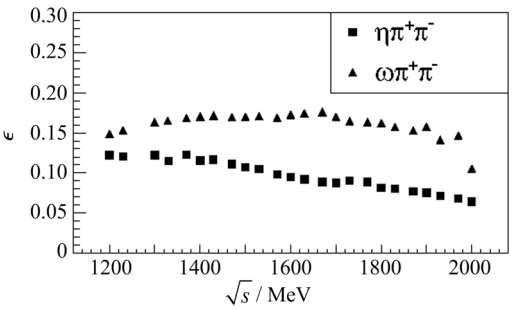

Fig. 10　Detection efficiencies

normal distributions. The fit functions from simulation are normalized to the number of signal events.

The experimental fit function consists of fit functions from simulations of $e^+e^-\to\eta\pi^+\pi^-$ and $e^+e^-\to\omega\pi^+\pi^-$ and Gaussian background. The fit function from simulation is shifted along mass axis and has a resolution correction. Shifts and resolution corrections in each center-of-mass energy point are free parameters. All parameters in simulation besides the number of events are fixed. The $\pi^+\pi^-\pi^0$ invariant mass distribution with a fit at the point 1540 MeV is shown in Fig. 11.

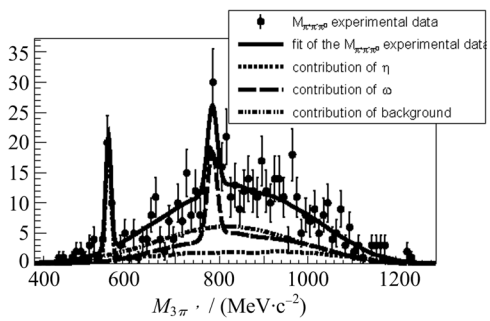

Fig. 11　$\pi^+\pi^-\pi^0$ invariant mass spectrum

In Fig. 11, $\pi^+\pi^-\pi^0$ invariant mass spectrum at 1540 MeV. $\chi^2/\nu = 127/195$, where χ^2 is chi square of the fit function and ν is the number of degrees of freedom.

3.4　Results and discussion

The Born cross sections for the $e^+e^-\to\eta\pi^+\pi^-$ and $e^+e^-\to\omega\pi^+\pi^-$ have been calculated in $\eta\to\pi^+\pi^-\pi^0$ and $\omega\to\pi^+\pi^-\pi^0$ channels, respectively, using the same technique as in the calculation of $e^+e^-\to\eta\pi^+\pi^-$ Born cross section in the $\eta\to\gamma\gamma$ channel. The results are presented in Figs. 12, 13. The preliminary estimation of a systematic uncertainty for the $e^+e^-\to\eta\pi^+\pi^-$ and $e^+e^-\to\omega\pi^+\pi^-$ Born cross sections is about 10%.

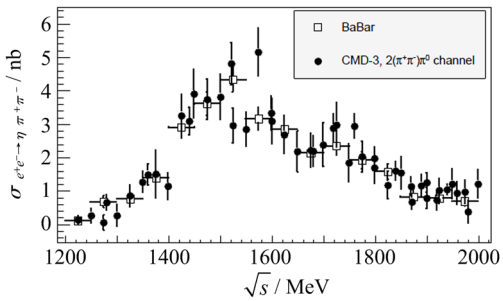

Fig. 12　The Born cross section for the $e^+e^-\to\eta\pi^+\pi^-$ process

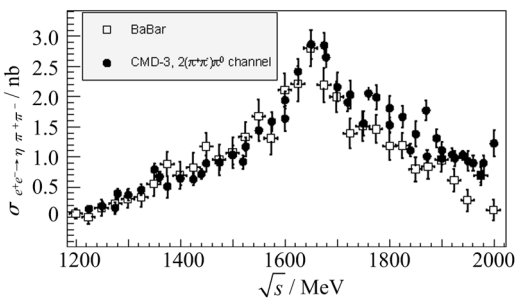

Fig. 13　The Born cross section for the $e^+e^-\to\omega\pi^+\pi^-$ process

References

[1] XIAO C W, DATO T, HANHART C, et al. Towards an improved understanding of $\eta\to\gamma^*\gamma^*$ [J]. Physics, 2015: arXiv:1509.02194.

[2] CHEREPANOV V, EIDELMAN S. Decays $\tau\to\eta(\eta)\pi\pi\nu$ and CVC[J]. Nuclear Physics Proceedings Supplements, 2011, 218(1): 231-236.

[3] AULCHENKO V M, ACHASOV M N, BARNYAKOV A Y, et al. Measurement of the $e^+e^-\to\eta\pi^+\pi^-$ cross section in the center-of-mass energy range 1.22-2.00 GeV with the SND detector at the VEPP-2000 collider [J]. Physical Review D, 2015, 91: 052013.

[4] DELCOURT B, BISELLO D, BIZOT J C, et al. Study of

the reactions $e^+e^-\to\rho\eta$, $\rho\pi$, $\varphi\pi$ and $\varphi\eta$ for total energy ranges between 1.4 and 2.18 GeV[J]. Physics Letters B, 1982, 113(1): 93-97.

[5] ACHASOV M N, BELOBORODOV K I, BERDYUGIN A V, et al. Measurement of the $e^+e^-\to\eta\pi^+\pi^-$ cross section in the $s\sqrt{s}$ = 1.04-1.38 GeV energy range with a spherical neutral detector at the VEPP-2M collider[J]. Journal of Experimental and Theoretical Physics Letters, 2010, 92(2): 80-84.

[6] BELOUS M, BAI J Z, BAI Y, et al. Study of J/ψ decays into $\eta K^{*0}\bar{K}^{*0}$[J]. Physics Letters B, 2010, 685(1): 27-32.

[7] GLASHOW K, SHAPKIN M, ADACHI I, et al. Measurement of cross sections of exclusive $e^+e^-\to VP$ processes at $s\sqrt{s}$ = 10.58 GeV[J]. Physics Letters B, 2009, 681: 400-405.

[8] AUBERT B, BONA M, BOUTIGNY D, et al. Erratum: The $e^+e^-\to2(\pi^+\pi^-)\pi^0$, $2(\pi^+\pi^-)\eta$, $K^+K^-\pi^+\pi^-\pi^0$ and $K^+K^-\pi^+\pi^-\eta$ cross sections measured with initial-state radiation[J]. Physical Review D, 2007, 76: 092005.

[9] AKHMETSHIN R R, ANASHKIN E V, AULCHENKO V M, et al. Study of the process $\varphi\to\pi^+\pi^-\pi^0$ with CMD-2 detector[J]. Physics Letters B, 2000, 489(1-2): 125130.

[10] ANTONELLI A, BALDINI R, CALCATERRA S, et al. Measurement of the reaction $e^+e^-\to\eta\pi^+\pi^-$ in the center of mass energy interval 1350-2400 MeV[J]. Physics Letters B, 1988, 212(1): 133-138.

[11] DRUZHININ V P, DUBROVIN M S, EIDELMAN S I, et al. Investigation of the reaction $e^+e^-\to\eta\pi^+\pi^-$ in the energy range up to 1.4 GeV[J]. Physics Letters B, 1986, 174(1): 115-117.

[12] AKHMETSHIN R R, ANISYONKOV A V, AHOKHIN S A, et al. First results from the CMD-3 detector at the VEPP-2000 collider[J]. Nuclear Physics B Proceedings Supplements, 2012, 225-227: 69-71.

[13] KURAEV E A, FADIN V S. Radiative corrections to the cross section for single-photon annihilation of an e^+e^- pair at high energy[J]. Soviet Journal of Nuclear Physics, 1985, 41(733): 466-469.

[14] ACHASOV N N, KARNAKOV V A. Reaction $e^+e^-\to\eta\pi^+\pi^-$[J]. Journal of Experimental and Theoretical Physics Letters, 1984, 39: 285-290.

[15] OLIVE K A, AGASHE K, AMSLER C, et al. Review of particle physics[J]. Chinese Physics C, 2014, 38(9): 090001.

[16] GILMAN F J. τ decays involving the η meson[J]. Physical Review D, 1987, 35(11): 3541-3547.

Article ID:0253-2778(2016)06-0523-05

Study of the $e^+e^- \to VP$ reactions at the VEPP-2000 e^+e^- collider with the SND detector

BOTOV A. A. (for the SND collaboration)

(*Budker Institute of Nuclear Physics*, *Novosibirsk* 630090, *Russia*)

Abstract: The reactions $e^+e^- \to \rho\pi$, $\omega\pi$, $\rho\eta$, $\omega\eta$ have been studied in the energy region 1.05-2.00 GeV. The experiment has been carried out at the VEPP-2000 e^+e^- collider with the SND detector. The measured cross sections have been fitted in the vector meson dominance model.

Key words: VEPP-2000; SND detector

CLC number: O572.3 **Document code**: A doi:10.3969/j.issn.0253-2778.2016.06.012

Citation: BOTOV A A(for the SND collaboration). Study of the $e^+e^- \to VP$ reactions at the VEPP-2000 e^+e^- collider with the SND detector[J]. Journal of University of Science and Technology of China, 2016,46(6): 523-527.
BOTOV A A(代表 SND 合作组). 用 SDN 探测器研究 VEPP-2000 对撞机上 $e^+e^- \to VP$ 的反应[J]. 中国科学技术大学学报,2016, 46(6): 523-527.

用 SDN 探测器研究 VEPP-2000 对撞机上 $e^+e^- \to VP$ 的反应

BOTOV A. A(代表 SND 合作组)

(俄罗斯布德克尔核物理研究所, 新西伯利亚 630090, 俄罗斯)

摘要:研究了 1.05-2.00 GeV 能区 $e^+e^- \to \rho\pi$, $\omega\pi$, $\rho\eta$, $\omega\eta$ 的反应,用 SDN 探测器在 VEPP-2000 对撞机上进行了实验,测量的截面适合用矢量介子模型来拟合.

关键词:强子; 信号/本地分离; 截面

0 Introduction

The transitions into the VP final states, where V and P denote vector and pseudoscalar mesons, respectively, are dominant decay modes for excited states of the vector ρ, ω, and ϕ mesons. In the center-of-mass(c.m.) energy region $\sqrt{s}$ = 1-2 GeV, where these vector resonances are located, the reactions $e^+e^- \to VP$ constitute a significant part of the cross section $e^+e^- \to$ hadrons. In this paper we study the reactions of this type with $VP = \rho\pi$, $\omega\pi$, $\rho\eta$, $\omega\eta$ in the c.m. energy region 1.05-2.00 GeV with the SND detector[1] at the VEPP-2000 e^+e^- collider[2]. The measured cross sections are fitted with the vector meson dominance (VMD) model.

1 Processes overview

1.1 $e^+e^- \to \rho\pi$

The cross section of the process $e^+e^- \to \rho\pi$ with the decay $\rho \to \pi\pi$ has been measured in the energy

Received: 2015-11-30; **Revised**: 2016-04-20

Foundation item: Supported by the Russian Science Foundation(14-50-00080), Russian Ministry of Science and Education and the RFBR(15-02-01037).

Biography: BOTOV A. A.(corresponding author), PhD. Research field: electro-positron annihilation into hadrons. E-mail: A.A.Botov@inp.nsk.su

range $1.05 \leqslant \sqrt{s} \leqslant 2.00$ GeV[3]. The following criteria are applied to selected $\pi^+\pi^-\pi^0$ events.

(Ⅰ) Exactly 2 charged tracks originating from the e^+e^- interaction region.

(Ⅱ) Exactly 2 photons with energies $E_\gamma > 30$ MeV

(Ⅲ) The total energy deposition in the detector calorimeter $0.3 < E_{\rm tot}/\sqrt{s} < 0.8$.

Selected events are fitted to a common vertex. The quality of the vertex fit is characterized by the parameter χ^2_R, which is required to be less than 40. Then the kinematic fit to the hypothesis $e^+e^- \to \pi^+\pi^-\gamma\gamma$ is performed with requirements of the energy and momentum balance, and events are further selected with the following conditions:

(Ⅰ) $\chi^2_E < 30$, where χ^2_E is the χ^2 of the kinematic fit.

(Ⅱ) z coordinate of the vertex $|z_{\rm vertex}| < 10$ cm.

(Ⅲ) The polar angles of the charged tracks $30° < \theta_{\rm track} < 150°$.

(Ⅳ) the difference of charged track azimuthal angles $|\Delta\phi_{\rm track}| > 10°$.

(Ⅴ) The energy deposition in the calorimeter associated with the charged pions $(E_{\pi^+} + E_{\pi^-})/\sqrt{s} < 0.6$.

(Ⅵ) The total energy deposition in the calorimeter not associated with two charged particles and two photons $E^{\rm outer}_{\rm tot} < 70$ MeV.

The number of signal events is determined from the fit to the two-photon mass spectrum with a sum of signal (π^0 resolution function) and background distributions, whose shapes are obtained using signal and background ($e^+e^- \to \pi^+\pi^-\pi^0\pi^0$, $e^+e^- \to \pi^+\pi^-\gamma$, etc.) simulation. The measured $e^+e^- \to \pi^+\pi^-\pi^0$ cross section is shown in Fig. 1. Our results is in agreement with SND at VEPP-2M and BABAR measurements, but has better accuracy. The curve in Fig. 1 represents the result of the VMD fit with $\omega(782)$, $\phi(1020)$, $\omega(1450)$, and $\omega(1680)$ resonances.

In Fig. 1, The cross section for the process $e^+e^- \to \rho\pi$ measured in this work [SND (2011)]

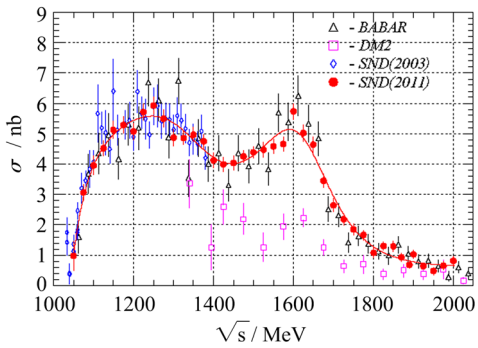

Fig. 1 The cross section for the process $e^+e^- \to \rho\pi$

together with previous measurements in the DM2[4], SND at VEPP-2M ([SND(2003)][5], and BABAR[6] experiments. The curve is the result of the VMD fit described in the text.

1.2 $e^+e^- \to \omega\pi$

The process $e^+e^- \to \omega\pi^0$ is studied in the decay mode $\omega \to \pi^0\gamma$ in the same energy range. Five-photon events are selected using the following conditions.

(Ⅰ) At least 5 photons.

(Ⅱ) No charged particles.

(Ⅲ) Less than 6 hits in the detector drift chamber.

(Ⅳ) The total energy deposition in the calorimeter $E_{\rm tot}/\sqrt{s} > 0.5$.

For selected events the kinematic fits to the hypotheses $e^+e^- \to 5\gamma$ and $e^+e^- \to \pi^0\pi^0\gamma$ are performed, whose qualities are characterized by the parameters $\chi^2_{5\gamma}$ and $\chi^2_{\pi^0\pi^0\gamma}$, respectively. Further selection is based on the following criteria.

(Ⅰ) $\chi^2_{5\gamma} < 30$.

(Ⅱ) $\chi^2_{\pi^0\pi^0\gamma} - \chi^2_{5\gamma} < 10$.

(Ⅲ) At least one of the two $\pi^0\gamma$ invariant masses $|m_{\pi^0\gamma} - M_\omega| < 200$ MeV.

The invariant masses in the latter condition is calculated using photon parameters obtained in the $e^+e^- \to \pi^0\pi^0\gamma$ fit. The number of signal events is obtained from the fit to the $m_{\pi^0\gamma}$ spectrum with a sum of signal and background distributions. The measured cross section is shown in Fig. 2. It should be noted that the CLEO cross section is calculated under the CVC hypothesis from the $\omega\pi$ spectral function in the $\tau \to$

$\omega\pi\nu_\tau$ decay. In Fig. 2, we present the result based on SND data collected in 2010-2012 runs. Our previous measurement based on 2010-2011 data was published in Ref. [7]. From the measured cross section the $\gamma^*\to\omega\pi$ transition form factor shown in Fig. 3 is extracted. The curves in Figs. 2 and 3 are the results of the SND data VMD fit with the $\rho(770)$, $\rho(1450)$ and $\rho(1700)$ resonances. The dashed curve in Fig. 3 is the fit result with the $\rho(770)$ only. It is seen that the VMD model cannot describe simultaneously our data on the transition form factor and data obtained in the NA60 from the $\omega\to\pi^0\mu^+\mu^-$ decay also shown in Fig. 3.

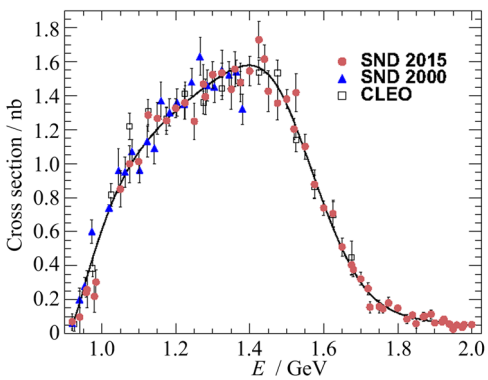

Fig. 2　The cross section for the process $e^+e^-\to\omega\pi$

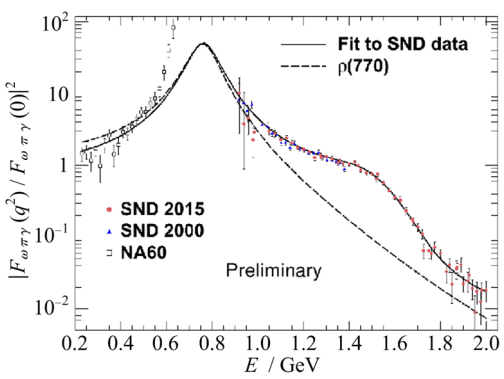

Fig. 3　The $\gamma^*\to\omega\pi$ transition

In Fig. 2, the cross section for the process $e^+e^-\to\omega\pi$ measured in this work (SND 2015) in comparison with previous measurements in the SND at VEPP-2M (SND 2000)[8] and CLEO[9] experiments. The curve is the result of the VMD fit described in the text. In Fig. 3, the $\gamma^*\to\omega\pi$ transition form factor measured in this work (SND 2015) in comparison with previous measurements in the SND at VEPP-2M (SND 2000)[8] and NA60[10] experiments. The curves are the result of the fit described in the text.

1.3　$e^+e^-\to\rho\eta$

The process $e^+e^-\to\rho\eta\to\pi^+\pi^-\eta$ has been studied in the decay mode $\eta\to\gamma\gamma$ in the energy range 1.22-2.00 GeV[11]. The following criteria are used to select $\pi^+\pi^-\eta$ events.

(Ⅰ) Exactly 2 charged tracks originated from the interaction region.

(Ⅱ) Exactly 2 photons with polar angles $36°<\theta<144°$.

(Ⅲ) The total energy deposition in the calorimeter $0.4<E_{\rm tot}/\sqrt{s}<0.9$.

(Ⅳ) The energy deposition of charged particles $E_{\rm track}/\sqrt{s}<0.65$.

The vertex fit and kinematic fit to the $e^+e^-\to\pi^+\pi^-\gamma\gamma$ hypothesis are performed for selected events. The final selection uses the following conditions.

(Ⅰ) $\chi^2_R<200$ and $\chi^2_E<60$.

(Ⅱ) The $\gamma\gamma$ invariant mass 400 MeV $<m_{\gamma\gamma}<$ 700 MeV.

The number of signal events is obtained from the fit to the $m_{\gamma\gamma}$ spectrum with a sum of signal and background distributions. The measured cross section is shown in Fig. 4. Our result agrees with BABAR data, but has better accuracy. The solid curve in Fig. 4 is the result of the VMD fit with $\rho(770)$ and $\rho(1450)$ resonances, while the dashed curve represents the fit with the $\rho(1700)$ contribution added. It is seen that the $\rho(1700)$ contribution is small. It is usually assumed that the dominant mechanism of the $e^+e^-\to\pi^+\pi^-\eta$ reaction is transition via $\rho^0(770)\eta$ intermediate state. We however observe a contribution of other mechanism, presumably $\rho^0(1450)\eta$[11]. From our cross section measurement, using the CVC hypothesis the branching ratio $B_{\rm CVC}(\tau^-\to\eta\pi^-\pi^0\nu_\tau)=(0.156\pm0.011)\%$ is calculated, which is in agreement with the measured value $B_{\rm exp}(\tau^-\to\eta\pi^-\pi^0\nu_\tau)=(0.139\pm0.010)\%$.

In Fig. 4, The cross section for the process $e^+e^-\to\rho\eta$ measured in this work (SND@ VEPP2000)

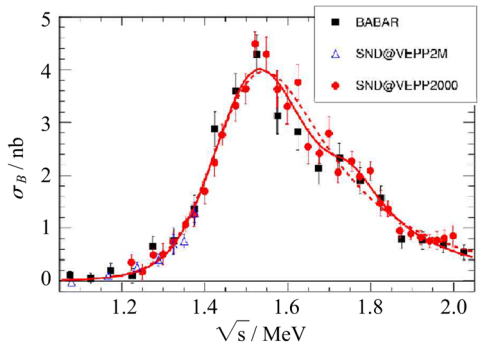

Fig. 4 The cross section for the process $e^+e^-\to\rho\eta$

in comparison with previous measurements in the SND at VEPP-2M (SND@VEPP2M)[12] and BABAR[13] experiments. The curves are the results of the VMD fits described in the text.

1.4 $e^+e^-\to\omega\eta$

The process $e^+e^-\to\omega\eta$ is studied in the decay mode $\omega\to\pi^+\pi^-\pi^0$ and $\eta\to\gamma\gamma$ in the energy range 1.34-2.00 GeV. Events are selected using the following criteria.

(Ⅰ) At least 2 charged tracks originated from the interaction region.

(Ⅱ) At least 4 photons.

(Ⅲ) The total energy deposition in the calorimeter $E_{\rm tot}>300$ MeV.

The vertex fit and kinematic fits to the $e^+e^-\to\pi^+\pi^-\pi^0\gamma\gamma$ hypothesis with the additional condition that the two photon invariant mass must be in the range $400\leqslant m_{\gamma\gamma}\leqslant 700$ MeV and to the $e^+e^-\to\pi^+\pi^-\pi^0\pi^0(\gamma)$ hypothesis are performed. The quality of the kinematic fits are characterized by the parameters $\chi^2_{\pi^+\pi^-\pi^0\gamma\gamma}$ and $\chi^2_{\pi^+\pi^-\pi^0\pi^0(\gamma)}$. The $e^+e^-\to\pi^+\pi^-\pi^0\pi^0$ process is the main source of background for the process under study. The following conditions are applied on the parameters obtained in the fits.

(Ⅰ) $\chi^2_{\pi^+\pi^-\pi^0\gamma\gamma}<30$ and $\chi^2_{\pi^+\pi^-\pi^0\pi^0(\gamma)}>200$.

(Ⅱ) The mass recoiling against $\gamma\gamma$, $0.65<m^{rec}_{\gamma\gamma}<0.9$ GeV for the $e^+e^-\to\pi^+\pi^-\pi^0\gamma\gamma$ fit.

The $\omega\eta$ signal is extracted from the fit to the $m_{\gamma\gamma}$ and $m_{\gamma\gamma}{}^{\rm rec}$ distributions. The measured cross section is shown in Fig. 5 in comparison with the previous BABAR measurement. It is fitted with a sum of the $\omega(1420)$ and $\omega(1650)$ contributions. Destructive interference between these two contributions is responsible for a very low level of the cross section observed above 1.8 GeV.

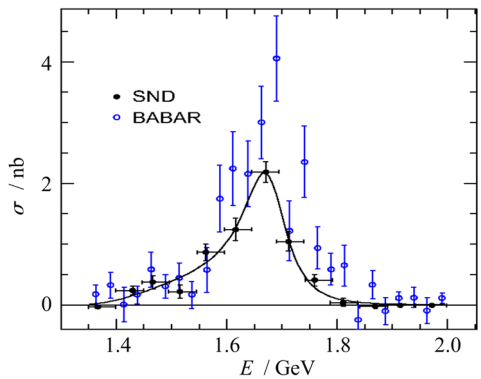

Fig. 5 The cross section for the process $e^+e^-\to\omega\eta$

In Fig. 5, the cross section for the process $e^+e^-\to\omega\eta$ measured in this work (SND) in comparison with previous measurements in the BABAR[14] experiment. The curve is the result of the VMD fit described in the text.

2 Conclusion

The cross sections for the processes $e^+e^-\to\rho\pi$, $\omega\pi$, $\rho\eta$, $\omega\eta$ have been measured in the SND experiment at the VEPP-2000 e^+e^- collider. All of these measurements have the best accuracies to date.

References

[1] ACHASOV M N, AULCHENKO V M, BARU S E, et al. Spherical neutral detector for VEPP-2M collider [J]. Nuclear Instruments and Methods in Physics Research, 1999, 449(1-2): 125-139.

[2] SHATUNOV YU M, EVSTIGNEEV A V, GANYUSHIN D I, et al. Project of a new electron-positron collider VEPP-2000 [C]// Proceedings of the 7th European Particle Accelerator Conference. Vienna, 2000: 439.

[3] AULCHENKO V M, ACHASOV M N, BARNYAKOV A YU, et al. Study of the $e^+e^-\to\pi^+\pi^-\pi^0$ process in the energy range 1.05-2.00 GeV [J]. Journal of Experimental and Theoretical Physics, 2015, 121(1): 27-34.

[4] ANTONELLI A, BALDINI R, BIAGINI M E, et al. Measurement of the $e^+e^-\to\pi^+\pi^-\pi^0$ and $e^+e^-\to$

$\omega\pi^+\pi^-$ reactions in the energy interval 1350-2400 MeV [J]. Zeitschrift Für Physik C, 1992, 56(1): 15-19.

[5] ACHASOV M N, AULCHENKO V M, BELOBORODOV K I, et al. Study of the process $e^+e^-\to\pi^+\pi^-\pi^0$ in the energy region $\sqrt{s}$ from 0.98 GeV to 1.38 GeV [J]. Physical Review D, 2002, 66(3): 032001.

[6] AUBERT B, BARATE R, BOUTIGNY D, et al. Study of $e^+e^-\to\pi^+\pi^-\pi^0$ process using initial state radiation with BaBar[J]. Physical Review D, 2004, 70(7): 072004.

[7] ACHASOV M N, AULCHENKO V M, BARNYAKOV A YU, et al. Study of $e^+e^-\to\omega\pi^0\to\pi^0\pi^0\gamma$ in the energy range 1.05-2.00 GeV with SND[J]. Physical Review D, 2013, 88: 054013.

[8] ACHASOV M N, BELOBORRODOV K I, BERDYUGIN A V, et al. The process $e^+e^-\to\omega\pi^0\to\pi^0\pi^0\gamma$ up to 1.4 GeV[J]. Physics Letters B, 2000, 486(1-2): 29-34.

[9] EDWARDS K W (CLEO Collaboration). Resonant structure of $\tau\to 3\pi\pi^0\upsilon_\tau$ and $\tau\to\omega\pi\upsilon_\tau$ decays [J]. Physical Review D, 1999, 61(7): 072003.

[10] ARNALDIR, BANICZ K, CASTOR J, et al. Study of the electromagnetic transition form factors in $\eta\to\mu^+\mu^-\gamma$ and $\omega\to\mu^+\mu^-\pi^0$ decays with NA60[J]. Physics Letters B, 2009, 677(5): 260-266.

[11] AULCHENKO V M(SND Collaboration). Measurement of the $e^+e^-\to\eta\pi^+\pi^-$ cross section in the center-of-mass energy range 1.22-2.00 GeV with the SND detector at the VEPP-2000 collider[J]. Physical Review D, 2014, 4(4): 323-328.

[12] ACHASOV M N, BELOBORRODOV K I, BERDYUGIN A V, et al. Measurement of the $e^+e^-\to\eta\pi^+\pi^-$ cross section in the $\sqrt{s}$ = 1.04 GeV-1.38 GeV energy range with a spherical neutral detector at the VEPP-2M collider[J]. JETP Letters, 2010, 92(2): 80-84.

[13] AUBERT B (BABAR Collaboration). The $e^+e^-\to 2(\pi^+\pi^-)\pi^0$, $2(\pi^+\pi^-)\eta$, $K^+K^-\pi^+\pi^-\pi^0$ and $K^+K^-\pi^+\pi^-\eta$ cross sections measured with initial-state radiation [J]. Physical Review D, 2007, 76(9): 092005.

[14] AUBERT B, BARATE R, BOUTIGNY D, et al. The $e^+e^-\to 3(\pi^+\pi^-)$, $2(\pi^+\pi^-\pi^0)$ and $K^+K^-2(\pi^+\pi^-)$ cross sections at center-of-mass energies from production threshold to 4.5 GeV measured with initial-state radiation [J]. Physical Review D, 2006, 71(5): 052003.

Article ID:0253-2778(2016)06-0528-05

Search for the decays $\eta' \to e^+ e^-$ and $\eta \to e^+ e^-$ at the VEPP-2000 $e^+ e^-$ collider

KARDAPOLTSEV L. V.[1,2](for the SND Collaboration)

(1. *Budker Institute of Nuclear Physics, SB RAS, Novosibirsk* 630090, *Russia*;
2. *Novosibirsk State University, Novosibirsk* 630090, *Russia*)

Abstract: A search for the rare decay $\eta' \to e^+ e^-$ has been performed with the SND detector at the VEPP-2000 $e^+ e^-$ collider. The inverse reaction $e^+ e^- \to \eta'$ and η' five decay chains have been used for this search. The upper limit $\Gamma_{\eta' \to e^+ e^-} < 0.002$ eV at the 90% confidence level has been set. A sensitivity of SND in a search for $\eta \to e^+ e^-$ decay has been studied. For this purpose a data sample with an integrated luminosity of 108 nb^{-1} collected in the center-of-mass energy range 520-580 MeV was analyzed. No background events for the reaction $e^+ e^- \to \eta$ with decay $\eta \to \pi^0 \pi^0 \pi^0$ have been found. In the absence of background, a sensitivity to $B(\eta \to e^+ e^-)$ of 10^{-6} can be reached during two weeks of VEPP-2000 operation.

Key words: VEPP-2000; SND; $e^+ e^-$; η'; η; electronic width

CLC number: O572.3 **Document code**: A doi:10.3969/j.issn.0253-2778.2016.06.013

Citation: KARDAPOLTSEV LV(for the SND Collaboration). Search for the decays $\eta' \to e^+ e^-$ and $\eta \to e^+ e^-$ at the VEPP-2000 $e^+ e^-$ collider[J]. Journal of University of Science and Technology of China, 2016, 46(6): 528-532.

KARDAPOLTSEV LV(代表SND合作组). 在VEPP-2000正负电子对撞机上寻找 $\eta' \to e^+ e^-$ 和 $\eta \to e^+ e^-$ [J]. 中国科学技术大学学报, 2016, 46(6): 528-532.

在 VEPP-2000 正负电子对撞机上寻找 $\eta' \to e^+ e^-$ 和 $\eta \to e^+ e^-$

KARDAPOLTSEV L. V.[1,2](代表 SND 合作组)

(1. 俄罗斯布德克尔核物理研究所, 新西伯利亚 630090, 俄罗斯; 2. 国立新西伯利亚大学, 新西伯利亚 630090, 俄罗斯)

摘要:在 VEPP-2000 正负电子对撞机上,用 SND 探测器研究了稀有衰变 $\eta' \to e^+ e^-$,研究中使用了逆过程 $e^+ e^- \to \eta'$ 和 η' 的五个衰变链. 90% 的置信度的 $\Gamma_{\eta' \to e^+ e^-}$ 上限被设定为 0.002 eV;还研究了用 SND 寻找 $\eta \to e^+ e^-$ 过程的灵敏度,为此分析了质心能量 520-580 MeV 之间积分亮度为 108 nb^{-1} 的数据,没有发现当 $\eta \to \pi^0 \pi^0 \pi^0$ 时,衰变 $e^+ e^- \to \eta$ 过程的本底事例. 在无本底情况下, VEPP-2000 运行两周时 $B(\eta \to e^+ e^-)$ 灵敏度即可达到 10^{-6}.

关键词:VEPP-2000; SND; 正负电子; 电子分宽度

Received:2015-11-30; **Revised**:2016-04-20

Foundation item: Supported by the IRFBR(15-02-03391-a), RSF Project(N 14-50-00080).

Biography: KARDAPOLTSEV L V(corresponding author), Professor/PhD. Research field: high energy physics. E-mail: l. v. kardapoltsev@inp.nsk.su

0 Introduction

Decays of pseudoscalar mesons to the pair of leptons $P \to l^+l^-$ are rare. In the standard model(SM) these decays proceed through the two-photon intermediate state as shown in Fig. 1 and therefore are suppressed as α^2 relative to the $P \to \gamma\gamma$ decays, where α is the fine structure constant. An additional suppression of $(m_l/m_P)^2$ arises from the approximate helicity conservation, where m_l and m_P are the lepton and meson masses, respectively. So, due to the low probabilitysuch decays are sensitive to possible contributions to new physics beyond the SM[1-2].

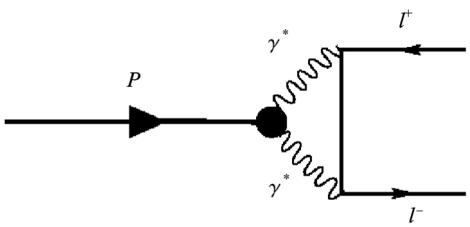

Fig. 1 Leading order QED contribution driving $P \to l^+l^-$ decays

The ranges of predictions for the $P \to l^+ l^-$ branching fractions obtained in different form-factors models[3-4] are listed in Tab. 1. For comparison, the last column of Tabl. 1 contains the current experimental values of the branching fractions. The value of $B(\pi^0 \to e^+e^-)$ differs from the theoretical prediction by about three standard deviations. This can have different explanations connected with theoretical uncertainty[5] or/and with new physics contributions[1-2].

Tab. 1 The theoretical predictions and experimental values for the $P \to l^+l^-$ branching fractions

parameter	prediction	experoment
$B(\pi^0 \to e^+e^-) \times 10^8$	6.23-6.38	7.49 ± 0.38[6]
$B(\eta \to e^+e^-) \times 10^9$	4.60-5.24	<2300[7]
$B(\eta \to \mu^+\mu^-) \times 10^7$	4.64-5.12	5.8 ± 0.8[8]
$B(\eta' \to e^+e^-) \times 10^{10}$	1.15-1.86	<56[9-10]
$B(\eta' \to \mu^+\mu^-) \times 10^7$	1.14-1.36	

This paper is devoted to the recent search for the $\eta' \to e^+e^-$ decay[9] with the SND detector[11-12] at the VEPP-2000 e^+e^- collider[13], in which the inverse reaction $e^+e^- \to \eta'$ is used. Also we consider the recent study of SND sensitivity in search for the $\eta \to e^+e^-$ decay with the use of the same technique[14].

1 SND detector

A detailed description of the SND detector can be found in Refs. [11-12]. It is a nonmagnetic detector, the main part of which is a three-layer spherical electromagnetic calorimeter based on NaI(Tl) crystals. The solid angle covered by the calorimeter is 90% of 4π. Its energy resolution for photons is $\sigma_E/E = 4.2\%/(E\ \mathrm{GeV})^{1/4}$, and the angular resolution is about 1.5°. The directions of charged particles are measured by a tracking system, which consists of a 9-layer drift chamber and a proportional chamber with readout from cathode strips. The tracking system covers a solid angle of 94% of 4π. The calorimeter is surrounded by a muon system, which is used, in particular, for cosmic-background suppression.

2 Search for $\eta' \to e^+e^-$ decay

For search for the decay $\eta' \to e^+e^-$ data with an integrated luminosity of about 2.9 pb^{-1} are used. They were accumulated in 2013 at the c. m. energy close to $m_{\eta'}c^2 = 957.78 \pm 0.06$ MeV[8]. During the data taking period the beam energy was monitored with an absolute accuracy of about 60 keV by the back-scattering-laser-light system[15]. As the collider energy spread (FWHM = 0.590 MeV) is significantly larger than the η' width $\Gamma_{\eta'} = (0.198 \pm 0.009)$ MeV[8], the resulting cross section is proportional to the electronic width.

$$\sigma_{\mathrm{vis}}(\mathrm{nb}) = (6.38 \pm 0.23)\Gamma_{\eta' \to e^+e^-}(\mathrm{eV}) \quad (1)$$

It should be noted that the radiative corrections and the energy spread lead to a reduction of the cross section compared to the Born one by a factor of four.

The search for the process $e^+e^- \to \eta'$ is performed in five decay chains: $\eta' \to \eta\pi^+\pi^-$ with the η decays to $\gamma\gamma$ and $3\pi^0$, and $\eta' \to \eta\pi^0\pi^0$ with the η decays to $\pi^+\pi^-\pi^0$, $\gamma\gamma$ and $3\pi^0$.

Detailed description of selection criteria for all decay chains can be found in Ref. [9]. Only main selection parameters will be discussed in this paper.

2.1 Decay chain $\eta' \to \pi^+\pi^-\eta$, $\eta \to \gamma\gamma$

For events passing a preliminary selection the kinematic fit to the $e^+e^- \to \pi^+\pi^-\eta$ hypothesis is performed. The input parameters for kinematic fit are

the polar and azimuthal angles of charged tracks and the angles and energies of photons measured in the calorimeter. The quality of the fit is characterized by the parameter χ^2_η. Another important parameter used for the final selection is the sum of energy depositions of charged particles in the second and third layers of the calorimeter $E_{2+3,\mathrm{char}}$. Since pions in the process under study are soft, they stop predominantly in the first calorimeter layer. The two-dimensional distributions of the parameters χ^2_η and $E_{2+3,\mathrm{char}}$ for data events and simulated events of the process under study are shown in Fig. 2. The rectangle in the bottom left corner corresponds to the selection criteria applied. No data events are selected.

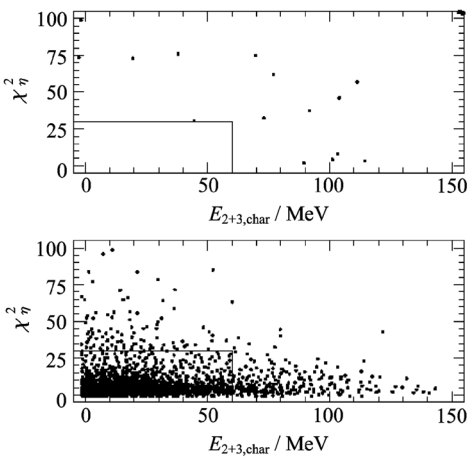

Fig. 2 The two-dimensional distribution of the parameters

In Fig. 2, the two-dimensional distribution of χ^2_η versus $E_{2+3,\mathrm{char}}$ for data events (top) and simulated events of the $e^+e^-\to\eta'\to\pi^+\pi^-\eta$, $\eta\to\gamma\gamma$ process (bottom). The rectangle in the bottom left corner of the plot corresponds to the selection criteria used.

The dominant sources of background for this decay mode are the processes $e^+e^-\to\eta\gamma$, $\eta\to\pi^+\pi^-\pi^0$ and $e^+e^-\to\pi^+\pi^-\pi^0\pi^0$. Additional fake photons can appear as a result of the splitting of electromagnetic showers, nuclear interaction of pions in the calorimeter, or superimposing beam-generated background. The number of background events estimated using MC simulation is 0.7 ± 0.1 and 0.10 ± 0.05 for the first and second processes, respectively.

There is also the nonresonant reaction $e^+e^-\to\pi^+\pi^-\eta$, that proceeds through the $\rho\eta$ intermediate state. It is suppressed due to the small phase space of the final particles. The contribution of the nonresonant process is estimated to be 0.2 events.

2.2 Decay chain $\eta'\to\pi^+\pi^-\eta$, $\eta\to3\pi^0$

For preliminary selected events the kinematic fit is performed to the hypothesis $e^+e^-\to\pi^+\pi^-3\pi^0$. The two-dimensional distributions of χ^2 of the kinematic fit ($\chi^2_{3\pi^0}$) versus the three π^0 invariant mass ($M_{3\pi^0}$) for data events and simulated events of $e^+e^-\to\eta'\to\pi^+\pi^-\eta$, $\eta\to3\pi^0$ processes are shown in Fig. 3.

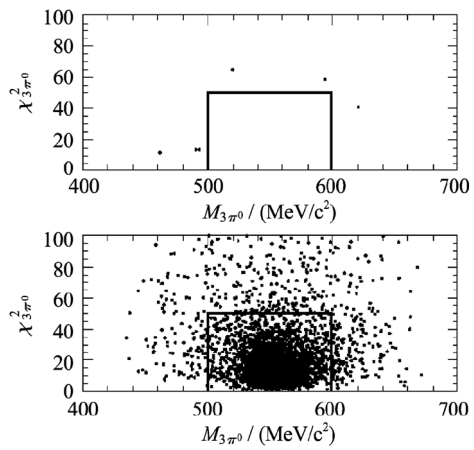

Fig. 3 The two-dimensional distribution of the parameters

In Fig. 3, the two-dimensional distribution of the parameters $\chi^2_{3\pi^0}$ and $M_{3\pi^0}$ for data events (top) and simulated $\eta'\to\pi^+\pi^-\eta$, $\eta\to3\pi^0$ events (bottom). The rectangle corresponds to the selection criteria used: $\chi^2_{3\pi^0}<50$ and $500<M_{3\pi^0}<600$ MeV/c^2.

The dominant background source for the $\pi^+\pi^-\pi^0\pi^0\pi^0$ final state is the process $e^+e^-\to\pi^+\pi^-\pi^0\pi^0$. The number of background events obtained using MC simulation is 2.7 ± 0.5. The contribution of the nonresonant background from the $e^+e^-\to\pi^+\pi^-\eta$ process discussed above is about 0.1 events.

2.3 Decay chain $\eta'\to\pi^0\pi^0\eta$, $\eta\to\gamma\gamma$

For events passing initial selection the kinematic fit to the $e^+e^-\to\eta'\to\eta\pi^0\pi^0\to6\gamma$ hypothesis is performed. The quality of the fit is characterized by the parameter $\chi^2_{\eta\pi^0\pi^0}$. The distributions of this parameter for data events, simulated signal events, and simulated background events from the process $e^+e^-\to\eta\gamma$, $\eta\to3\pi^0$ are shown in Fig. 4. The condition $\chi_{\eta\pi^0\pi^0}<15$ is applied. No data events satisfying the selection criteria

have been found.

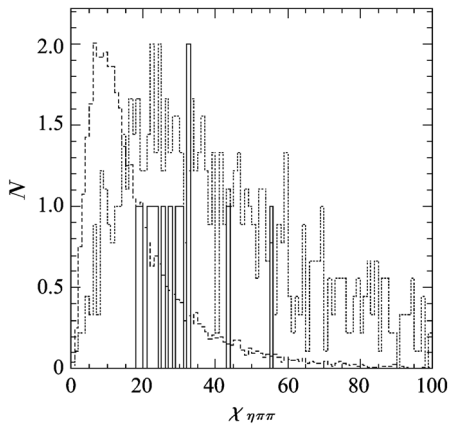

Fig. 4　The $\chi^2_{\eta\pi^0\pi^0}$ distribution

In Fig. 4, the $\chi^2_{\eta\pi^0\pi^0}$ distribution for data events (solid histogram), simulated signal $e^+e^- \to \eta' \to 2\pi^0\eta \to 6\gamma$ events (dashed histogram), simulated background events from the process $e^+e^- \to \eta\gamma$, $\eta \to 3\pi^0$ (dotted histogram).

The main background sources for this decay mode are the processes $e^+e^- \to \eta\gamma \to 3\pi^0\gamma$ and $e^+e^- \to \pi^0\pi^0\gamma$. The number of background events from these sources is calculated to be 1.3 ± 0.3 and 0.4 ± 0.1, respectively.

2.4　Decay chain $\eta' \to \pi^0\pi^0\eta$, $\eta \to 3\pi^0$

For this decay mode with ten photons in the final state there is no background from e^+e^- annihilation. The main source of background is cosmic-ray showers. We select events containing nine or more photons and no tracks in the drift chamber. The total energy deposition $E_{\rm cal}$ and the event momentum $P_{\rm cal}$ calculated using energy depositions in the calorimeter crystals must satisfy the following conditions:

$$\left.\begin{aligned} &0.7 < E_{\rm cal} < E_{\rm cm} < 1.2,\ cP_{\rm cal} < E_{\rm cm} \\ &E_{\rm cal}/E_{\rm cm} - cP_{\rm cal}/E_{\rm cm} > 0.7 \end{aligned}\right\} \quad (2)$$

No data events are selected after applying these criteria.

2.5　Upper limit

Since the number of selected data events is equal to zero, we set the upper limit on the cross section. The technique of Cousins and Highland[16] following the implementation of Barlow[17] is used to calculate the limit with all uncertainties included:

$$\sigma^{\rm exp}_{\rm vis} < 12.7 \text{ pb at } 90\% \text{ CL} \quad (3)$$

The limit on the cross section is translated using Eq. (1) to the upper limit on the η' electronic width

$$\Gamma_{\eta' \to e^+e^-} < 0.0020 (\text{eV}) \text{ at } 90\% \text{ CL} \quad (4)$$

The obtained limit is slightly better than the limit set recently in the CMD-3 experiment $\gamma_{\eta' \to e^+e^-} < 0.0024$ eV[10].

Using the Eq. (1) we combine the SND and CMD-3 data and obtain the combined upper limits on the electronic width

$$\Gamma_{\eta' \to e^+e^-} < 0.0011 (\text{eV}) \text{ at } 90\% \text{ CL} \quad (5)$$

and the branching fraction [$\gamma_{\eta'} = (0.198 \pm 0.009)$ MeV[8]].

$$B(\eta' \to e^+e^-) < 5.6 \times 10^{-9} \text{ at } 90\% \text{ CL} \quad (6)$$

The obtained upper limit is most stringent but still 30-50 times larger than theoretical predictions[1-2] made in the framework of the standard model.

3　Search for $\eta \to e^+e^-$ decay

For this study, VEPP-2000 parameters at c. m. energy close to $m_\eta c^2 = 548.862 \pm 0.018$ MeV[8] such as luminosity, accuracy of the energy setting, energy spread, are important. In 2013 SND did not record data exactly at this energy. Therefore, we analyze data from four energy points near $m_\eta c^2$, with c. m. energies of 520, 540, 560, and 580 MeV. The integrated luminosity collected at these energy points measured using the reaction $e^+e^- \to \gamma\gamma$ is 108.1 ± 2.0 nb^{-1}.

In the proposed experiment the collider energy must be set and monitored with an accuracy better than the collider c. m. energy spread of about 150 keV. This is provided by the beam-energy-measurement system described above.

The most suitable η decay mode for the search for the $e^+e^- \to \eta$ reaction at SND is $\eta \to \pi^0\pi^0\pi^0 \to 6\gamma$, for which physical background is small. The main source of background is cosmic-ray events. For the search for $e^+e^- \to \eta$, events with six or more detected photons and with the energy deposition in the calorimeter larger than $0.6E$ are selected. Background from events with charged particles is rejected by the selection condition that the number of fired wires in the drift chamber is less than four. Cosmic-ray background is suppressed by the veto from the muon detector.

For events passing the preliminary selection, a kinematic fit to the $e^+e^- \to \pi^0\pi^0\pi^0 \to 6\gamma$ hypothesis is performed. The quality of the kinematic fit is

characterized by the parameter χ^2. The condition $\chi^2 < 100$ is used to select η candidates. No events satisfying the selection criteria are found. So, we set the upper limit on the $e^+e^- \to \eta$ cross section

$$\sigma_{\exp} < 170 \text{ pb at } 90\% \text{ CL} \quad (7)$$

corresponding to $N_s = 0$ and integrated luminosity 108 nb^{-1}. Using the same technique as in section 2.5, we can estimate sensitivity to the search for the decay $\eta \to e^+e^-$ to be

$$B(\eta \to e^+e^-) < 2.9 \times 10^{-6} \text{ at } 90\% \text{ CL} \quad (8)$$

This result is close to the upper limit $B(\eta \to e^+e^-) < 2.3 \times 10^{-6}$ set recently in the HADES experiment[7]. With a VEPP-2000 luminosity of $0.34 \times 10^{30} \text{cm}^{-2}\text{s}^{-1}$ the current upper limit can be reached in a week of data taking. In two weeks a sensitivity at the level of 10^{-6} can be reached.

4 Conclution

A search for the rare decay $\eta' \to e^+e^-$ has been performed with the SND detector at the VEPP-2000 e^+e^- collider. The inverse reaction $e^+e^- \to \eta'$ and five decay chains of η' have been used for this search. The following upper limit has been set on the decay width: $\Gamma_{\eta' \to e^+e^-} < 0.002$ eV at the 90% confidence level. Also a sensitivity of SND in a search for decay $\eta \to e^+e^-$ has been studied. For this perpose we have analyzed a data sample with an integrated luminosity of 108 nb^{-1} collected with the SND detector in the center-of-mass energy range 520-580 MeV. There are no background events for the reaction $e^+e^- \to \eta$ with decay $\eta \to \pi^0\pi^0\pi^0$ have been found. In the absence of background, a sensitivity to $B(\eta \to e^+e^-)$ of 10^{-6} can be reached duringtwo weeks of VEPP-2000 operation.

References

[1] KAHN Y, SCHMITT M, TAIT M. Enhanced rare pion decays from a model of MeV dark matter[J]. Physics Review D, 2008, 78(11): 115002.

[2] CHANG Q, YANG Y D. Rare decay $\pi^0 \to e^+e^-$ – constraints on the light CP-odd Higgs in NMSSM[J]. Physics Letters B, 2009, 676(1-3): 8893.

[3] PETRI T. Anomalous decays of pseudoscalar mesons[J]. Physics, 2010: arXiv:1010.2378.

[4] DOROKHOV A E. Rare decay $\pi^0 \to e^+e^-$ as a test of standard model[J]. Physics Particle and Nuclear Letters, 2010, 7(4): 229-234.

[5] HUSEK T, KAMPF K, NOVOTNY J. Rare decay $\pi^0 \to e^+e^-$: on corrections beyond the leading order[J]. European Physics Journal C, 2014, 74: 3010(1-11).

[6] ABOUZAID E, ARENTON M, BARKER A R, et al. Measurement of the rare decay $\pi^0 \to e^+e^-$[J]. Physics Review D, 2007, 75(1): 012004.

[7] AGAKISHIEV G, BALANDA A, BELVER D, et al. Searching a Dark Photon with HADES[J]. PhysicsLetters B, 2014, 731(2): 265-271.

[8] OLIVE K A, GOLWALA S, VOGEL P, et al. Review of particle physics[J]. Chinese Physics C, 2014, 38(9): 090001.

[9] ACHASOV M N, AULCHENKO V M, BARNYAKOV A, et al. Search for the $\pi^0 \to e^+e^-$ decay with the SND detector[J]. Physical Review D, 2015, 91: 092010.

[10] AKHMETSHIN R R, ANISENKOV A V, AULCHENKO V M, et al. Search for the process $e^+e^- \to \eta*(958)$ with the CMD-3 detector[J]. Physics Letters B, 2015, 740: 273-277.

[11] ACHASOV M N, BERKAEV D E, BOGDANCHIKOV D A, et al. First experience with SND calorimeter at VEPP-2000 collider[J]. Nuclear Instruments and Methods in Physics Research Section A, 2009, 598(1): 31-32.

[12] AULCHENKO V M, BOGDANCHIKOV A G, BOTOV A A, et al. SND tracking system: Tests with cosmic muons[J]. Nuclear Instruments and Methods in Physics Research Section A, 2009, 598(1): 102-104.

[13] SHATUNOV YU M, EVSTIGNEEV A V, GANYUSHIN D I, et al. Project of a new electron positron collider VEPP-2000[C]// Proceedings of the 7th European Particle Accelerator Conference. Vienna, Austria, 2000: 439-441.

[14] ACHASOV M N, BARNYAKOV A Y, BELOBORODOV K I, et al. On the search for the $\eta \to e^+e^-$ decay at the VEPP-2000 e^+e^- collider[J]. Journal of Experimental Theoretical Physics Letters, 2015, 102(5): 266-270.

[15] ABAKUMOVA V, ACHASOV M N, BERKAEV D E, et al. A system of beam energy measurement based on the Compton backscattered laser photons for the VEPP-2000 electron-positron collider[J]. Nuclear Instruments and Methods in Physics Research Section A, 2014, 744(5): 35-40.

[16] COUSINS R D, HIGHLAND V L. Incorporating systematic uncertainties into an upper limit[J]. Nuclear Instruments and Methods in Physics Research Section A, 1992, 320(1-2): 331335.

[17] BARLOW R. A calculator for con_dence intervals[J]. Computer Physics Communications, 2002, 149(2): 97-102.

List of Participants

Name	E-mail	Institution	City	Country
Prof. ACHASOV, Nikolay	achasov@ math. nsc. ru	Sobolev Institute for Mathematics	Novosibirsk	Russian
Prof. AN, Qi	anqi@ ustc. edu. cn	USTC	Hefei	China
Dr. BALDINI FERROLI, Rinaldo	baldini@ lnf. infn. it	INFN-LNF	Frascati	Italy
Dr. BARSUK, Sergey	sergey. barsuk@ cern. ch	Laboratoire de l'Accélérateur Linéaire (FR)	Orsay	France
Mr. BELOBORODOV, Konstantin	K. I. Beloborodov@ inp. nsk. su	NSU / BINP	Novosibirsk	Russian
Prof. BERGER, Niklaus	niberger@ uni-mainz. de	JGU Mainz	Mainz	Germany
Mr. BEYER, Axel	axel. beyer@ mpq. mpg. de	MPQ	Garching	Germany
Mr. BOTOV, Alexander	a. a. botov@ inp. nsk. su	BINP	Novosibirsk	Russian
Prof. CAI, Hao	hcai@ whu. edu. cn	Wuhan University	Wuhan	China
Mr. CAO, Zheng	caoz@ ihep. ac. cn	IHEP	Beijing	China
Dr. CARLONI CALAME, Carlo	carlo. carloni. calame@ pv. infn. it	University of Pavia	Pavia	Italy
Mr. CHEN, Rui	chenr2012@ lzu. edu. cn	Lan Zhou University	Lanzhou	China
Prof. CHEN, Shenjian	sjchen@ nju. edu. cn	Nanjing University	Nanjing	China
Dr. CZARNECKI, Andrzej	andrzejc@ ualberta. ca	University of Alberta	Edmonton	Canada
Prof. CZYZ, Henryk	czyz@ us. edu. pl	University of Silesia	Katowice	Poland
Dr. DE LEO, Veronica	veronica. deleo@ roma3. infn. it	INFN Sezione Roma 3	Roma	Italy
Prof. DENIG, Achim	denig@ kph. uni-mainz. de	JGU Mainz	Mainz	Germany
Dr. DIMOVA, Tatyana	baiert@ inp. nsk. su	NSU / BINP	Novosibirsk	Russian
Dr. DING, Guijun	dinggj@ ustc. edu. cn	USTC	Hefei	China
Prof. DRUZHININ, Vladimir	druzhinin@ inp. nsk. su	NSU / BINP	Novosibirsk	Russian
Dr. ESCRIBANO, Rafel	rafel. escribano@ ifae. es	U. Barcelona	Barcelona	Spain
Dr. FAEL, Matteo	fael@ itp. unibe. ch	University of Bern	Bern	Switzerland
Ms. FANG, Xin	fangx@ mail. ustc. edu. cn	USTC	Hefei	China
Mr. FANG, Shuangshi	fangss@ ihep. ac. cn	IHEP	Beijing	China
Prof. FEDOTOVICH, Gennady	fedotovich@ inp. nsk. su	BINP	Novosibirsk	Russian
Prof. GAO, Daoneng	gaodn@ ustc. edu. cn	USTC	Hefei	China
Prof. GAO, Haiyan	yijun. gu@ dku. edu. cn	Duke Kunshan University	Kunshan	China
Mr. GAO, Xinlei	gaoxinl@ mail. ustc. edu. cn	USTC	Hefei	China
Mr. GAO, Zhen	gaozhen@ mail. ustc. edu. cn	USTC	Hefei	China
Dr. GAUZZI, Paolo	paolo. gauzzi@ roma1. infn. it	U. Roma / INFN Roma	Rome	Italy
Prof. GOLTERMAN, Maarten	maarten@ sfsu. edu	SF State U.	San Francisco	United States
Dr. GONNELLA, Francesco	francesco. gonnella@ lnf. infn. it	INFN	Frascati	Italy
Mr. GRIESSINGER, Konrad	griess@ slac. stanford. edu	Mainz University	Mainz	Germany
Dr. GUO, Zhihui	dr_guozhihui@ 163. com	Hebei Normal University	Shijiazhuang	China
Prof. HUANG, Guangshun	hgs@ ustc. edu. cn	USTC	Hefei	China
Prof. HU, Haiming	huhm@ ihep. ac. cn	IHEP	Beijing	China
Dr. IGNATOV, Fedor	ignatov@ inp. nsk. su	BINP	Novosibirsk	Russian
Mr. IVANOV, Vyacheslav	vyacheslav_lvovich_ivanov@ mail. ru	BINP	Novosibirsk	Russian
Dr. JIAO, Jianbin	jiaojb@ sdu. edu. cn	Shandong University	Jinan	China
Prof. JOHANSSSON, Tord	tord. johansson@ physics. uu. se	Uppsala University	Uppsala	Sweden
Mr. KARDAPOLTSEV, Leonid	l. v. kardapoltsev@ inp. nsk. su	BINP / NSU	Novosibirsk	Russian
Dr. KARSHENBOIM, Savely	savely. karshenboim@ mpq. mpg. de	MPQ	Garching	Germany
Dr. KIM, SeungCheon	sk2528@ cornell. edu	Cornell University	Ithaca	United States
Dr. KISELEV, Alexey	kiselev@ math. nsc. ru	Sobolev Institute for Mathematics / NSU	Novosibirsk	Russian
Mrs. KONG, HUI	kid007@ mail. ustc. edu. cn	USTC	Hefei	China
Dr. KOROL, Aleksandr	a. a. korol@ inp. nsk. su	NSU / BINP	Novosibirsk	Russian
Mr. KOZYREV, Evgeny	eakozyrev09@ gmail. com	NSU / BINP	Novosibirsk	Russian
Dr. KUPSC, Andrzej	Andrzej. Kupsc@ physics. uu. se	Uppsala University	Uppsala	Sweden
Dr. LEE, Hye-Sung	hyesung. lee@ cern. ch	IBS CTPU	Daejeon	Republic of Korea
Dr. LI, Cui	cui. li@ physics. uu. se	Uppsala University	Uppsala	Sweden
Prof. LI, Haibo	lihb@ ihep. ac. cn	IHEP	Beijing	China
Dr. LI, Lei	lilei@ ihep. ac. cn	BIPT	Beijing	China
Mr. LI, Longke	lilongke@ mail. ustc. edu. cn	USTC	Hefei	China

Ms. LI, Peilian	lipl@ mail. ustc. edu. cn	USTC	Hefei	China
Mr. LI, Peirong	lipeirong11@ mails. ucas. ac. cn	UCAS	Beijing	China
Mr. LIU, Dong	dliu13@ mail. ustc. edu. cn	USTC	Hefei	China
Prof. LIU, Jianbei	liujianb@ ustc. edu. cn	USTC	Hefei	China
Dr. LIU, Landiao	liulandiao@ gmail. com	Peking University	Beijing	China
Prof. LIU, Shubin	liushb@ ustc. edu. cn	USTC	Hefei	China
Prof. LIU, Xiang	xiangliu@ lzu. edu. cn	Lanzhou University	Lanzhou	China
Prof. LIU, Yanwen	yanwen@ ustc. edu. cn	USTC	Hefei	China
Prof. LU, Caidian	lucd@ ihep. ac. cn	IHEP	Beijing	China
Dr. LUSIANI, Alberto	alberto. lusiani@ pi. infn. it	Scuola Normale Superiore	Pisa	Italy
Dr. LYU, Xiaorui	xiaorui@ ucas. ac. cn	UCAS	Beijing	China
Prof. MAGGIORA, Marco	marco. maggiora@ to. infn. it	INFN-TO	Turin	Italy
Dr. MA, Hailong	mahl@ ihep. ac. cn	IHEP	Beijing	China
Prof. MALTMAN, Kim	kmaltman@ yorku. ca	York University	Toronto	Canada
Dr. MASSRI, Karim	karim. massri@ cern. ch	University of Liverpool	Liverpool	UK
Dr. NICHOLSON, Caitriana	c. nicholson@ ihep. ac. cn	IHEP	Beijing	China
Mr. NIU, Pengyu	niupengyu14@ mails. ucas. ac. cn	IHEP	Beijing	China
Dr. PACETTI, Simone	simone. pacetti@ pg. infn. it	U. Perugia / INFN	Perugia	Italy
Dr. PASSERA, Massimo	passera@ pd. infn. it	INFN Padova	Padova	Italy
Mr. PENG, Junbo	vortex@ mail. ustc. edu. cn	USTC	Hefei	China
Dr. PEREZ DEL RIO, Elena	eperez@ lnf. infn. it	INFN Frascati	Frascati	Italy
Dr. PIMINOV, Pavel	piminov@ inp. nsk. su	BINP SB RAS	Novosibirsk	Russian
Mr. POPOV, Alexandr	aspopov1@ inp. nsk. su	BINP	Novosibirsk	Russian
Prof. QIAO, CONGFENG	qiaocf@ ucas. ac. cn	University of CAS	Beijing	China
Dr. REDMER, Christoph Florian	redmer@ kph. uni-mainz. de	JGU Mainz	Mainz	Germany
Prof. ROBERTS, B. Lee	roberts@ bu. edu	Boston University	Boston	United States
Dr. ROIG, Pablo	proig@ fis. cinvestav. mx	Dpto. Fisica Cinvestav	Mexico DF	Mexico
Dr. RONGGANG, Ping	pingrg@ ihep. ac. cn	IHEP	Beijing	China
Dr. SAVRIE', Mauro	savrie@ fe. infn. it	University of Ferrara and INFN	Ferrara	Italy
Prof. SHEN, Chengping	shencp@ ihep. ac. cn	Beihang University	Beijing	China
Prof. SHEN, Xiaoyan	shenxy@ ihep. ac. cn	IHEP	Beijing	China
Prof. SHWARTZ, Boris	shwartz@ inp. nsk. su	BINP / NSU	Novosibirsk	Russian
Dr. SUN, Yanjun	yjsun@ mail. ustc. edu. cn	Northwest Normal University	Lanzhou	China
Mr. TAN, Yaxing	tanyx@ mail. ustc. edu. cn	USTC	Hefei	China
Dr. TODYSHEV, Korneliy	todyshev@ inp. nsk. su	BINP	Novosibirsk	Russian
Dr. WANG, Boqun	boqunwg@ ucmail. uc. edu	U. Cincinnati	Cincinnati	United States
Dr. WANG, Dayong	dayong. wang@ pku. edu. cn	Peking University	Beijing	China
Dr. WANG, Ping	wangp@ IHEP. ac. cn	IHEP	Beijing	China
Prof. WANG, Qun	qunwang@ ustc. edu. cn	USTC	Hefei	China
Mr. WANG, Weiping	cloud13@ mail. ustc. edu. cn	USTC	Hefei	China
Prof. WANG, Xiaolian	wangxl@ ustc. edu. cn	USTC	Hefei	China
Dr. WANG, Yadi	wangyd@ ihep. ac. cn	HIM-GSI	Mainz	Germany
Mr. WANG, Yaqian	whyaqm@ gmail. com	KPH	Mainz	Germany
Dr. WANG, Zhihong	wzh1988@ mail. ustc. edu. cn	USTC	Hefei	China
Mr. WANG, Zhiyong	wangzy@ ihep. ac. cn	IHEP	Beijing	China
Mr. WEI, Yifeng	weiyf@ mail. ustc. edu. cn	USTC	Hefei	China
Ms. XUE, Mingxuan	xuemx@ mail. ustc. edu. cn	USTC	Hefei	China
Mr. XUE, Sirun	xuesr@ ihep. ac. cn	IHEP	Beijing	China
Mr. XU, Qingnian	xuqingnian10@ mails. ucas. ac. cn	UCAS	Beijing	China
Dr. XU, Xinping	xuxp@ ihep. ac. cn	Soocow Univ.	Suzhou	China
Prof. YAN, Wenbiao	wenbiao@ ustc. edu. cn	USTC	Hefei	China
Prof. YUAN, Changzheng	yuancz@ ihep. ac. cn	IHEP	Beijing	China
Mr. ZENG, Zhe	zengzhe@ mail. ustc. edu. cn	USTC	Hefei	China
Mr. ZHANG, Bingxin	zhangbx@ ihep. ac. cn	IHEP	Beijing	China
Dr. ZHANG, Jingzhi	jingzhi@ ihep. ac. cn	IHEP	Beijing	China
Dr. ZHANG, Liming	liming_zhang@ tsinghua. edu. cn	Tsinghua University	Beijing	China
Mr. ZHANG, Yateng	zyt1988@ mail. ustc. edu. cn	USTC	Hefei	China
Dr. ZHANG, Zhenyu	zhangzhenyu@ ihep. ac. cn	Wuhan University	Wuhan	China
Prof. ZHANG, Ziping	zpz@ ustc. edu. cn	USTC	Hefei	China
Mr. ZHANG, Jielei	zhangjielei@ ihep. ac. cn	IHEP	Beijing	China
Prof. ZHAO, Qiang	zhaoq@ ihep. ac. cn	IHEP	Beijing	China
Prof. ZHAO, Zhengguo	zhaozg@ ustc. edu. cn	USTC	Hefei	China
Dr. ZHEVLAKOV, Alexey	zhevlakov@ phys. tsu. ru	Tomsk State University	Tomsk	Russian
Ms. ZHOU, Xiaorong	zxrong@ ustc. edu. cn	USTC	Hefei	China
Mr. XIA, Lei	jessemcc@ mail. ustc. edu. cn	USTC	Hefei	China
Dr. ZHENG, Bo	zhengb@ ihep. ac. cn	University of South China	Hengyang	China